

Structural damage to Dutch terraced houses due to flood actions

Lise Jansen



Structural damage to Dutch terraced houses due to flood actions

Master Thesis (final report)

by

Lise Jansen

to obtain the degree of Master of Science
at the Delft University of Technology.

Student number: 4289013
Project duration: September 3, 2018 – June 6, 2019
Date of report: June 6, 2019
Thesis committee: Dr. J. D. Bricker, TU Delft, Chairman
Dr. K. M. de Bruijn, Deltares
Prof. Dr. Ir. S.N. Jonkman, TU Delft
Ir. P. A. Korswagen Eguren, TU Delft
Ir. S. Pasterkamp, TU Delft

Preface

This thesis concludes my masters in Structural Engineering with specialization Hydraulic Structures of the faculty of Civil Engineering and Geosciences at the Delft University of Technology. During my studies, I discovered my passion for establishing bridges between the field of structural and hydraulic engineering. The topic of structural damage to buildings due to flooding is perfect to further examine this interface of the two fields of interest. On top of that as the Dutch, we are always aware of the fact that the biggest part of our country can be flooded by water from the North Sea or one of the big rivers crossing our country. But the question arises if our Dutch residences can resist these flood actions or that they will be washed away... Before you start reading my work, I would like to thank those people who contributed to the process of writing this thesis and supported me along the way:

First of all, I would like to thank my committee members for their advice, ideas, supervision and support, without you it would not have been the level of quality as it is right now! A special thanks to Jeremy Bricker for initiating this graduation topic and chairing the committee. You made me realize that not all ideas can be explored into detail in a master thesis which, in combination with your endless enthusiasm for all the ideas, helped me throughout the whole process. You also introduced me to Karin de Bruijn, who was especially important in defining the research questions and gave me a lot of the input concerning flood models and the way Deltares is dealing with flooding.

Thank you Paul Korswagen-Eguren for carefully reading everything I have written and providing me with the right remarks both on the content and the use of the English language. It helped me improve the report into the smallest details. On top of that, your experience with this topic and particularly masonry made it easier for me to go in depth and ask you for advice if I ran into a brick wall. Sander Pasterkamp was very helpful with all the questions about buildings and loads in general. You could always find a moment to help me thinking of possible solutions in a creative and constructive way. Furthermore, Bas Jonkman was essential in increasing the comprehensibility of my thesis and placing it in a more realistic view. I really appreciate the critical comments and ideas to improve the report.

Furthermore, I am grateful for the opportunity to conduct my own experiments in the Fluid Mechanics Laboratory and for the staff of the lab and technicians, who helped me out whenever they could. It would be impossible to conduct the experiments without you installing the instruments, constructing the essential 'building' and advising me based on your experiences with all kind of experiments in the laboratory.

Last but not least, I cannot forget to thank my friends and housemates for all the lazy evenings hanging on the couch, cosy dinners with "just one glass of wine" and your excellent persuasiveness which made me join many more social activities than planned. Amongst all the fun, you also lent a sympathetic ear (or a coffee card), gave me advice when I needed it the most and a particular thanks to Floor for helping me out with her design skills. Let me conclude by expressing my very special thanks to my family and boyfriend Wouter, who unconditionally gave me love and understanding during the whole process.

Overall, I really enjoyed my college days and am proud to conclude these with this report. I wish you a pleasant and interesting reading!

*Lise Jansen
Delft, May 2019*

Abstract

'De Watersnood van 1953', the largest Dutch flood in recent history, caused the death of 1795 people in the Netherlands directly from the flood conditions, while in the UK, 315 were recorded. Most of them were among those whose residence collapsed due to high water depth, quick rise rate of the water or strong flow velocity. Based on historical data of floods with similar flood characteristics and comparable buildings, mortality functions were developed to estimate the number of fatalities. These functions are still used, but the correlation between the flood characteristics and the damage observation is not clear according to multiple studies. The current study contributes to improving these functions by investigating which *flood conditions may lead to collapse of the residences in the current Dutch building stock*.

From the BAG-registration (in Dutch: Basisregistratie Adressen en Gebouwen) it is found that 50% of the Dutch live in terraced houses (in Dutch: rijtjeshuizen), which is similar in the areas which are most likely to be affected by flooding. Most of these residences are built in the period of the housing shortage between 1965 and 1975 and the energy crisis between 1975 and 1994, which are considered as 'the typical Dutch residence'. This residence type consists of cavity walls with a load-bearing leaf of concrete or unreinforced masonry (URM), which can be clay or calcium-silicate. This inner leaf is tied to the outer leaf of URM consisting of perforated clay units, wood-based materials, or concrete. Stability is provided by piers in the façades in case of the URM walls or rigid connections between the concrete floor and walls. To define the properties of the building materials, existing experimental research on the masonry is used.

Experiments with a physical model were conducted herein to measure the quasi-steady load in the form of pressures acting on different elements of the residence. This enables the comparison of the quasi-steady flood load and the lateral load due to wind on different elements of a building. Similar to FEMA (2011), it was found that the pressure coefficient decreases when the width-to-water depth ratio decreases. However, higher coefficients are found from the experiments than those provided by FEMA, resulting in higher hydrodynamic loads. Furthermore, the orientation of the residence compared to the flow direction changes the angle of attack. When the flow is perpendicular to the wall, the pressure coefficient is the largest. Decreasing the angle of attack causes a decrease of the pressure due to equal flood conditions.

The pressure coefficients obtained from the experiments are used to define the hydrodynamic load due to flooding. The resistance of the load-bearing cavity walls, windows and piers were compared to the acting moment due to different depth-flow velocity combinations. The resistance of out-of-plane bending of the load-bearing wall is the critical failure mechanism for typical Dutch residences. Residences with calcium-silicate masonry walls and system floors have a higher resistance than residences with clay masonry walls and timber floors. Cracks start to develop at a small lateral load resulting in zero tension strength after cracking and an eccentricity of the normal force. This makes the influence of the dead weight carried by the wall, in combination with the compression strength and the thickness, more important than the flexural bending strength.

All types of residences, using design values, already collapse before the h_v -product (water depth times flow velocity) of $7 \text{ m}^2/\text{s}$ is reached according to Clausen (1989). A water depth of ± 1.2 meters for the older residences (1965-1975) and ± 1.8 meters for the newer residences (1975-1994), already cause the design moment resistance of the wall without taking the velocity or wave action into account. If the flood water has a flow velocity of 2 m/s or waves are generated by a wind speed of 29.5 m/s over a fetch of 100 m , the critical water depth reduces to respectively ± 0.9 and 1.5 meters.

List of symbols

α	[°]	rotation of the building
α_{im}	[-]	factor for impulsive load
β	[-]	bending moment coefficient
γ_M	[-]	material factor
δ_0	[m]	vertical shift in wave height due to interaction with wall
θ	[°]	crack angle
λ	[-]	scale ratio
λ	[-]	hydrodynamic load in choked flow
μ	[-]	orthogonality ratio
μ	[-]	viscosity
μ_N	[-]	mean
ρ	[kg/m ³]	density water
ρ_{wind}	[kg/m ³]	density wind
σ	[MPa]	surface tension
σ_m	[MPa]	bending stress
σ_n	[MPa]	compression stress
σ_N	[-]	deviation
ϕ	[°]	flow incidence / angle of attack
b	[m]	width of the flume
c_0	[m/s]	wave celerity
c_f	[-]	force coefficient
c_{fr}	[-]	friction coefficient
$c_s c_d$	[-]	structural factor
dh/dt	[m/hr]	rise rate
f_{cd}	[MPa]	design compression strength
f_{ck}	[MPa]	characteristic compression strength
$f_{ctk0,05}$	[MPa]	characteristic tension strength
f_b	[MPa]	mean compressive strength
f_{xk}	[MPa]	characteristic flexural strength
f_{vk}	[MPa]	characteristic shear strength
f_{vk0}	[MPa]	initial characteristic shear strength
f_{wk}	[MPa]	characteristic flexural bond tensile strength
g	[m/s ²]	gravity acceleration
h	[m]	water depth
h_0	[m]	impoundment depth
hv	[m ² /s]	depth-velocity product
k	[-]	wave number
l	[m]	length
n	[-]	number of piers in facade
p	[MPa]	pressure
p_f	[-]	annual failure probability
q	[m ³ /s]	discharge
q_{Ed}	[N/m ²]	design load
q_p	[N/m ²]	peak velocity pressure
t	[s]	time
t_{op}	[s]	time of opening of the gate

u	[m/s]	hourly extreme wind velocity
u	[mm]	displacement
v	[m/s]	flow velocity
v_{min}	[MPa]	characteristic shear strength
w_e	[MPa]	pressure on outside walls
w_i	[MPa]	pressure on inside walls
x	[m]	distance from gate
x_u	[m]	concrete compression zone
z_e	[m]	reference height
A	[m ²]	footprint object
A_c	[m ²]	concrete area
A_{fr}	[m ²]	friction area
A_{ref}	[m ²]	impact area
B	[m]	width / length side normal to the flow
B/b	[-]	blockage ratio
C_D	[-]	drag coefficient
C_{D0}	[-]	unbounded drag coefficient
C_H	[-]	hydrostatic coefficient
C_P	[-]	pressure coefficient
C_R	[-]	coefficient of resistance
D	[m]	depth / length side aligned with the flow
E	[MPa]	modulus of elasticity
E_{ex}/E_{in}	[N]	external / internal work
EI	[Nm]	bending stiffness / flexural rigidity
F	[m]	fetch
F_b	[N/m]	buoyancy load
F_d	[N/m]	quasi-static/hydrodynamic load per meter width
$F_{D,T}$	[-]	mortality fraction in transition zone
$F_{D,B}$	[-]	mortality fraction in breach zone
$F_{D,O}$	[-]	mortality fraction in zone with slowly rising water levels
$F_{D,S}$	[-]	mortality fraction in zone with rapidly rising water levels
F_h	[N/m]	hydrostatic load per meter width
F_i	[N]	load due to dynamic debris
F_s	[N/m]	impulsive load per meter width
F_w	[N/m]	wind load per meter width
G	[kg/m ²]	weight
G_n	[°]	natural slope
H	[m]	height of the building
H_s	[m]	significant wave height
I	[mm ³]	moment of inertia
N_{Ed}	[N/m]	design normal load
N_{Rd}	[N/m]	design normal resistance
M_{Ed}	[Nm/m]	design moment load
M_{Rd}	[Nm/m]	design moment resistance
L	[m]	length / wave length
T_s	[s]	significant wave period
U	[m/s]	wind velocity
V	[m ³]	volume
V	[kN/m]	shear force per meter width
W	[mm ³]	section modulus

Contents

Abstract	v
List of symbols	vii
1 Introduction	1
1.1 Motive	1
1.1.1 Background	1
1.1.2 Problem description	3
1.2 Research aim, objectives and methodology.	3
1.2.1 Research objectives	3
1.2.2 Methodology	4
1.3 Reading guide	5
2 The impact of Dutch floods on buildings	7
2.1 Impact of Dutch floods	7
2.1.1 Dutch mortality functions	7
2.1.2 Flood modelling.	9
2.2 Flood actions on buildings	10
2.2.1 Overview of flood actions	11
2.2.2 Quasi-static load	13
2.2.3 Wind waves.	15
2.3 Summary and conclusions of literature review on loads	17
2.3.1 Gaps in the current literature.	17
3 Typical Dutch residences	19
3.1 Building stock.	19
3.2 Description of case-study residences	21
3.2.1 Load-bearing walls	21
3.2.2 Façades.	23
3.2.3 Floors and roof	23
3.3 Failure mechanisms	24
4 Experimental quantification of design flood loads	27
4.1 Experimental set-up	27
4.1.1 Instrumentation	29
4.1.2 Scaling and scale effects.	29
4.1.3 Methodology	30
4.2 Results of experiments.	34
4.2.1 Geometry	35
4.2.2 Orientation	38
4.2.3 Conclusions on quasi-steady load.	39
4.3 Overview of flood loads	40
5 Structural damage of typical Dutch residences	43
5.1 Approach	43
5.1.1 Schematization	43
5.1.2 Load bearing walls	45
5.1.3 Stability	47
5.1.4 Windows	48

5.2	Resistance	49
5.2.1	Load-bearing walls	49
5.2.2	Stability	52
5.2.3	Non-structural elements: windows.	53
5.3	Structural damage	54
5.3.1	Load-bearing walls	54
5.3.2	Shear walls	56
5.3.3	Conclusions on structural damage.	56
6	Discussion, Conclusions and Recommendations	61
6.1	Discussion	61
6.2	Conclusions.	63
6.3	Recommendations	64
A	Durability of masonry	69
B	Damage grade	71
B.1	Vulnerability matrices.	71
C	Impact modelling	73
C.1	Dutch mortality functions.	74
D	Flood actions	75
D.1	Flood infiltration rate	76
D.2	Impulsive load	76
D.3	Blockage effect	77
E	Drag and pressure coefficients	79
E.1	Windload according to NEN-EN 1991-1-4.	79
F	Selection of case-study residences	81
F.1	Type of residence BAG.	81
F.2	Building quality over the years.	82
F.3	Case-study residences.	84
G	Material models and properties for structural analyses	87
G.1	Model approaches	87
G.2	Material properties	88
H	Experimental set-up	89
H.1	Instrumentation	89
H.2	Scaling	90
H.3	Analytical solution for a dam-break wave	93
I	Linear elastic approach	95
I.1	Edge conditions.	95
I.2	Linear elastic response.	96
I.3	Load distribution over shear walls	98
J	Tie and window failure	99
J.1	Tie failure	99
J.2	Windows	100
K	Failure graphs without the safety factors	101

Introduction

1.1. Motive

In the last years, there have been floods all over the world which have a lot of influence on the lives of people living in these flood-prone areas. Their residences could be damaged, they may need to evacuate, could be surprised by the water or even drown in the flood. The most extreme flood in the Netherlands occurred in 1953 and is known as the "Watersnoodramp". In this introduction, some recent floods of low-lying areas protected by flood defences from various forms of flooding, like coastal, river and pluvial floods are described. The way countries deal with damage and fatality estimates, give more insight into the room for improvements of the Dutch situation and help to formulate the objectives of this study.

1.1.1. Background

In the night of 31 January to 1 February 1953, a storm surge on the North sea flooded large areas at the east coast of the United Kingdom, northwest of Belgium and southwest of the Netherlands. Many fatalities occurred due to the collapse of buildings behind levee breaches, which were mainly caused by the high water depth, rise rate of the water and flow velocity. In the Netherlands 1795 people died directly from the flood conditions, while in the UK, 315 were recorded. This gives a mortality rate for both areas of just below 1% (Jonkman, 2007), where mortality is defined as the fraction of those who died directly from the flood out of all the people present at the onset of flooding after evacuation excluding the persons in shelters.



(a) Schouwen Duiveland. Nieuwerkerk



(b) Rescue Dreischor through hole in the roof

Figure 1.1: Watersnoodramp 1953 in the Netherlands from Nationaal Archief and Beeldbank Zeeland

In the flooded areas of Zuid-Holland in the Netherlands 1649 out of a total of 1687 collapsed residences were poor-quality working-class houses, presumably built with the traditional building method. To fix the bricks, mortar was used based on chalk instead of cement (Slager, 1992). This is a problem when these buildings are near the sea since the air and water contain salt, $NaCl$, which reacts with the calcium-carbonate, $CaCO_3$, to calcium-chloride, $CaCl_2$. When water is penetrating the wall, the mortar can dissolve and the interface conditions between the bricks become worse.

Similarly, in the United Kingdom a large number of fatalities were observed in seaside shanty-towns of mainly wooden prefabricated bungalows, which were not meant to be occupied in winter. People were surprised by the water in the night when they were asleep and could not escape due to collapse or rise rate of the water (Lumbroso and Vinet, 2011).

Recent floods

One of the most recent extreme flood events occurred on the 10th of October 2018 when Hurricane Micheal made landfall near Mexico Beach, Florida as a category 4 hurricane. When the hurricane travelled land inwards, flash floods were triggered in the Carolinas and Virginia due to a high storm surge. At Mexico Beach 237 of the 440 buildings (54%) were totally destroyed and 99 (23%) were severely damaged. These were almost all residential structures built around the seventies before the new construction code, which is known to be extremely strict on windstorm resistance. Witnesses saw the wind lifting buildings and the flood spreading downed trees and debris all over the town. One of the few residences still standing is built especially to withstand extreme events like this and is made from poured concrete, reinforced by steel cables and rebars. In the corners, additional concrete piers are situated and the whole structure is elevated from the ground on approximately 12 meter high piles. Further from the coast more small buildings withstood the wind, but were affected by the flood water (New York Times).

Also a category 4, Hurricane Harvey made landfall near Rockport, Texas on August 25 2017, but this hurricane is known for its extreme rainfall and flood-related damages. An estimation by the Houston Chronicle on September 6th 2017 is made of 119,000 damaged residences from which 800 totally collapsed. 54 of the 78 direct fatalities were due to drowning, most of them (confirmed for 18) while driving a vehicle or by getting out of a car (Sebastian et al., 2017). This is also found to be the most frequent cause of death in data analysis of 13 flood events from Europe and the United States considering mainly inland flooding, which is considered to be representative for the current Dutch situation according to Jonkman (2007) in Figure 1.2.

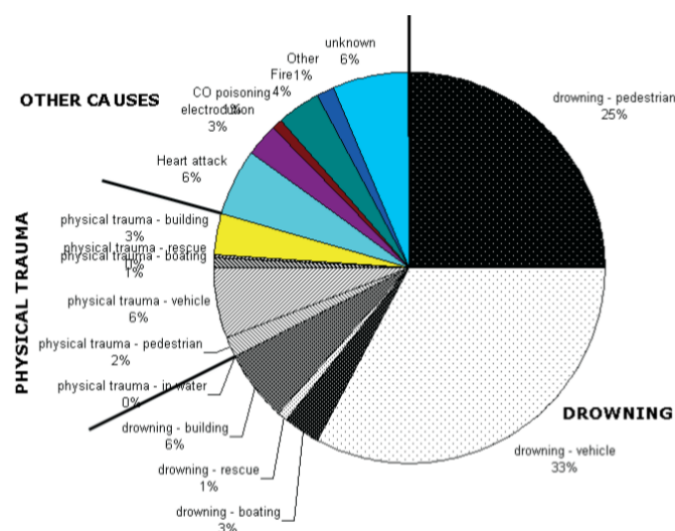


Figure 1.2: Distribution of causes and circumstances of death (Jonkman, 2007)

The storm Xynthia hit the French Atlantic coast on 28th of February 2010. The combination of storm surge, high tide and large waves caused failure of the flood defences along the coast, which was not expected by the authorities. People prepared for the storm by seeking shelter in their bungalows and closed the electric shutters. When the flood arrived, they had no escape route due to lack of a first floor, resulting in people getting trapped inside their own residence. Several residences also had steel bars in front of their windows as advised by insurance companies or could not open their shutters due to the power cut. From the 65 direct fatalities, 47 people died as result of the flood (drowning, hypothermia and exhaustion) from which 41 were trapped in their residence (Lumbroso and Vinet, 2011). A total of 500,000 residences were damaged by the storm all over France, from which 682 were destroyed in the flooded area 682 (Kolen et al., 2010).

1.1.2. Problem description

Although it is difficult to subscribe the damage to the severe forces from the wind or flood, it becomes clear that residential building quality is an important issue in mortality. In Figure 1.3 this can be accommodated under the factor "People vulnerability & behaviour", but has also an influence on the need of "Preventive evacuation" and the possibility of "Sheltering during flooding".

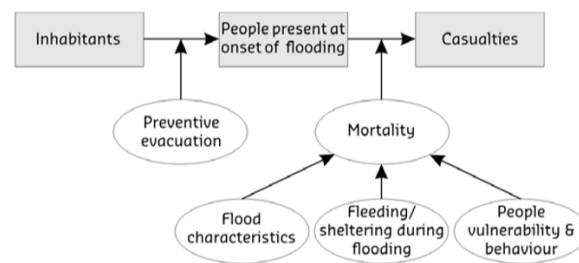


Figure 1.3: Overview of factors which influence the number of flood fatalities (De Bruijn and van Kester, 2015)

To estimate the number of fatalities due to flooding the Dutch government uses mortality functions, which provide mortality as a function of the flood characteristics such as water depth, flow velocity and water level rise rate. These are developed by analyzing empirical information from historical floods between 1934 and 1965. Implicitly, the building quality is taken into account, but this quality has changed over the years with new building regulations and development of knowledge, materials and construction techniques. For example, the classification of masonry based on their environment with strict requirements for buildings in the coastal area to prevent degradation of the mortar like during the Watersnoodsramp, see Appendix A.

Luckily after this period, no flood has occurred with similar flood characteristics and comparable buildings, so improving those functions based on new representative data is difficult. Empirical studies which compare the flood characteristics to the strength and stability of current residences could be the outcome.

1.2. Research aim, objectives and methodology

The aim of this study is to determine which flood conditions can cause structural damage to residential structures. First, the research objectives are formulated as research questions followed by the methodology.

1.2.1. Research objectives

The focus of this study is on the (partial) collapse of residences. Other damage, as described in Appendix B, is not taken into account. Better insight into the failure mechanisms of the current residences can contribute to the improvement of mortality estimates. The following main research question is drawn up with two main objectives to be able to answer this main

question:

Which flood conditions may lead to collapse of typical Dutch residences?

1. *Which loads act on a building in a flood?*

The flood actions on buildings due to Dutch flood conditions are quantified based on previous studies and new experiments with a physical model. The focus is on the hydrostatic and dynamic loads in relation to the orientation of the residence compared to the flow direction and ratio between the dimensions of the residences and water depth. The design load due to flooding is determined by combining several actions.

2. *What is the strength of typical Dutch residences?*

First, typical Dutch residences which are most likely to be affected by flooding are selected based on the location, time of construction, and type of residence. Their properties and most common failure mechanisms during flooding are defined as well in order to describe the strength of the structural elements of the residences.

When the load due to flood actions (sub-question 1) is larger than the maximum load that can be resisted by an element of the residence (sub-question 2), the element will collapse. The flood conditions which cause this load, are considered as the maximum flood conditions the residence can withstand before collapsing.

1.2.2. Methodology

In order to answer the two main objectives the following methodology is used:

- *Define the relevant flood actions on buildings:*
The known flood actions on buildings and flood conditions which could occur in the Netherlands are described in the literature review. Some can already be quantified by previous studies.
- *Select the typical Dutch residences:*
The typical Dutch residences prone to flooding are found to combine the building stock information in the BAG-registration (Basisregistratie Adressen en Gebouwen) with the inundation maps from the Klimaatatlas in a Geographic Information System (GIS). Based on the description of residences categorized per time of construction from the literature review, the physical properties of 3 typical Dutch residences are defined.
- *Describe the typical Dutch residences and their failure mechanisms:*
The last couple of years physical tests are conducted to investigate the properties and behaviour of masonry residences in the context of the earthquakes in the Groningen, North of the Netherlands. These studies are used as input of the material properties as addition to properties defined in the Eurocode. The failure mechanisms are defined based on studies on failure mechanisms of similar buildings or building elements due to flooding and earthquakes.
- *Quantify the quasi-steady flood load:*
To characterize this flood load on buildings different experiments with a physical model are conducted. The loads are measured as pressures on different sides of the building to make it possible to approach the quasi-static part of the dynamic load in the same way as the wind load on buildings. Similar experiments of bluff objects in both wind tunnels and flumes from the literature review are used to validate the used physical model.
- *Determine the resistance of the residences:*
When the strength of typical Dutch residences and the loads on buildings due to flood actions are known, a structural schematization can be made for both. The maximum loads which the residences can withstand are determined analytically with both linear elastic and non-linear calculations.

1.3. Reading guide

This study can roughly be divided into two parts which belong to the two sub-questions: determination of the strength of typical Dutch residences on one hand and the quantification of the loads due to flood actions on the other hand. In the reading guide in Figure 1.4 this is visualized by the use of orange for the strength and blue for the loads. The main question can be answered by combining both parts.

First, a literature analysis is done to explore the current knowledge in the field of flood actions on buildings. Starting in *Chapter 2* with describing the development in flood impact modelling. The loads on buildings due to the Dutch flood conditions are determined based on various studies. This chapter ends with a summary of the literature review and the identified gaps. In *Chapter 3* the typical Dutch residences are determined and described. Followed up by the most common failure mechanisms for these kinds of residences. *Chapter 4* deals with the experiments needed to quantify the quasi-steady flood load and compare this to the wind-load on buildings. This leads to design loads, which are schematically used to find the resistance of the residences in *Chapter 5*. The maximum loads the residences can resist are compared with the flood conditions which can cause these loads, to be able to answer the main research question in *Chapter 6*. Finally, recommendations are presented in this chapter as well.

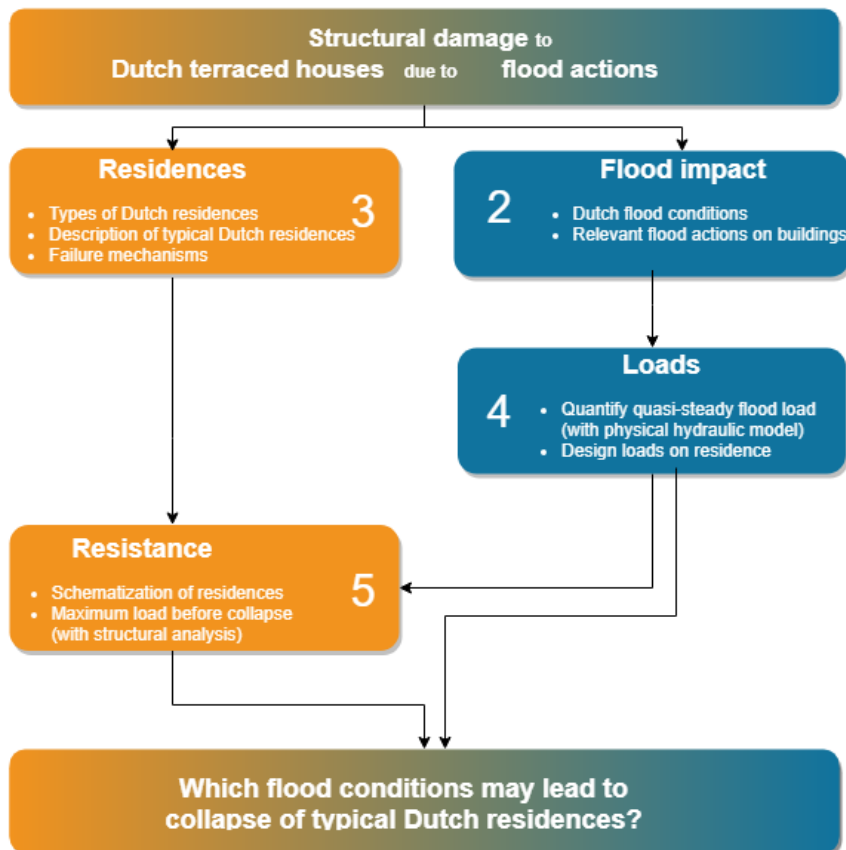


Figure 1.4: Research outline (per chapter)

The impact of Dutch floods on buildings

In this chapter a literature review is given on the role of the collapse of buildings due to Dutch floods, starting with the description how to cope with the impact of flooding nowadays. The generation of flood parameters by hydraulic models needed as input of the mortality functions and the inclusion of collapse of the buildings are discussed, followed by a description of different flood actions. Based on the identified gaps in the literature, it is described how this study will contribute to the improvement of estimating the collapse of residences.

2.1. Impact of Dutch floods

To assess the impact of flooding, a hydraulic model is developed to simulate flood hazards, which generate spatial flood characteristics. To translate these characteristics to the impact, relations or functions between the damage or mortality fraction and the flood are needed. The impact of large scale floods from the main Dutch watercourses is assessed with the 'Standard Flood Damage and Fatality Assessment Model' (Slager and Wagenaar, 2017) or in Dutch 'Standard Schade en Slachtoffer Model' (SSM2017).

2.1.1. Dutch mortality functions

In the Dutch model, the flooded area is divided into four typical hazard zones depending on their flood characteristics. Based on empirical data from historical flood events and literature, for each of the zones a mortality function is determined by Jonkman (2007) and adapted by Maaskant et al. (2009). The collapse of residences is especially in the breach zone and zone with rapidly rising water levels a major cause of fatalities. These relationships are shown in Figure 2.1a (Appendix C.1 for the actual functions) followed by a description per zone.

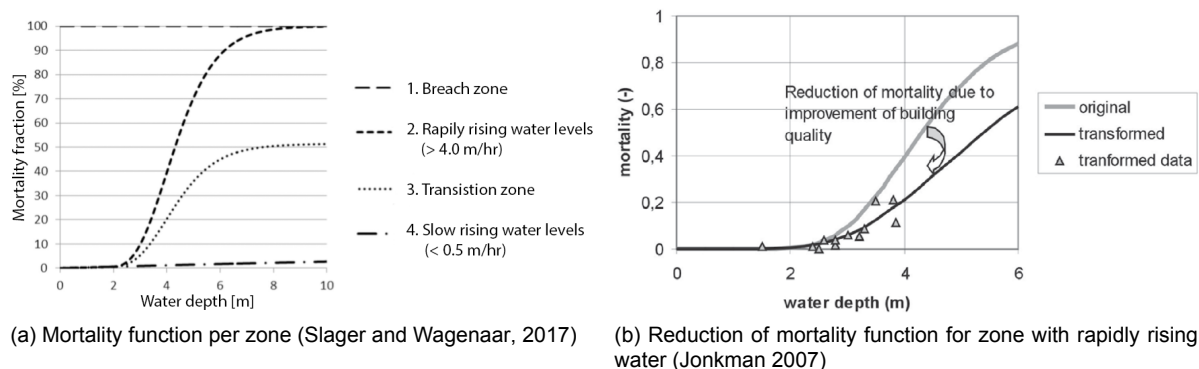


Figure 2.1: Dutch mortality functions

Breach zone

This area is generally directly behind the breach and has characteristic high flow velocities ($v \geq 2\text{ m/s}$), high products of depth and flow velocity ($hv \geq 7\text{ m}^2/\text{s}$) and fast-rising water levels. Many functions are developed to define total collapse of a building based on data of a historic event or empirically obtained by experiments, where the Clausen criterion (1989) of total collapse (dashed black line at $hv = 7\text{ m}^2/\text{s}$ in Figure 2.2) can be seen as the upper limit. That is why the boundaries of this zone are defined by this criterion for total destruction of brick and masonry houses, based on data from the Dale Dyke dam failure in the UK in 1864. The hv is based on a point depth in the flood in combination with the average speed in the direction of the flow, but locally higher velocities could occur.

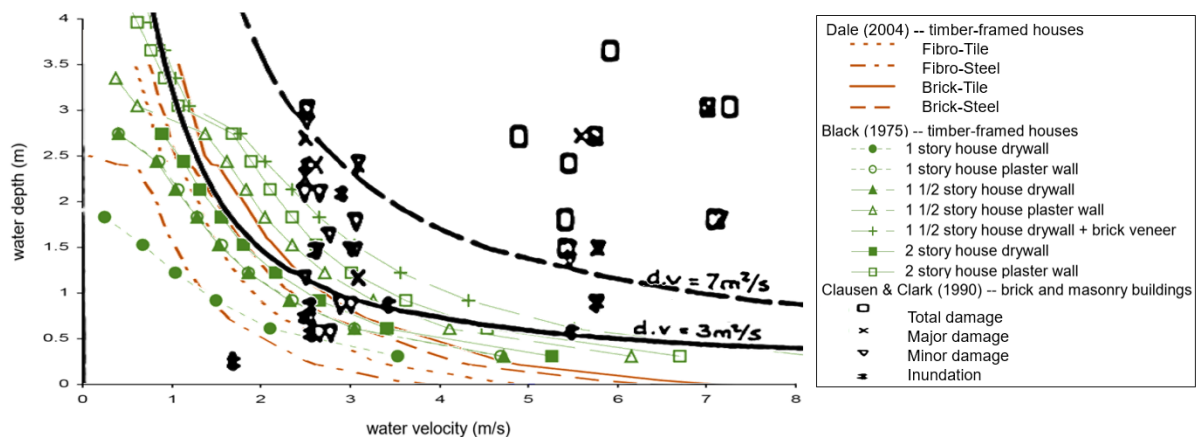


Figure 2.2: Damage curves for different kind of buildings (upper limit by Clausen (1989): partial collapse above solid black line and total collapse above dashed black line)

In the Netherlands, this mortality function is rarely used, since these flood characteristics only occur really close to the breach, locally near blockage of the water due to a higher elevation (road, levee, wall of residence etc.) or tidal current. Since the probability to survive the outside conditions is negligible, people are assumed to stay indoors and do not survive the collapse. This leads to the conservative assumption that none of the people exposed to the flood in this zone will survive, so $F_{D,B} = 1$ (Jonkman, 2007).

Zone with rapidly rising water levels

In this zone, there is not enough time for people to find shelter due to high water level rise rate over the first 1.5 m water depth. In combination with high water levels, there is also the danger of being trapped on higher floors. The relationship between water depth and mortality in this zone is mainly based on data of the 1953 floods in the Netherlands, where many fatalities among the working-class occurred due to building collapse (Slager, 1992). Asselman (2005) used damage data of Goeree and Schouwen Duiveland during the 1953 flood and the damage curves developed by Roos (2003), to investigate the decrease in collapse ratio if these houses were built with present-day cavity or concrete walls, which would respectively be 20 and 93%.

Based on the study of Asselman (2005), Jonkman (2007) made a first-order estimate to correct the original function for improved building quality by assuming a 50-50 distribution of cavity and concrete walls. In Figure 2.1b the original mortality function and the reduction of the log-normal mortality function are shown. This transformed mortality function is based on assumptions and purely transformed due to improvement of building quality. So this is not yet implemented in the SSM2017, but it emphasizes the importance of understanding the impact of building quality.

Transition zone

Jonkman (2007) defined 0.5 m/hour as a threshold for rapidly water level rise leading to fatalities, which was based on limited data. To reduce the sensitivity of the results due to a small difference in rise rate around this threshold, Maaskant et al. (2009) modified this by introducing an extra zone with a mortality function linearly interpolated between rapidly and slow rising water levels.

Zone with slow rising water levels

Due to the slow rising of the water people have better possibilities to reach shelter on higher grounds or floors of buildings, so in this zone the relationship between collapse of buildings and mortality is less strong.

2.1.2. Flood modelling

For SSM2017 Delft-FLS and Sobek-1D2D are mostly used to perform the hydrodynamic calculations to provide a hazard map. From land-use maps, the roughness can be defined per cell and buildings are usually taken into account by applying a high roughness for the urban areas, for example using the Withe-Colebrook formula with Nikuradse equivalent roughness value of $K_n = 10$ m. Applying this roughness to every cell where a building is situated leads to neighbourhoods or even cities where the flow velocity in those cells are highly restricted (generally less than 0.5 m/s) and is mainly directed around. Local flood characteristics inside these areas with high urbanization rates are not adequate enough to asses individual structures (Tennakoon, 2004).

Nowadays models and elevation data is available with a higher resolution, like 3Di, D-flow FM, HEC-RAS etc. Single residential buildings and levees can be modelled at the right location, by using their actual elevation or use the ground elevation (flat area) with a high roughness for the area of the building only instead of the whole urban area (Beretta et al., 2018). If detailed data is available, this way of modelling could generate a more accurate estimation of the local flood characteristics which can differ per street, building or even per side of the building.

Flood characteristics

From the flood models, parameters can be obtained which characterize the flood. In various studies, the following input flood characteristics are considered as critical for the collapse of buildings:

- *Water depth, h [m]*
The inundation depth is one of the most influential parameters for the loss of life and damage to buildings. Markings are left by the water, so after a flood these can be estimated quite accurately and used to validate the flood models. In the Netherlands water depths till approximately 6 m can occur at the deepest polders.
- *Flow velocity, v [m/s]*
The speed of the moving water in a flood has a large influence on the possibility of evacuation and the hydrodynamic pressure on objects in the flood. The actual velocity in a flood is hard to estimate, but is done by reports from eye-witnesses, from video records or flood modelling. For most locations in the Netherlands, these velocities are below 2 m/s.
- *Depth-velocity product, hv [m²/s]*
This product is derived from the momentum flow in Equation 2.1, where hv is the only variable of the load since the density of the water and the horizontal area (footprint of the building) remain constant. The combination of these parameters determines if humans are still stable in the flood and the magnitude of the forces on buildings.

$$\text{momentum flow} = mv = \rho V \cdot v = \rho BL \cdot hv \quad (2.1)$$

Dutch hazard map

To determine the areas of interest in the Netherlands the current flood map from the Climate Impact Atlas is used. In this flood map, the effects due to flooding as a result of failure of primary and regional flood defences are combined with the unprotected areas outside the levees. The flooding scenarios are defined in the Flood Risk in the Netherlands (VKN2) project and used by the Delta Programme to derive the flood protection standards, determined by the most strict standard based on the following three criteria:

1. *Equity principle*: Individual risk or annual probability of dying cannot exceed 1/10,000.
2. *Societal risk*: Probability of events with large numbers of fatalities should be limited.
3. *Economic optimization*: Balancing the benefit of risk reduction to the cost of protection.

As the name of the atlas gives away, the effects of climate change are implemented in this model based on the VKN2 (Rijkswaterstaat, 2019). For the Netherlands, the KNMI has developed four climate scenario's based on global temperature increases and the changes in airflow patterns. The worst case scenario takes into account an increase of 2°C and a high change in airflow patterns, which result in the maximum water depths shown in Figure 2.3a.

The flood map has a spatial resolution of 100x100 meters and the water depths are defined in ranges. Since most of the damage will be caused by high water depths, the areas with a water depth of 2.0 meters and higher are defined as the areas of interest in this study as shown in Figure 2.3b. To take into account the used grid the areas of interest is expanded with half the grid-size, to include the buildings within a distance of 50 m as well.

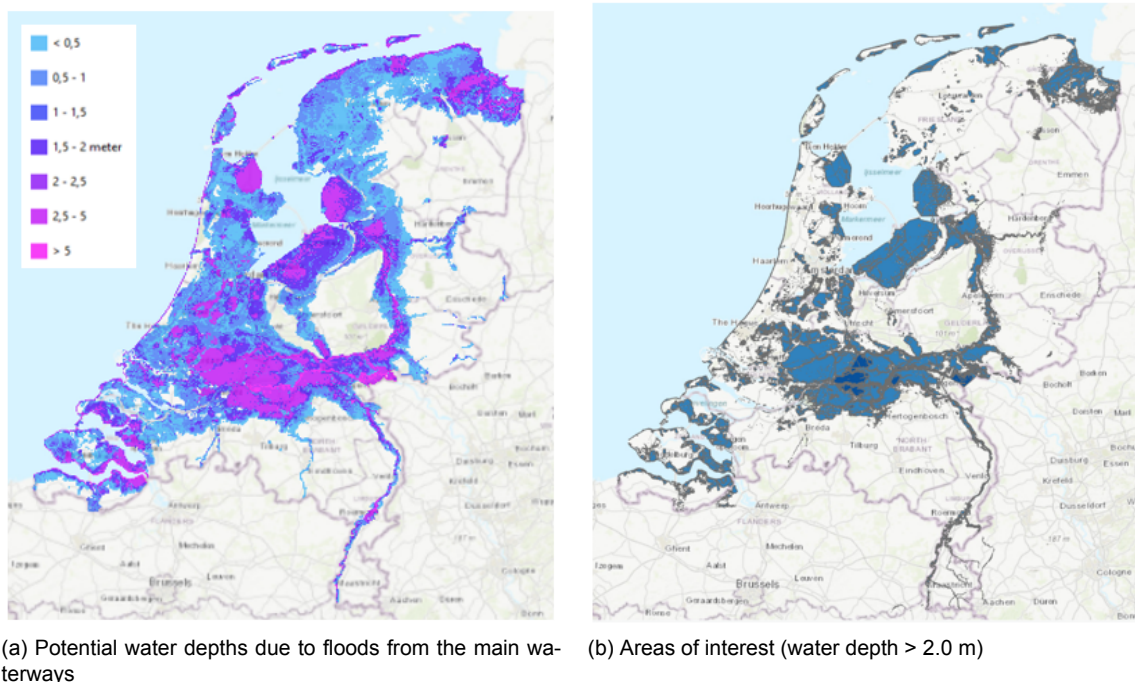


Figure 2.3: Maximum water depths due to the flooding scenario's based on the VKN2 (including the effects of climate change)

2.2. Flood actions on buildings

Much research is done on flood actions due to a dam-break, tsunami and levee breach with both experimental and analytical methods. The flood characteristics of this different kind of floods around buildings are comparable, since it is commonly assumed that the flood propagates as a bore or a wave in-land after breaking. First, a brief overview of all the flood actions is given, followed by a more elaborated quantification of the loads which are included in the structural analysis.

2.2.1. Overview of flood actions

An overview of the different flood actions on a building is given in this section based on those defined by Kelman (2002). The capital letters are used for the dimensions of the building and small letters for the flood characteristics as shown in Figure 2.4a, where the most important flood actions are pictured.

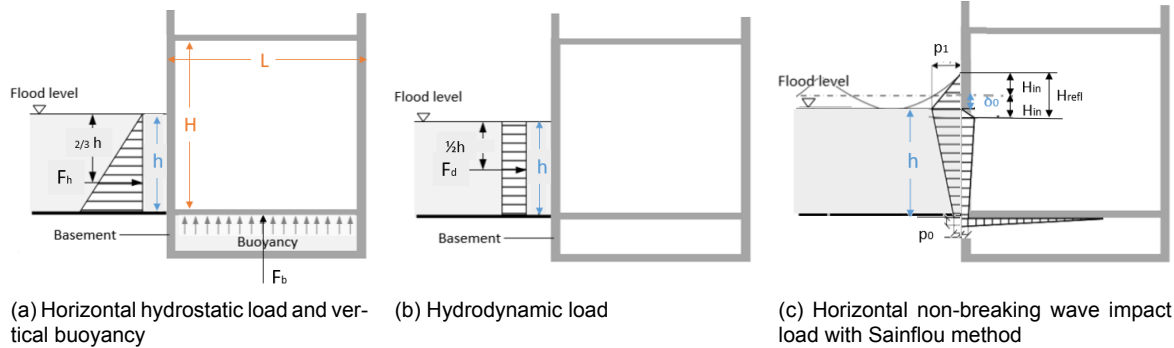


Figure 2.4: Hydrostatic and hydrodynamic flood actions (adapted from Chen, 2016)

Hydrostatic actions

Flood water causes a difference in water level inside, h_i , and outside, h_o the building until these levels are equalized after some time. This difference, Δh , causes a load per meter width with a horizontal and vertical component and on top of that capillary rise could occur:

- *Lateral pressure* is acting on the vertical elements like walls, windows and doors, see Figure 2.4a:

$$F_h = \int \rho g \Delta h \, dh = \frac{1}{2} \rho g (h_o^2 - h_i^2) \quad (2.2)$$

- The vertically upward pressure acting on the horizontal elements like floors is also known as *buoyancy*. This uplift can cause floating away of light buildings, like timber frame residence, when these are not anchored or cause bursting up of the floors, when water cannot penetrate these, see Figure 2.4a:

$$F_b = \rho g (h_o - h_i) B \quad (2.3)$$

- Water penetrating building material or the surrounding soil due to *capillary rise*, can cause damage above the actual water level. Depending on the type of material and duration of inundation, this can cause an extra load or a decrease in the strength of the building.

Hydrodynamic actions

Hydrodynamic actions are load induced by waves and velocity. Actions due to flow around an object can be divided into the quasi-steady load and impact load per meter width.

- *Quasi-static loads*, generated by drag/velocity-dominated floods, include for example non-breaking wave loads and inland actions from flash floods and tsunamis. This load can be determined with the standard form drag equation with drag coefficient, C_D , and flow velocity, v , see Figure 2.4b:

$$F_d = \frac{1}{2} C_D \rho v^2 h \quad (2.4)$$

- Inertia/acceleration-dominated floods occur close to a breach or at the wave front of a tsunami, which induce *impulsive loads* on top of the quasi-static load. This force can be seen as the transfer of kinetic energy when bore impinge on a building. It only acts on the leading edge member and can be determined by amplifying the quasi-static load by a factor $\alpha_{i,m}$, see Figure 2.4c:

$$F_s = \alpha_{i,m} F_d \quad (2.5)$$

- Wind can generate *waves* on top of the current water level, which are related to the water depth, wind velocity and fetch length. The wave height and wave period can be calculated with the Sverdrup-Munk-Brettschneider method and used as input for the Method of Sainflou (Equation 2.2.3) to approach the load of standing (i.e. non-breaking) regular waves in a simplified manner.

Geotechnical actions

Due to large flow velocities, the flood water can cause moving of the soil in two main manners:

- *Erosion* occurs when high water velocities wash away the soil around the building. These scour holes can cause instability or even turning over in case of shallow foundations. In case of a pile foundation, erosion can expose these piles and create direct contact with the moving water and sediment. This increases the abrasion of the piles and they become vulnerable to debris action as well.
- *Deposition* of soil occurs when sediment-loaded water slows down and the sediment settle down. The deposition can generate an extra lateral loading on the walls.

Debris action

If there is not only water that is moved by the flood, other materials can hit the building also known as *debris*. A difference can be made between static and dynamic debris:

- *Static debris* or damming of waterborne debris can be caused by an accumulation of debris mass, such as tree branches, becomes fixed to the building. The debris does not cause a dynamic force anymore, but it change the geometry, so drag resistance of the building.
- A single object dragged by the flow can be pushed to the building. According to the study of Roos (2003) these *dynamic debris* are the determining load case for failure of the walls. This load is based on various assumptions, but can in reality variate extremely from cars to small furniture.

Non-physical actions

On top of the physical effects of the flood, there also effects from the water-material contact depending on the quality, composition and temperature of the flood water and the exposure time to these effects:

- An example of a *chemical action* is the dissolving of the chalk between the bricks in the salty seawater after some inundation time in the 1953 flood (Slager, 1992). Due to corroding of steel elements, like the ties between the cavity walls, it is likely to assume a decrease in strength.
- Since the flood water can flow over soil, streets or even through factories before it comes in contact with buildings, *contamination* of the flood water is not unusual. This can be in the form of oil, fuel or even chemical waste.
- Forming of *mould* depends on the vulnerability of the material which is in contact with the water and the temperature of the water. It could cause a lot of damage to timber building materials, insulation material and the interior of the building.

Selection of flood actions

Although not all actions are taken into account in this study since the focus is on *collapse* and not *damage*, see Appendix B. Based on the effect of the flood actions on the collapse of residences in the Netherlands, a selection is made which actions to include in this study, see Table 2.1. In Appendix D the choices to include or exclude a flood action can be found.

Table 2.1: Selection of flood actions

Flood action	Load	Structural analysis	Experiments (physical model)	Elaboration
Hydrostatic	Lateral pressure Buoyancy & Capillary rise	x	x	Section D.1 -
Hydrodynamic	Quasi-static Impulsive Wind waves	x x	x	Section 2.2.2 Section D.2 Section 2.2.3
Geotechnical				-
Debris				-
Non-physical				-

2.2.2. Quasi-static load

Objects in the water need to withstand the quasi-static load (Equation 2.4) caused by the movement of the water. The drag coefficient, C_D , is used to calculate this load, which depends on the shape and roughness of the object and the flow condition of the medium. If an object is streamlined, the skin friction is overwhelmingly larger than the form drag. Buildings with their sharp edges are the opposite and can be accommodated under bluff objects, so skin friction can be neglected. For these objects the drag coefficient remains relatively constant for $Re > 100$, since the separation point generally occurs at the same place considered as the sharp corners of the leading edge (Massey, 1970).

Buildings are designed to withstand the load from wind on the structure, which is also defined in Eurocode NEN-EN 1991-1-4 as a quasi-static load per meter width, see Equation 2.6. The peak velocity pressure, q_p , needs to be calculated from the hourly extreme wind velocity, u , at a certain reference height, z_e . When the height is larger than the width of the building, the shape of the profile of the velocity pressure is assumed to be uniform with as reference height the height of the building, see Figure E.3. As the structural factor, $c_s c_d$, can be taken as 1 for buildings less than 15 m, both the formula and the profile of the wind load are comparable to those of the hydrodynamic force. The difference can be found in the coefficients, c_f and C_D , and the area where the pressure is acting on, which is the water depth, h , for the hydrodynamic load and the total height of the building, H , for the aerodynamic load.

$$\left. \begin{aligned} F_w &= c_s c_d c_f q_p(z_e) h_{ref} \\ q_p(z_e) &= \frac{1}{2} \rho_{wind} u^2 \end{aligned} \right\} F_w = c_f \left(\frac{1}{2} \rho_{wind} u^2 \right) H \quad \text{vs.} \quad F_d = C_D \frac{1}{2} \rho v^2 h \quad (2.6)$$

NEN-EN 1991-1-4 NB gives the highest wind speeds for buildings located in the coast of the Netherlands in area I. In this area, the characteristic 10 minutes mean velocity at 10 m above ground level with a return period of 50 years, u_b , is 29.5 m/s. The hourly extreme velocity, u , can be found by combining this average wind speed and the maximum gust in an hour. The wind pressure due to this peak velocity is determined by multiplying the basic pressure, q_b , with an exposure factor, c_e , which is a function of height above ground level and the roughness of the terrain. For a height of 5 meters (\approx height of two storeys) in a coastal area, a peak pressure of 1.36 kPa is found. A pressure with the same magnitude is caused due to a flow velocity of 1.65 m/s or a hydrostatic load due to a water depth of 0.28 m:

$$\begin{aligned} q_p &= c_e q_b = c_e \cdot \left(\frac{1}{2} \rho_{wind} u_b^2 \right) = 2.5 \cdot \frac{1}{2} \cdot 1.25 \cdot 29.5^2 = 1.36 \text{ kPa} \\ q_w = q_d &: \quad q_p = \frac{1}{2} \rho v^2 \quad \rightarrow v = 1.65 \text{ m/s} \\ F_w = F_h &: \quad q_p h = \frac{1}{2} \rho g h^2 \quad \rightarrow h = 0.28 \text{ m} \end{aligned}$$

In the calculation above the coefficients in Equation 2.6 are not taken into account yet. The force coefficient, c_f , for the quasi-static load is defined as the drag coefficient, C_D , where the forces are considered as one load on a stiff structure. In the Eurocode, this force coefficient is defined as the pressure coefficient, C_p . The force due to the wind velocity is divided into separate loads acting on different sides of the building, see Figure 2.5 and Appendix E.

The drag coefficient, C_D , is equal to the integrated value of pressure coefficient of the faces perpendicular to the flow direction, $C_{p,front}$ and $C_{p,rear}$, and the friction coefficient, $C_{friction}$, along the faces parallel to the flow direction (sides and top face). The effect of friction along the faces is relatively small compared to the perpendicular pressures, so this is not taken into consideration in this study, leading to the definition in Equation 2.7.

$$C_D = \frac{F_{horizontal}}{\frac{1}{2}\rho v^2 h} \quad \text{vs.} \quad C_p = \frac{p}{\frac{1}{2}\rho v^2} \quad \rightarrow \quad C_D = \int_{y=0}^{y=B} C_{p,front} + C_{p,rear} \, dy \quad (2.7)$$

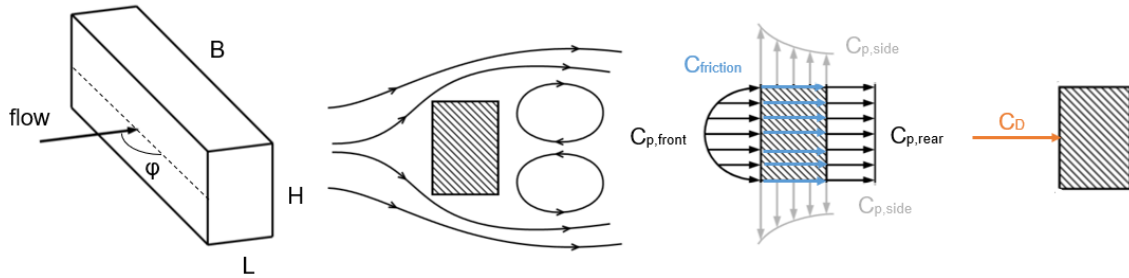


Figure 2.5: Pressure on a building in uniform flow (adapted from slides CT5145 Random Vibrations)

To determine the values of the drag coefficients, many tests and experiments are done in wind tunnels and flumes varying the side ratio, defined as the ratio between the side aligned with the flow, L , and the side normal to the flow, B , and the flow incidence or angle of attack, ϕ . In Figure 2.6 graphs from the research of Norberg (1993) are displayed where these influences are quantified. The maximum drag coefficient for a rectangular cylinder occurs when the length compared to the width is approximately 2:3. FEMA P-55 gives drag coefficients based on the ratio width-to-water depth, B/h , which increases from 1.25 to 2.0 as the ratio increases from 1 to 120 and larger, see Appendix E. Árnason (2005) varied this ratio as well, but did not find an clear dependency.

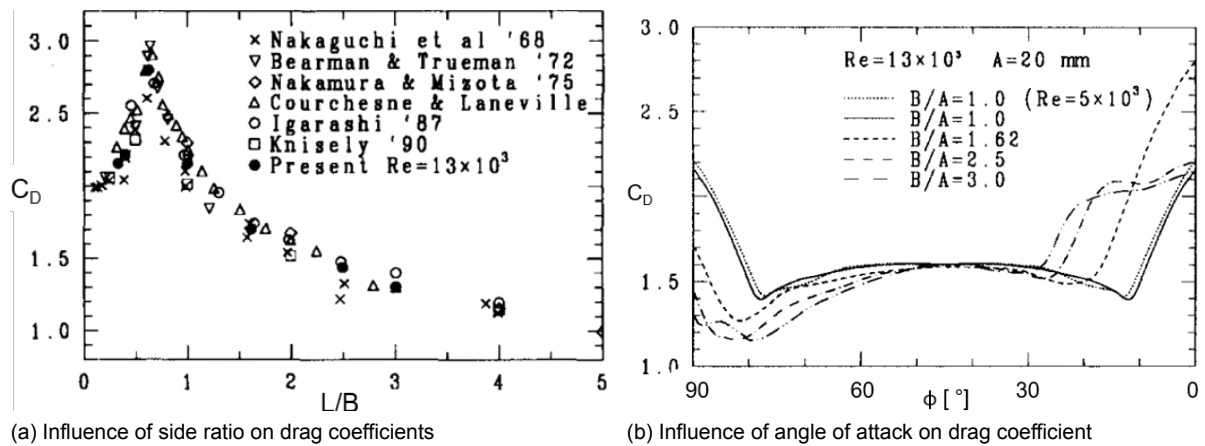


Figure 2.6: Influence of the side ratio and angle of attack on steady flow drag coefficients (Norberg, 1993)

For buildings with a rectangular footprint, the pressure coefficients for external positive and negative pressures due to wind are given depending on the aspect ratio, H/L , given in Figure E.2. These external pressures are averaged over the sides from wind tunnel tests and computational fluid dynamics (CFD) simulations. In Figure 2.7 the results of the experiments and the simulation of Nore et al. (2010) are shown. The pressure coefficients along the sides of a cubic structure for two different angles of attack are compared to the values for $H/L = 1$ from the Eurocode in Figure 2.7a. It can be seen that the Eurocode is using just conservative values.

From Figure 2.7b can be concluded that the pressure on the walls, except for the leeward wall, decreases as the angle of attack increases from 0° to 45° , which is in accordance to the influence on the angle of attack to the drag coefficient in Figure 2.6b and the experiments of Cuomo et al. (2008) on cubic structures. Figure 2.6b shows a minimum drag coefficient at an angle of attack between 5° and 15° depending on the side-ratio, which is in case of a square a decreases from ± 2.1 to ± 1.4 .

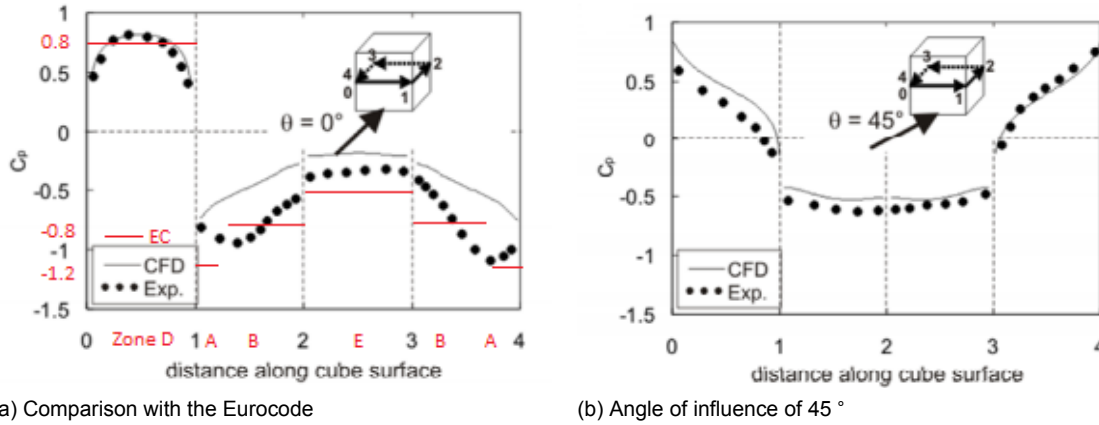


Figure 2.7: Mean pressure coefficient, C_p , along horizontal trajectory 0-1-2-3-4 for (a) $\theta = 0^\circ$ and (b) $\theta = 45^\circ$ (Nore et al., 2010)

According to the Eurocode causes an increase of the aspect ratio, H/L , an increase in the pressure coefficients on the walls. The same can be seen by comparing the results from Figure 2.7 with the same figures for high rise buildings from Oka and Ishihara (2009). The height where the pressure is acting on, which is the water depth in case of flooding, is taken into account in FEMA P55 by the width-to-water depth ratio, B/h .

The ratio of the width of the building to the width of the flume is known as the blockage ratio, B/b , and can be used to take into account the presence of adjacent buildings. Empirically determined drag coefficients are strongly influenced by the blockage, which causes an increase of the average flow outside the wake. In some cases, there is also a water level difference between the upstream and downstream side of the building, which causes a contribution of hydrostatic pressure to the streamwise load. Recent research on the impact of this effect on the hydrodynamic force is summarized in section D.3.

2.2.3. Wind waves

Due to the wind velocity, waves can be developed which cause an additional water height on top of the still water level. The significant wave height, H_s , and period, T_s , are calculated with the Sverdrup-Munk-Brettschneider method (SPM, 1984) in Equation 2.8. For the velocity, U , the basic wind velocity of 29.5 m/s is taken (wind area I in NEN-EN 1991-1-4 NB). It is unlikely that this peak velocity has an influence on the development of the wind waves over the entire fetch, because the gust has a short duration compared to the wave period, so these gusts are not taken into account. For the fetch, F , three values are used to show the influence of the water depth on the significant wave height. According to Roos (2003), a fetch length of 0.1 km is comparable to a building density of more than 15 buildings per hectare. For the buildings at the edge of the city, a larger fetch of 10 km is used.

$$\begin{aligned}
 H_s &= \frac{U^2}{g} 0.283 \tanh \left[0.578 \left(\frac{gh}{U^2} \right)^{0.75} \right] \tanh \left[\frac{0.0125 \left(\frac{gF}{U^2} \right)^{0.42}}{\tanh \left[0.578 \left(\frac{gh}{U^2} \right)^{0.75} \right]} \right] \\
 T_s &= \frac{2\pi U}{g} 1.20 \tanh \left[0.833 \left(\frac{gh}{U^2} \right)^{0.375} \right] \tanh \left[\frac{0.077 \left(\frac{gF}{U^2} \right)^{0.25}}{\tanh \left[0.833 \left(\frac{gh}{U^2} \right)^{0.375} \right]} \right]
 \end{aligned} \tag{2.8}$$

The additional pressure due to wind waves is calculated with the Sainflou method in Figure 2.8. This is an approximation for the loads of non-breaking waves on a vertical wall, based on Stokes' second order wave theory and complete reflection of the incoming waves in this case caused by the wind: $H_{refl} = 2H_{in} = 2H_s$. Using the linear wave theory, the wave number, k , and length, L , in shallow water can be calculated from the significant wave period:

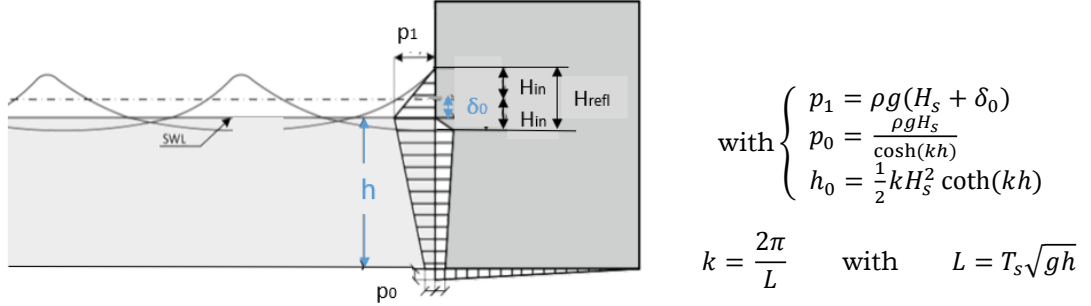


Figure 2.8: Sainflou: pressure of non-breaking waves on a vertical wall (adapted from en Waterstaat et al. (2007))

To determine if the pressure due to the wind-induced waves is an important load, this pressure is defined as a line load along the width of the structure. This load is divided by the line load per meter width due to the hydrostatic pressure, leading to the following ratio:

$$\frac{F_{wave}}{F_h} = \frac{p_0 h + \frac{1}{2}(p_1 - p_0)h + \frac{1}{2}p_1(\delta_0 + H_s)}{\frac{1}{2}\rho g h^2} \quad (2.9)$$

As can be seen in Figure 2.9a the significant wave height increases to 1 meter as the fetch length or water height increases (with a fetch of 10 kilometres and a water height equal to the floor level). Especially for the lower water heights and high fetches, the influence of the wave load is large and can be up to 80% higher than the hydrostatic load from the water height itself. As the water height increases, the load due to the wind-induced wave becomes smaller compared to the hydrostatic load. Although in all cases, the load due to the wind waves should not be neglected.

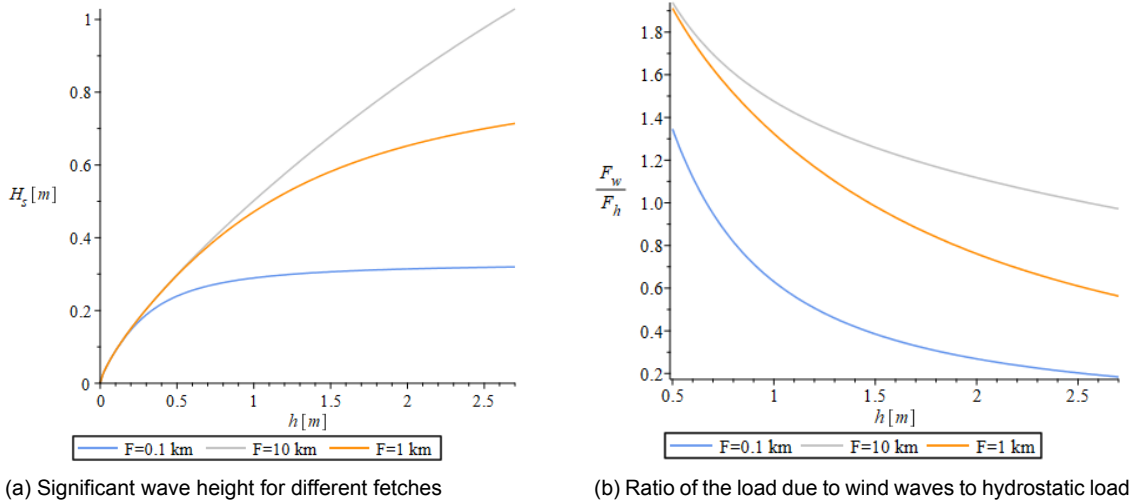


Figure 2.9: Wind induced waves for different fetches with a wind velocity of 29.5 m/s

2.3. Summary and conclusions of literature review on loads

The correlation between the flood characteristics and the damage observation is not clear according to multiple studies as stated in the research on residential damage due to flooding of New Orleans after hurricane Katrina by Pistrika and Jonkman (2010). In these described studies, damage data sets of historic flood events are compared to the existing damage curves such as the Clausen criterion, where the following conclusion can be drawn: *The uncertainty of damage estimates decreases with an increasing number of flooded buildings.*

The current curves which indicate collapse of buildings, are based on empirical damage data from different events and calculation or simulation of the flood characteristics at a low spatial resolution. This choice of spatial aggregation level can cause a large difference in the flood characteristics per flood model, due to averaging the variations of flood depth and velocity over the used grid cell. So when looking at structural damage with a high spatial resolution, so blocks groups and blocks, the local flood characteristics are not adequate enough to assess these buildings as individual structures.

Nowadays the modelling of local flood characteristics is still evolving, so more accurate local flood parameters will be presumably available in the future. Approaches where the strength of the building is compared to loads due to local flood characteristics could be useful to adapt the current damage and mortality functions. The resistance of the buildings is now implicitly accounted for, but this is changing over time (Asselman, 2005) and could be different in other regions than Zeeland. That is why the determination of a correction factor for the quality of current buildings is considered as one of the most important factors (De Bruijn and van Kester, 2015) to improve the flood mortality functions in the Netherlands.

2.3.1. Gaps in the current literature

It has become clear that the flood actions on buildings are needed to predict whether the current buildings can resist the flood conditions in an event. Much research is done to determine these actions, but up to now buildings in a flooded area are assessed as fixed bodies in a flow similar to bridge piers in a river. However, the shape of a building differs significantly and a building does not necessarily behave like a stiff structure. This study takes both differences into account to make the determination of the quasi-static hydrodynamic load better applicable for buildings. The flood characteristics, h and v , referred to in the report are those generated from hydraulic models or experiments without the building being present.

- Multiple experiments are conducted to find the influence of the building geometry on the flow around the building and the induced forces. In most studies, the orientation of the flow is not taken into account or this is only done for cubic objects. Since most buildings in the Netherlands do not have a rectangular footprint, the influence of the combination of *the orientation of the flow and the geometry* on the loads is one of the objectives in this study.
- Secondly, considering the building as a stiff structure or solid body implies that all the loads act in one point or on a surface. The point of action is considered to be the frontal area of the wall drawn in Figures 2.4 and 2.5. In reality, the loads due to the flow act on different elements of the building instead. The wind causes loads on the building in the same way as the water does, which are described as pressures acting on different sides of the building. If it is possible to *link these wind-induced load to the hydrodynamic load*, a similar or even the same design code can be used to design buildings resistant to hydrodynamic loads.

3

Typical Dutch residences

From the current flood model used in the Netherlands, the areas which are most likely to be flooded are described as the areas of interest, see Figure 2.3. The residences which are located in this area are of interest in this research and the different types are elaborated in this chapter. To define "the typical Dutch residence" which is most likely to be affected by flooding, building stock data from the BAG-registration (in Dutch: Basisregistratie Adressen en Gebouwen) is combined with flood characteristics. The type of building where most of the population is living in, is chosen to be the "typical Dutch residence".

3.1. Building stock

With the 61% of the Dutch population, the percentage of people living in a semi-detached, corner or terraced house (in Dutch: twee-onder-een-kap, hoekwoning of rijtjeshuis/ tussenwoning) is the highest in Europe, with the United Kingdom on a second place with 60%. When similarity is found in terms of structural and stability building elements, the failure mechanisms of a corner house can be compared to a semi-detached house. As stated by Asselman (2005) the distribution of building types does not necessarily need to be the same among the country. To determine if the most common type of building is also likely to be affected by flooding, the location of the buildings is also of interest since the distribution of building types differ per area. This can be found by importing the geodatabase of the BAG-registration in a Geographic Information System (GIS).

Building type

In the BAG-database different types of information are collected, such as the footprint, floor area, height and the number of residences in a building. A building in this research is comparable with a "pand" in the BAG, which is defined as the smallest functional and structural individual unit direct connected and able to enter from the ground floor. A residence can be defined as the smallest individual unit with the function of living.

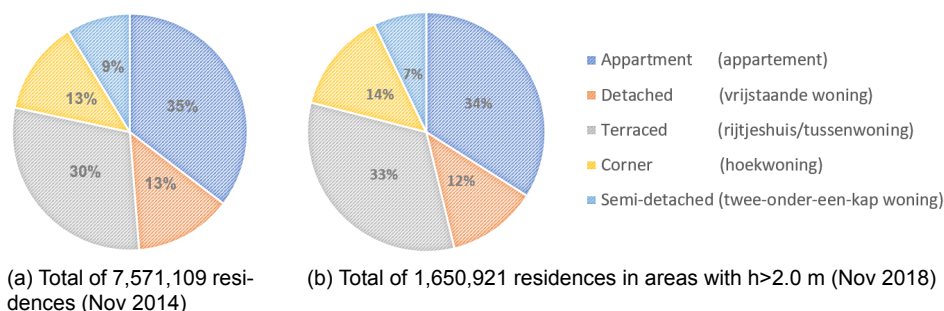


Figure 3.1: Building stock from BAG (Dutch building stock)

Unfortunately, the building typology is not available in the latest BAG-data of November 2018, so the approach in Appendix F.1 is used to find this information. Since there is a total of 7,571,109 residences, it takes a lot of time to sort the residences based on their types. In the BAG-data from November 2014, this distribution is available and shown in Figure 3.1a. Assuming an even amount of people per residence, 35% of the population lives in a terraced house and 15% in a corner house. In the areas of interest, sorting according to Appendix F.1 gives the distribution in Figure 3.1b, which is almost similar to the national distribution. A row of houses is taken as a typical Dutch residence to focus on in this study, because the majority of the Dutch live in this kind of houses.

Year of construction

The building parameters depend on the time of construction of the residence. There are five general periods when the majority of the single-family residences are built with their specific points of attention described in Appendix F.2. The amount of terraced and corner residences in the area of interest are displayed as columns per period in Figure 3.2.

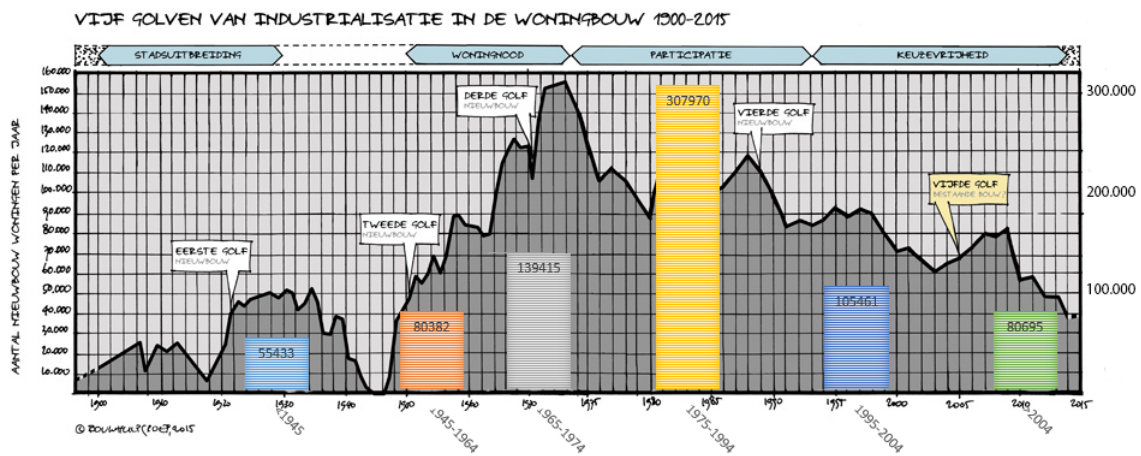


Figure 3.2: Building development of the years (Kenniskbank Bestaande Woning Bouw)

The considered building is a terraced house built in the period of the housing shortage between 1965 and 1975 and the energy crisis between 1975 and 1994, see Figures 3.3 and 3.4. Due to the use of precast concrete panels as floor (in Dutch: breedplaatvloer) in 1970, floors could span one residence with a width of 5.4 meter, which leads to a new plan without an additional load-bearing wall inside the residence. Furthermore, a storey-height of 2.7 m is used and since blocks of 4 to 8 residences are common, the width of these blocks are 21.6 to 43.2 meters. A suitable depth of the structure of 8.64 meters is chosen to work with two different buildings with a width, B , to depth, D , ratio of 2.5 and 5. Testing the effect of this ratio could also be used for other buildings with a similar footprint like apartments.



(a) Block of residences



(b) Facade

Figure 3.3: Typical Dutch terraced houses (Agentschap,2011)

3.2. Description of case-study residences

A few generalities are found in the construction of the terraced house: The residences consist of two floors with an inclined roof construction and the load-bearing walls are the party walls which separate the residences from each other. Over the years there has been a lot of variation between the used materials and building method, so the choice is made to create the following 3 case-study residences pictured in Appendix F.3 with typical floorplans in Figure 3.4. The different elements of the case-study residences are described in this section.

1. Traditionally built < 1970: masonry (clay) cavity walls and timber floors
2. Traditionally built > 1970: masonry (calcium silicate) cavity walls and system floors
3. In-situ concrete walls and floors

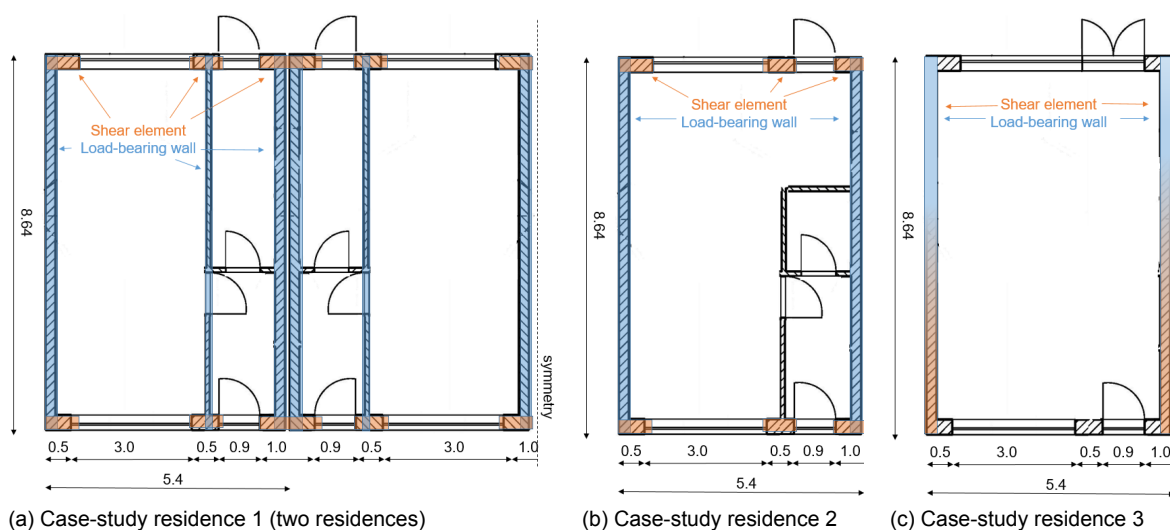


Figure 3.4: Common floorplans of typical Dutch terraced houses with their key-elements

3.2.1. Load-bearing walls

The structural walls of residence 3 consist of concrete, which can be reinforced (RC) or unreinforced (URC) shown in Figure F.5. In residence 1 and 2 the walls are made of unreinforced masonry (URM), which is defined in Eurocode 6 as "an assemblage of masonry units laid in a specified pattern and joined together with mortar". The masonry unit can be made of different materials such as clay, calcium silicate or concrete. From the second half of the 19th century, the load-bearing elements are usually the inner leaves of a cavity wall. The outer leaf is self-supporting and connected to the inner leaf with steel ties, which increase the resistance of the wall. The space in between can be hollow or filled with insulation, see Figure 3.5. The party walls often consist of untied leaves or massive walls to prevent noise pollution from the neighbours.

- *Ties*

The ties prevent out-of-plane bending due to horizontal loads such as the wind or in-plane eccentric pressure and contribute to preventing of buckling of the inner leaf due to centric pressure. The ones used between 1945 and 1980 are made of galvanized steel, so vulnerable for corrosion if moisture is settled between these walls, which is especially the case for hollow cavities. These kinds of ties are not allowed to use anymore according to the Bouwbesluit, because of the lifespan which is assumed to be lower than the required 50 years.

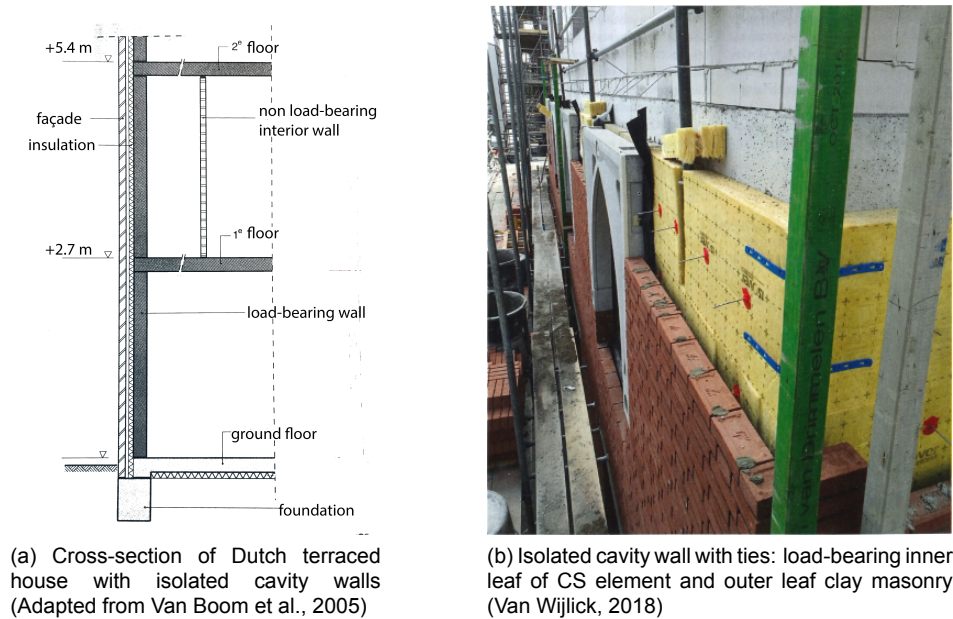


Figure 3.5: Cavity wall

- *Masonry*

To model this composite material, three common approaches are described in Appendix G. Jafari et al. (2017) determined the material properties of masonry by performing destructive laboratory tests on samples of existing buildings in the Northern part of the Netherlands. These samples composed of masonry units in a running bond and general purpose mortar with a joint thickness of 10 mm. It can be assumed that these characteristic values are comparable for masonry in the rest of the country. Esposito et al. (2016) used replicated masonry to perform standardized tests to characterize the material. The properties defined in both studies are summarized in G.2.

The samples for the existing buildings show higher strength, but also have a higher coefficient of variation due to the difference in the quality of the sample. The choice is made to use the values of the replicated masonry for the perforated clay and calcium silicate bricks. Since no replicated solid clay bricks are tested, the values of the sample are used leading to the strengths in Table 3.1.

- *Concrete*

Constructing a residence with concrete walls, there are multiple options to provide for stability as shown in Figure F.5. The unreinforced end walls with a small thickness have the worst moment resistance, so are taken into consideration in this study in combination with the lowest quality URC used for residences C20/25 (Van Boom et al., 2005).

Table 3.1: Characteristic material properties for masonry and wall ties (see Appendix G.2 for derivation)

Case	Test specimen	f_k [MPa]	f_{xk1} [MPa]	f_{xk2} [MPa]	f_{vk0} [MPa]	μ [-]	$q_{Rd,tie}$ [MPa]
1+2+3	Perforated clay	12.72	0.27	0.75	0.12	0.87	
1	Solid clay > 1945	6.64	0.29	0.81	0.36	0.89	-2.61 to +3.84
2	Calcium-Silicate	5.05	0.14	0.51	0.11	0.43	-1.48 to +3.40
3	Concrete	20	1.55	1.55	0.44	1	

3.2.2. Façades

The longitudinal façades on both sides of the residences create the connection between inside and outside by the windows and doors which are placed in this wall. For the traditionally built residences, part of this wall also has a stabilizing function. The location of the openings for the windows and doors are similar for these residences since masonry piers are needed in between the openings to provide stability. For the in-situ concrete residences, the façades have no structural function, so can be designed without any restrictions. In all cases, this is a self-supporting cavity wall with an outer leaf of masonry and an inner leaf of masonry, wood-based material or concrete.

In residences built in the period between 1945 and 1970, the windows of the lower and upper floor were often coupled, leading to a continuous façade over two storeys. For the windows, single glazing from float glass is used in pinewood frames. These residences are recognized as cheap and industrial, so from the seventies complete masonry façades were built again. From then on double-glazing is introduced in a frame of tropical hardwoods, PVC, steel or aluminium. The thickness of the glass panes is determined by the requirement that the glass should resist the lateral wind load according to (NEN 2608 and NPR 3599).

The dimensions of the windows vary from 1 to 3 meters in width and 0.5 to 2 meters in height (Chen, 2016). Typically in terraced houses, there are windows on both sides of the lower floor, which have dimensions of approximately 3 by 2 meters. The height above the ground level is 0.7 m in that case, which corresponds to the value found by Roos (2003). This part of the facade can consist of one large window with glass pane of 2.8 by 1.8 meters (assuming a frame of 100 mm width) or a combination of multiple windows as shown in Figure 3.6.

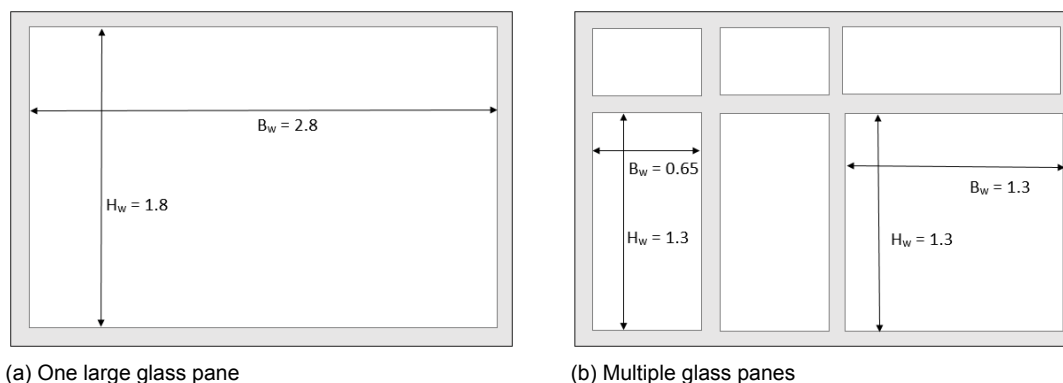


Figure 3.6: Dimensions of windows

The strength of the glass corresponds to a failure probability of 1%, 50% and 99%, which give a maximum bending resistance of respectively 20 MPa, 60 MPa and 80 MPa (Kelman, 2002). If both panels have an equal geometry, the double glazed-unit is assumed to be twice as strong a single-glazed unit. Usually, there is a millimetre difference between the two panes to prevent interference, leading to a well-accepted thickness of the outer leaf of 5 mm, a cavity of 15 mm and an inner leaf of 4 mm (NEN 2608).

3.2.3. Floors and roof

The floors function as horizontal supports for the walls, so transfer the loads from these walls through the stabilizing walls to the foundation. On top of that, the dead weight of the floors, the roof and the live loads on top of these elements should be carried by the load-bearing walls. The in-plane strength and stiffness of these floors are of interest to define the applicable support conditions. Over the years the following three types of floors are commonly used, which resemble the case-study residence with the similar number:

1. *Timber floors* mainly span two fields, since the width of the residences is too large to span in once resulting in a load-bearing wall in the middle of the residence for example in the "Doorzonwoning" in Figure 3.3b. Timber beams span in the direction of the load-bearing walls with cross boards nailed on top with a total weight of 0.3 kN/m^2 . The beams can be connected to the load-bearing walls by simple interlocking, which connection can be improved by anchoring in the walls by means of steel ties.
2. "*System floors*" are concrete floors consisting of prefabricated reinforced slabs, in some cases filled up with in-situ concrete. In the Netherlands, the most commonly used are the wide-slab floor (in Dutch: breedplaatvloer) and hollow-core beam floor (in Dutch: kanaalplaatvloer) with a weight of 550 to 600 kg/m^2 . These slabs are placed on top of the load-bearing walls and fixed with mortar.
3. When the *concrete floor* is fixed to the load-bearing walls by pouring concrete at the edges and continuous or overlapping reinforcement through the elements, stability can be found without adding piers. This floor-type is usually combined with in-situ concrete walls as well. The thickness depends on the span of the floor, which is 5.4 meters in these cases, leading to a minimum thickness of 180 mm in case of massive party walls and 200 to 210 mm in case of untied cavity walls (VOBN).

The roof of terraced houses usually consists of a timber saddle roof with the ridge parallel to the longitudinal façade. Timber purlins carry the weight of the battening and roof tiles to the party walls, which gives a dead load of 0.75 kN/m^2 . Another type of roof is the rafter roof, which transfers the forces to the floor. Both load paths give the same line load on the party walls, since the floors span in between these party walls. The inclination of the roof is assumed to be 45 degrees, which lead to the following line load on the party walls:

$$q_{roof} = \frac{G_{roof}B/2}{\cos \alpha} = \frac{0.75 \cdot 5.4/2}{\cos 45} = 2.86 \text{ kN/m} \quad (3.1)$$

3.3. Failure mechanisms

A building is likely to collapse if one of the key structural elements fails, such as the foundation, load bearing walls or elements which provide stability. These are designed to withstand the loads according to the building regulations at the time of construction. When higher loads due to flooding are acting on the building, one of these key elements can fail and the loads are redistributed over the other elements as shown in Figure 3.7. If these forces remain high, total collapse of the building due to one of the following failure mechanisms could occur. In this research partial collapse of a key structural element will be assigned to total collapse of the building. Other damage to the building as described in Appendix B is not considered.



(a) Scour failure due to hurricane Katrina in 2004 (Robertson et al., 2007)



(b) Failure of external walls in Zwijndrecht during the 1953 flood (Historische Vereniging Zwijndrecht)

Figure 3.7: Failure mechanisms of residences due to flooding

Scour of foundations

Scour occurs if the velocity of the flood water washes away the top layer of soil resulting in a lack of lateral support or undermining of the foundation and exposing the foundation. In the case of a piled foundation, the stability is unlikely to become a problem. For buildings on shallow foundations, instability can occur resulting in damage to part of the foundation and resting wall on top or even toppling over of the building, see Figure 3.7a.

Roos (2003) concluded that this failure mechanism causes only a small fraction of the damage due to Dutch levee breaches, since less than 5% of the buildings would partially collapse in only 31% of the affected postal code areas. This can be explained by looking at the critical velocity for eroding of the top layer of the soil, which is 0.6 m/s for unprotected clay or gravel, and up to 5.0 m/s for grass or paving. On top of that, most newer Dutch residences have pile-foundations, which are far less vulnerable for scouring than shallow foundations.

Failure of load-bearing walls

For the failure of the load bearing (and non-load bearing) walls two basic failure modes can be considered: in-plane shear failure and out-of-plane bending failing. Building materials for these walls, like concrete and masonry, are weak in tension resulting in cracks at the side in tension. The forces redistribute in the uncracked area leading to more cracks when the force remains constant until the structure shift along these cracks and fails as in Figure 3.7b. In masonry walls, these cracks are usually located at the interface of the bricks and mortar, for concrete the location is more difficult to predict due to the more homogeneous behaviour of the material. Important factors in the magnitude of the resistance of the wall are the support reactions of the edges, orthogonal strength ratio and dimensions (Chen, 2016).

Kelman (2002) studied the failure of different elements of a building. For cavity walls is stated that load transfer between the outer and inner leaf through the ties is negligible. The behaviour of the cavity wall is conservatively assumed to be comparable with a single-leaf wall, so the leaves fail independently of each other. Since the failure pressures are close, a binary system in which the panel either fail or not is more likely.

Instability

When an element that is part of the stability construction fails, horizontal loads from the flood cannot be distributed well to the vertical members and these load-bearing parts could collapse. To resist the lateral force on the side of the corner residence, the different residences in a row work together by transferring this load through the anchors between the higher level floors. The diaphragm action of the floors distributes this load into the load-bearing walls to the foundation. In a residence itself, the stability can be achieved in different ways:

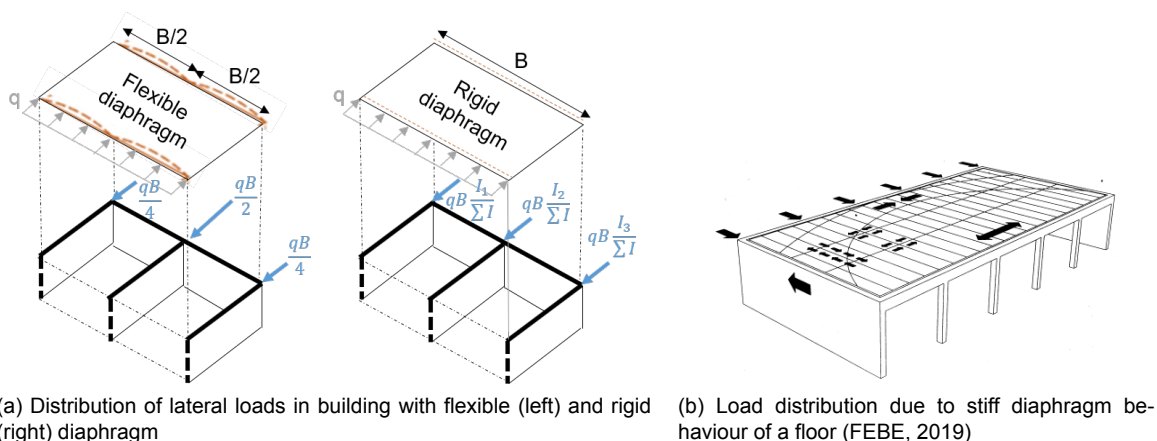


Figure 3.8: Distribution of lateral loads in building with flexible (left) and rigid (right) diaphragm }

- *Wall-diaphragm connection and piers*

In traditionally built residences this method is generally achieved by the connection of the load-bearing walls with their perpendicular inner walls or wall parts in the façades. In the façades, the masonry walls in between the openings for windows and doors are assumed to behave as a series of relatively slender piers. The walls are connected to the floor and roof to avoid out-of-plane buckling of the load-bearing walls. These diaphragms could be flexible or rigid, which behave differently in the way lateral loads are distributed into the vertical members to the foundation, as shown in 3.8. For a flexible diaphragm, for example anchorage of the timber floor beams in the façades, the force distribution can be compared to a horizontal beam spanned over two walls. For a rigid diaphragm, this distribution depends on the relative rigidity of the wall to the diaphragm.

- *Box like behaviour due to fixed connections*

In other building methods like "Gietbouw", the connections of rigid concrete walls and floors are fixed due to casting of the ends of the prefab-walls and box-like behaviour is created. In residences walls in two directions needs to be fixed, where this can be just in one direction when a stability core is created, for example around an elevator shaft.

Failure of non-structural elements

Local failure of non-structural elements like windows, door and façades, creates openings in the building envelope. Flood water can enter the building and the interior gets exposed to the floodwater, which cause a change of the load distribution on different elements. Research to failure of these elements are done in several studies, for example Kelman (2002) and Chen (2016). Since the failure of this kind of elements does not immediately lead to the collapse of a building, only the impact of the openings on the building will be elaborated further.

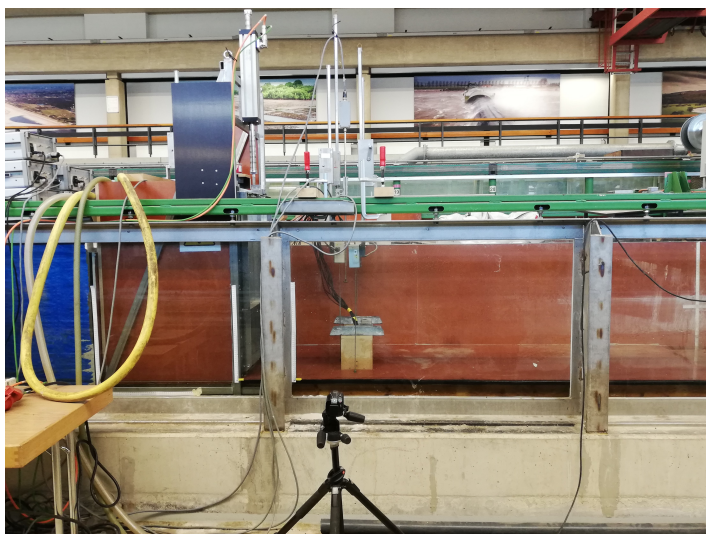
4

Experimental quantification of design flood loads

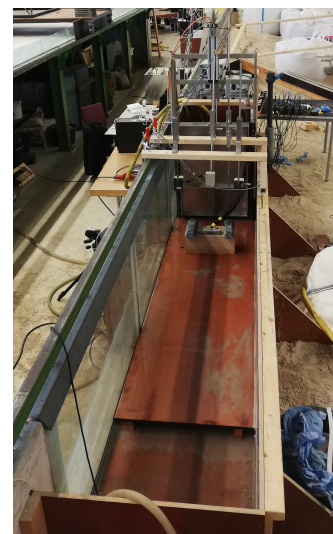
The loads due to flooding should be quantified to determine which flood conditions lead to failure of a terraced house. For hydrostatic and wind-induced waves, the loads are already defined in section 2.2.3 based on literature. The quasi-steady load is defined in a different way than in previous studies by determining the pressure on different elements of the residence. This makes it possible to compare this quasi-steady flood load to the wind load defined in Eurocode. This chapter starts with the description of the set-up and procedure of these experiments, followed by the obtained results. From these results, conclusions are drawn as regards the application of the pressure coefficients. Finally, the design loads on the residences are defined by combining different flood actions.

4.1. Experimental set-up

The experiments are conducted with a hydraulic model (scale 1:50) at the Fluid Mechanics Laboratory of the Department of Hydraulic Engineering at the University of Technology Delft. The Wave Overtopping Simulator designed by Rietmeijer (2017) is used to generate a typical dam-break wave. The different elements of the set-up are pictured in Figure 4.1 and described below.



(a) Side view



(b) Top perspective view

Figure 4.1: Experimental set-up at the TU Delft

The water from the reservoir can enter the prismatic flume through a removable gate from the reservoir and run into the "building". The pressures due to these flood waves, with accompanying water height and flow velocity are measured.

Flume

The flume has a width of 0.81 m and a length of 3.5 m. A false bottom is created at a height of 12 mm and has a length of 2.5 m. The reservoir upstream of the flume has a width of 0.67 m. It is filled to an initial still water level, referred to as the impoundment depth, h_0 . Since minimum leakage through the frame of the gate is hard to avoid and the instruments need to be underwater to be able to measure, an initial water depth in the flume, h_f , is present before opening the gate.

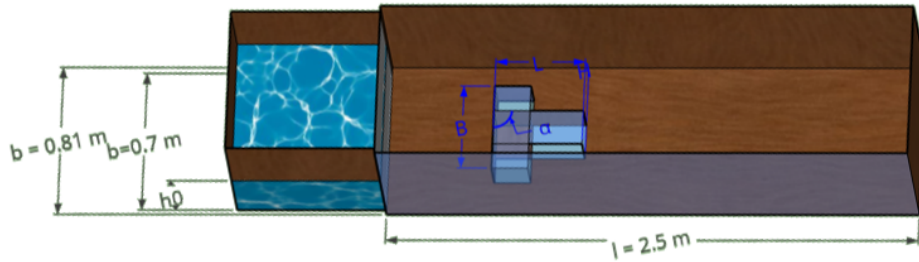


Figure 4.2: Schematic figure of the flume with two different angles of the building

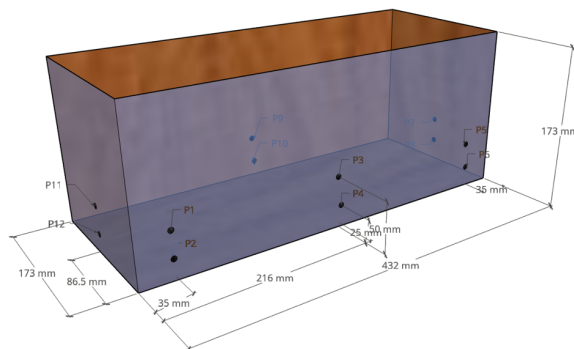
Gate

The gate is lifted to enable water to flow into the flume. To make sure the opening time does not influence the free-falling movement of the particles near the free surface and the formation and propagation of the dynamic wave, the opening period of the gate is set to be short enough according to the criteria in Equation 4.1, see Appendix H.1.

$$t_{op} \leq \begin{cases} \sqrt{\frac{2h_0}{g}} & \text{Lauber and Hager (1998)} \\ 1.25 \sqrt{\frac{h_0}{g}} & \text{Vischer and Hager (1998)} \end{cases} \quad (4.1)$$

Building

Experiments are conducted on the residences described in 3.1 with a width, B , to length, L , ratio of 2.5 and 5. The building is represented as a rectangular structure made out of wood. 6 pressure sensors with a range of 0.5 psi (pounds per square inch) are located at 2 different elevations ($h_{sensor} = 25 \text{ mm}$ and 50 mm) at every side of the structure as shown in Figure 4.3. These are used to determine the pressure coefficients and compare them with the Eurocode for wind loads.



(a) Schematic representation of the "building"



(b) Topview physical model of the "building"

Figure 4.3: Building 4R resembles 4 residences ($B = 432 \text{ mm}$ and $L = 173 \text{ mm}$)

4.1.1. Instrumentation

Different measurement instruments are needed to capture the time-history of the water surface elevation, velocity and pressures. The data is continuously recorded on one computer to make sure the data from different instruments can be compared by using the time as reference. The raw output signals (in volt) of the instruments are saved using the software DasyLab in ASC-files. The files are imported in Python, where calibration formulas are used to convert these data into water depth and flow velocity. A moving-average of 0.015 seconds is used to reduce the effect of turbulence and errors in the measurements. Since a frequency of 1000 Hz is used, this average interval contains 15 measurements. Only the impulsive load has a short duration, but since the focus is not on these load but the more steady dynamic load, this frequency of ± 65 Hz should be sufficient.

Wave gauges generate electric signals (in volt), which correspond to a certain water depth. The location of these wave gauges are presented in Figure 4.4 and calibration of the instruments can be found in Appendix H. The free stream velocity is measured at the location of the front side of the building without the building being present, see Figure 4.4a. An electromagnetic velocity sensor (EMS) is located at a height of 15 mm to assume the measured velocity to be uniform of the height of the building (Wüthrich et al., 2018), resulting in an initial water depth in the flume, h_f , of 15 mm as well.

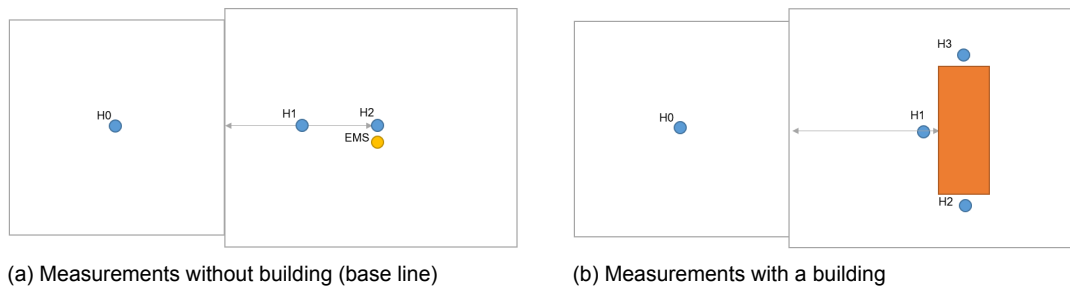


Figure 4.4: Schematic representation of the topview of the physical model

4.1.2. Scaling and scale effects

A physical model is used to conduct experiments, which is on a different scale (1:50) than a real flood situation would be. A perfect simulation by the physical model without any scale effects is met when mechanical similarity (or similitude) occurs as described in Appendix H.2.

- *Scaling*

Since gravity and inertia are the most important parameters, scaling according to Froude's law is applied in the experiments: The dimensionless Froude number, $Fr = \frac{v}{\sqrt{gh}}$, should be equal in the model and in reality as well. The scaling of different parameters can be found in Figure H.3a. An example is given for velocity: Since the gravity is the same in the model as in reality, $\lambda_g = 1$ and the length is scaled according to the scale of the model, $\lambda_L = \lambda$, the flow velocity should be scaled with $\lambda_v = \sqrt{\lambda}$, to provide $\lambda_{FR} = 1$. A measured flow velocity of 1 m/s during the experiments, corresponds with a real flow velocity of $v_{model} \cdot \sqrt{\lambda} = 1 \cdot \sqrt{50} = 7.1$ m/s. Scaling of the building material, in this case masonry and concrete, is hard due to the difficulty in scaling down of the modulus of elastic, stiffness, density and interaction between the blocks. Since only pressures on the faces are measured, timber is chosen as material.

- *Scale effects*

Since the model is made based on Froude scaling and the model fluid is identical to the real-world fluid (water), only one force ratio can be met and dynamic similarity is not possible. The remaining force ratios result in scale effects, which increase with the scale ratio. To minimize these effects, the dimensionless numbers are checked in Appendix H.2.

4.1.3. Methodology

In the first runs, the water depth and velocity are measured for different impoundment depths without any obstacles in the flume to find the suitable depths and location of the objects. The analytical solution of a dam break wave over a wet bed is used to validate the measured values. Also, control of the gate and continuity during all the experiments is important to maintain. These factors influence the water depth and velocity near the obstacle, which should be in the range of the expected Dutch flood parameters.

Analytical solution of wet bed bore

The propagation of a dam break wave over still water with an initial water depth is displayed in Figure 4.5. It can be described as a propagating bore, which is similar to a turbulent and highly aerated hydraulic jump (Chanson, 2004).

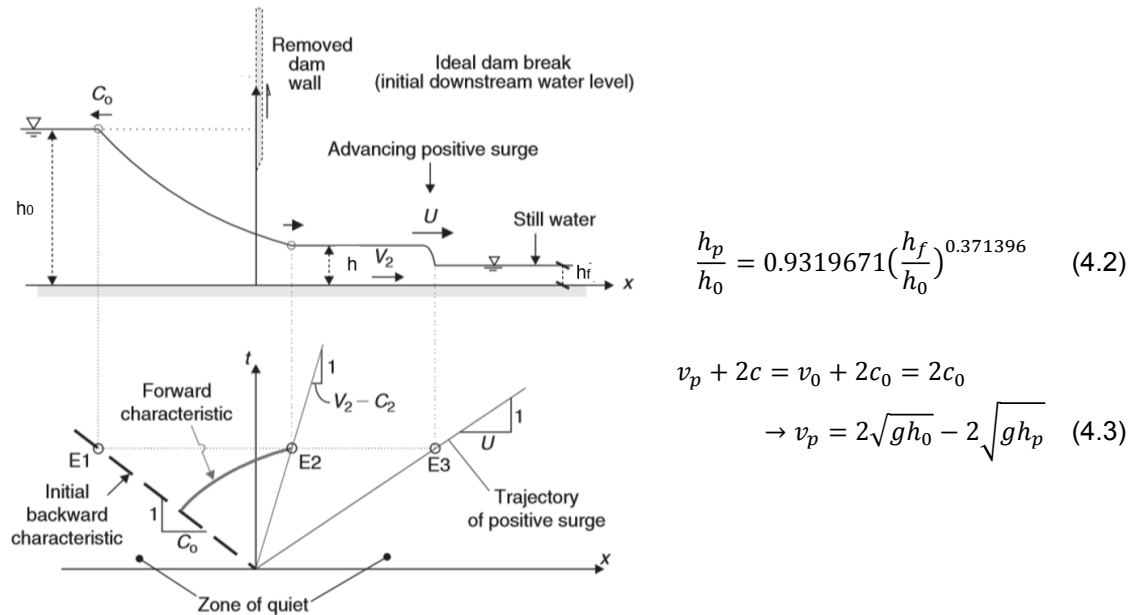


Figure 4.5: Sketch of dam break wave in a horizontal channel initially filled with water for $h_f < 0.1383h_0$ (Chanson, 2004)

The propagation of the wave in Figure 4.5 can be divided in four main regions (from upstream to downstream):

1. This solution assumes an infinite reservoir like a lake or river with constant initial water depth, h_0 . In the present experiments, the end of the reservoir probably affects the bore before the full water depth of the bore is developed. This results in lower water depth and a higher flow velocity compared to the analytical solution.
2. The theory of Ritter (1892), see Appendix H.3, for a dam-break wave on a dry bed can be applied on the region between point E2 and the leading edge of the negative wave in E1.
3. Between E2 and the leading edge of the positive surge in E3 an almost constant water depth is observed, which is referred to as a *plateau*. The height of this plateau can be predicted by deducing the momentum and continuity equation to Equation 4.2 introduced by Chanson (2004). From the forward characteristics also the flow velocity can be predicted with Equation 4.3.
4. The last region is the turbulent bore front with significant air entertainment travelling over an initial water depth, h_f . A value between 5 and 20 mm is used in the current study, which is too small to measure correctly with only the water gauges, so a video camera is used to determine this value.

Baseline measurements

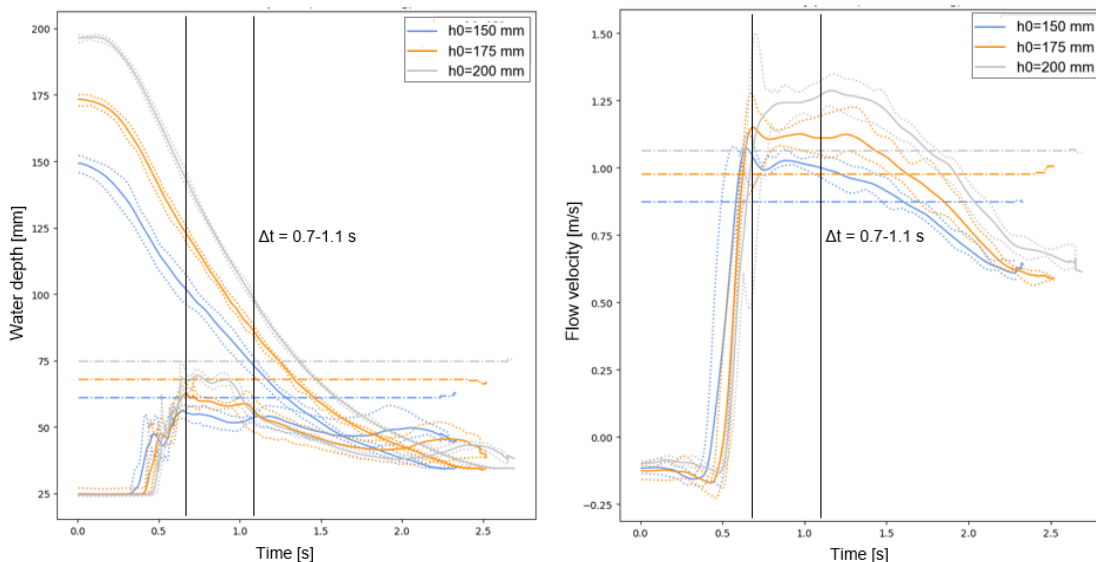
Different experiments are conducted by combining the following variables summed up in Table 4.1: 3 different impoundment depths, 5 angles of attack and 2 buildings. These chosen impoundment depths correspond with flood water depths up to 3.5 m and flow velocities up to 9 m/s at the location of the building at full scale (in reality). Based on these situations, the influence of the different variables on the pressure coefficient is investigated.

Table 4.1: Different situations of experiments

Angle of attack [°] →	0	15	45	75	90	
Impoundment depth, h_0 [mm] ↓						
150	■	■	■	■	■	■ 4 residences = 4R
175	■	■	■	■	■	■ 8 residences = 8R
200	■	■	■	■	■	

To find the influence of these variables, experiments without the building and an impoundment depth of 150, 175 and 200 mm are conducted referred to as the 'baseline' measurements. The water depth and velocity from these experiments are used in further calculations. The dimensionless numbers are checked for the results from five runs with an impoundment depth of 200 mm to see if scale effects should be taken into account. In Figure H.4 it can be seen that these numbers are well above the critical values of 120 for the Weber number and 2000 for the Reynolds number, so scale effects can be neglected.

The average water depth and flow velocity of the five runs are displayed as the mean per impoundment depth in Figure 4.6a and 4.6b, the dotted lines are the measured maximum and minimum values. Figure 4.6a shows the water depth inside the reservoir, h_0 , which follows the parabolic curve described by Ritter (1892) and the water depth at the location of the building without being present. It can be seen that the water level shows a plateau between $t \approx 0.7$ and 1.1 s, which is lower than the analytical value from Equation 4.2 as expected due to the finite reservoir. Figure 4.6b shows the flow velocity at the building location, which is higher than the analytical value in Equation 4.3. At the interval where the plateau occurs, the flow is considered to be quasi-steady. On this interval, the water depth and free stream velocity (or flow velocity without the building being present) at the location of the building are almost constant.



(a) Water depth at reservoir (parabolic curves) and at location of the building (show plateau) (b) Velocity at location of the building

Figure 4.6: Mean values of 5 different runs per h_0 (solid lines = mean value, ... = minimum/maximum value, -.- = plateau value)

Between the different runs per configuration and the upcoming experiments with the buildings, there could be a minor difference between the impoundment depths, h_0 , or initial water depth in the flume, h_f . To take into account these differences, the normalized values dependent on the time, $h_n(t)$ and $v_n(t)$, are used for further calculations as described in Equation 4.4. The time-averaged base values over the quasi-steady interval and corresponding standard deviations are presented in Table 4.2.

$$h_n(t) = \frac{h(t) - h_f}{h_0 - h_f} \quad (4.4)$$

$$v_n(t) = \frac{v(t)}{\sqrt{g(h_0 - h_f)}}$$

Table 4.2: Time-averaged values from the baseline measurements based on 5 runs (standard deviation between brackets)

h_0 [mm]	h_n [-]	h_{base} [mm]	h_{real} [m]	v_n [-]	v_{base} [m/s]	v_{real} [m/s]
150	0.28	53.1 (1.18)	2.65	0.89	1.01 (0.01)	7.24
175	0.27	58.8 (1.18)	2.94	0.90	1.12 (0.01)	8.13
200	0.26	64.8 (4.50)	3.24	0.93	1.23 (0.03)	8.84

Buildings

To investigate the influence of the geometry, orientation and different ratios on the pressure, the building is placed at the location of the velocity sensor and second wave gauge. The geometry of the buildings and side ratio, L/B , can be found in Table 4.3. The width-to-water depth ratio used by FEMA (2011) and aspect ratio, h/L , used by the Eurocode in Appendix E vary as the water depth varies over time during an experiment, so the time-averaged value is given for the three impoundment depths (150, 175 and 200 mm).

Table 4.3: Geometry and time-averaged ratios for three impoundment depths (150, 175 and 200 mm)

	Sort	Width, B [mm]	Length, L [mm]	L/B	B/h	h/L
8R - 0°	8 residences	864	173	0.4	13.4-14.7-16.3	0.30-0.34-0.37
4R - 0°	4 residences	432	173	0.2	6.7-7.4-8.1	0.30-0.34-0.37
4R - 90°	4 residences	432	173	2.5	2.7-2.9-3.3	0.12-0.14-0.15

The building placed with its longest side, B , parallel to the flow, is the original orientation (Figure 4.7b). The angle between the front side of this original orientation and the new orientation caused by rotating the building is referred to as α . The angle of attack or flow incidence, ϕ , is different for the sides. The distance between the centerline of the frontal area (P3/4) and the gate remains constant, shown in Figure 4.7 for all orientations except for 4R-90°, where this constant distance is between the frontal area (P11/12) and the gate.

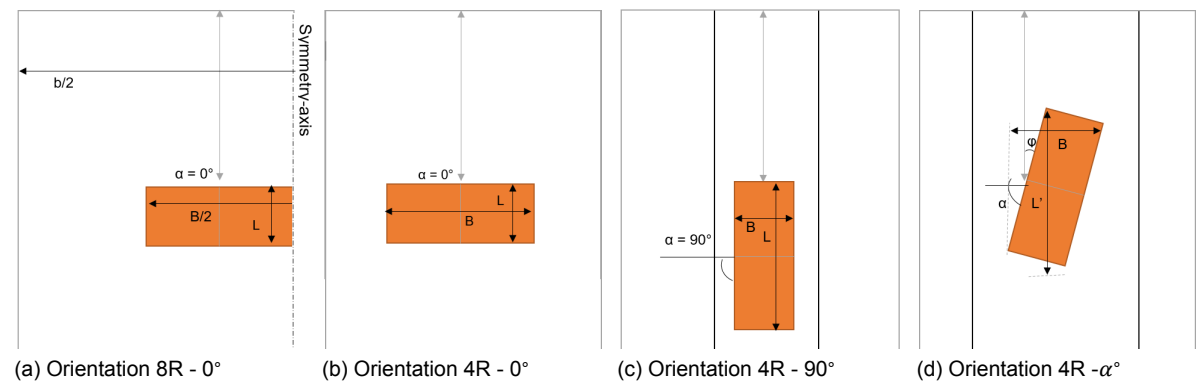


Figure 4.7: Orientations of the building (with $\alpha=15, 45$ or 75)

Due to the limited width of the flume, building 8R which resembles 8 residences, does not fit in this flume without changing the scale. Since there is uniform flow, it is assumed water will flow around the building similar at both sides. The line parallel to the length of the flume through the middle of the building can be seen as a symmetry axis (Figure 4.7a). By placing building 4R, which is half the width of building 8R, to the side of the flume, the pressures on one half of the building can be measured. Due to symmetry, these same pressures will act on the other half as well. Although, symmetry is only present when the angle of attack of the flow is at 90° or 0° , so other orientation of the building cannot be investigated in these experiments.

By changing the orientation of the building, also the blockage ratio, B'/b change according to Equation 4.5. To prevent the blockage ratio having any influence on these experiments, temporary walls are placed in the flume to maintain a constant blockage ratio (black lines in Figures 4.7c and 4.7d). Depending on the angle of rotation of the building, the walls are positioned to create the width as given in Figure 4.7. The projected width of the building at each orientation, B' , divided by the flume width, b , give ratio's between the 0.53 and 0.57. For orientation 4R- 90° (Figure 4.7c) and 4R- 0° (Figure 4.7b), this is comparable with respectively the width of a bicycle path (± 3.5 m) and access road for car drivers, cyclists and pedestrians (± 9 m) on both sides of the building.

$$\text{ratio} = B'/b \quad \text{with} \quad B' = L \sin \alpha + B \cos \alpha \quad (4.5)$$

Process of dam-break wave colliding into building

In Figure 4.8 three successive video frames are presented for three different orientations, showing three different stages of a bore or wave colliding into a building. These stages are also observed in the pressure profiles of the sensors at the frontal face of the building. The pressures obtained from 4R- 90° with different impoundment depth, expressed in the water column with corresponding hydrostatic pressure, are shown in Figure 4.9. Due to different stages, the pressure profiles show the characteristic 'church-roof' shapes. Also, it can be seen that the highest impoundment depth of 200 mm results in the highest pressures.

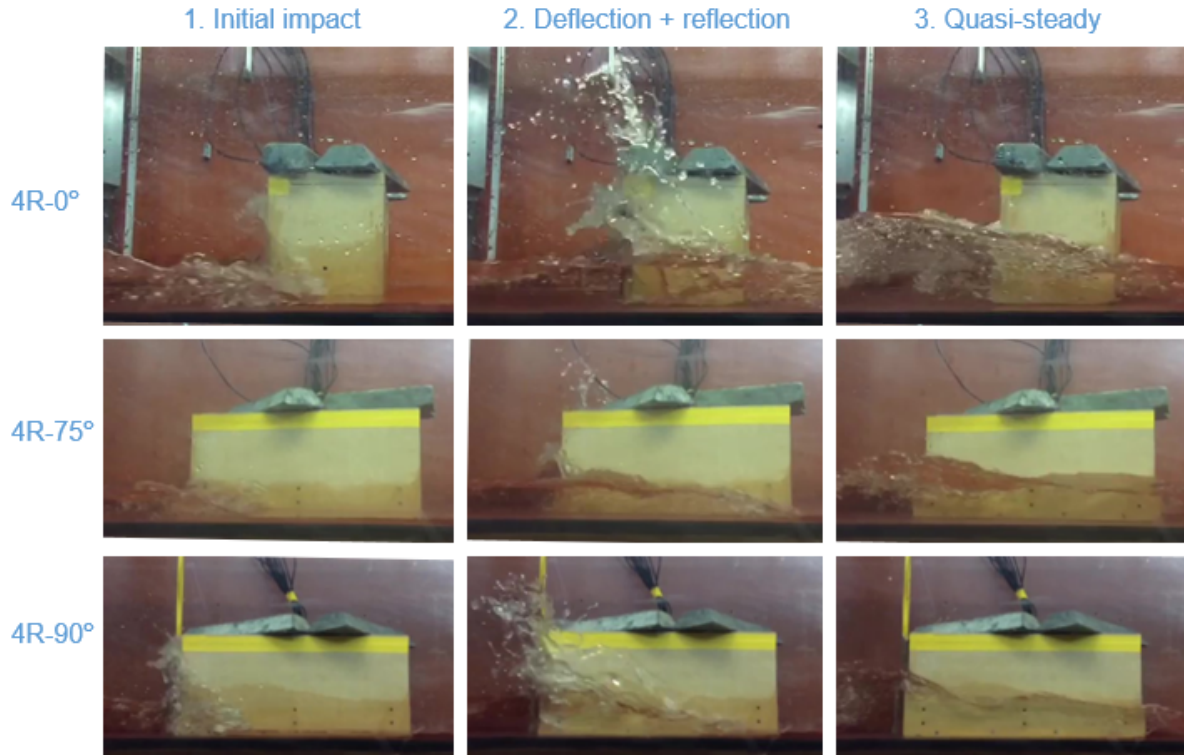


Figure 4.8: Snapshots of the experiments for three different orientations ($h_0 = 175$ mm)

1. *Initial impact*: When the bore runs into the building, the flow direction is suddenly changed at the location of the building. A sharp peak in the pressure profile can be observed at the frontal face due to the impulsive load. The first snapshots are taken just after this peak pressure, where a reflected wave causes an increase of the water surface in front of the building.
2. *Deflection + reflection*: Due to the blockage of the flow, the steep front cannot be maintained at the front side of the building. Besides the reflection, the bore is deflected causing a thin tongue of water running up the upstream face of the building. Simultaneously with the highest splash-up, the maximum height of the tongue of water is reached and falls back over itself sending a volume of water back upstream. The splash-up at the upstream side is considerably smaller for the flow perpendicular to the face of the building (4R-0° and 4R-90°) compared to other cases (4R-α°).
3. *Quasi-steady*: The third snapshots are taken when only reflection (or no deflection) is observed and a quasi-steady state is developed. A smaller second peak with a longer duration is visible in the pressure profile. From the snapshots, a difference between the water level upstream and downstream of the building can be observed especially for the flow perpendicular to the face of the building.

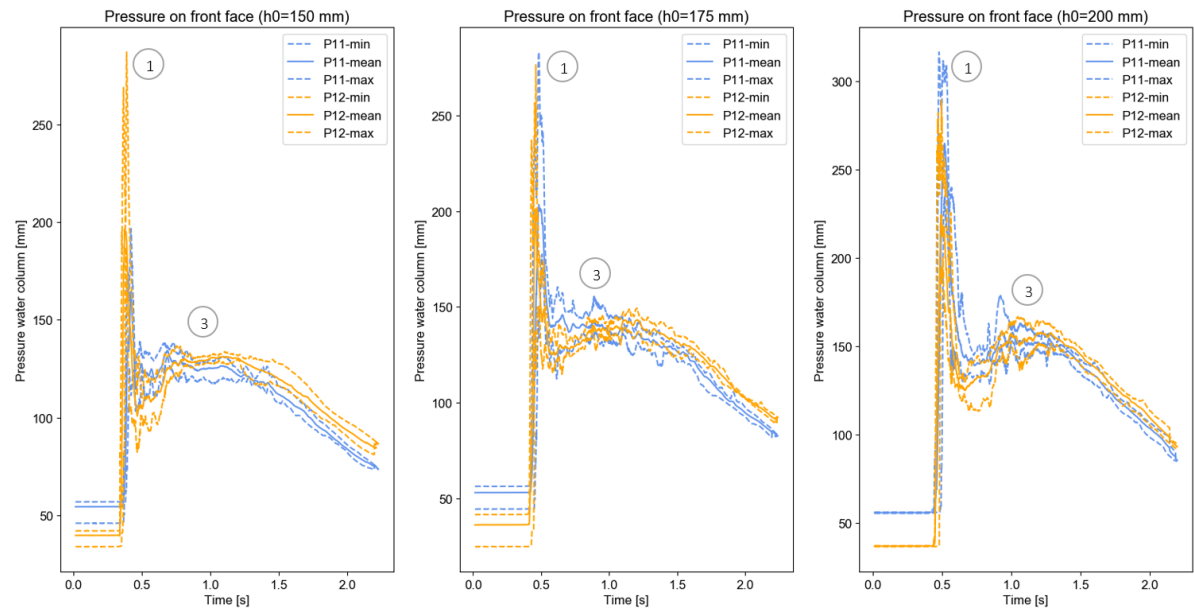


Figure 4.9: Time averaged pressure of the sensors at the upstream face for all 3 impoundment depths (average from 5 runs)

4.2. Results of experiments

The difference between the measured pressure by the sensors and the pressure due to the water depth is caused by the flow velocity. Since both flow velocity and direction change due to the presence of the building, the normalized water depths and free-stream velocity from the baseline experiments are used for the calculation of the pressure coefficient (Table 4.2). At the location where both the flow velocity and water depth are measured in the baseline experiments, the centerline of the front-face (line of P3/P4) of the building is placed. Based on these base values, the pressure coefficient which belongs to the quasi-steady pressure can be calculated according to Equation 4.6. The average pressure coefficient during quasi-steady

flow is taken at the time interval from 0.7 to 1.1: $C_p = \frac{\sum C_p(t)}{\Delta t}$

$$C_p(t) = \frac{\rho g(h(t) - h_{base}(t))}{\frac{1}{2}\rho v_{base}(t)^2} = \frac{2g\Delta h(t)}{v_{base}(t)^2} \quad \text{with} \quad \begin{cases} h_{base}(t) = h_n(t)(h_0 - h_f) + h_f \\ v_{base}(t) = v_n(t)\sqrt{g(h_0 - h_f)} \end{cases} \quad (4.6)$$

4.2.1. Geometry

The influence of the geometry of the buildings and the ratio of the water depth on the pressure is investigated by the use of two different buildings. Only the experiments for an angle of attack of 0° and 90° are used to analyze the influence of these ratios.

The time average pressure coefficients, C_p , belonging to the frontal face (P1 t/m 6) are displayed with the corresponding width-to-water depth ratio in Figure 4.10. Despite the locally higher flow velocity near the edges, the pressure coefficient is significantly lower at this location of the building’s face (P2 and 6). The direction of this flow is mainly parallel to the face of the building, which results in a small component perpendicular to the face. Since the velocity of the baseline experiment or free stream velocity is used, this results in a lower pressure coefficient. The choice is made to exclude these values from the mean pressure coefficient and show these values individually in Figure 4.10, so the higher values are the mean of the time average pressure coefficients from P1, P3, P4 and P5.

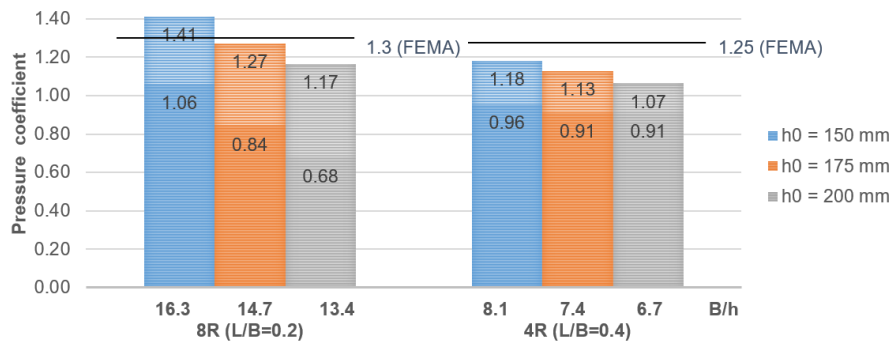


Figure 4.10: Mean pressure coefficients at the frontal area for different B/h-ratio's

P-55, Coastal Construction Manual (FEMA, 2011) provides drag coefficients for different ranges of the B/h -ratio, which belong to the highest aspect ratio of the interval. For example, a drag coefficient of 1.25 is prescribed for all building with a ratio between the 1 and 12, see Appendix E. This should result in an upper value for B/h -ratios in this range, which values are also drawn in Figure 4.10. However, the value corresponding with the highest B/h -ratio exceeds the upper value given by FEMA. This could be explained by the side ratio, L/B , of 0.2, which is quite low when looking at detached residences. Since the majority of the residences in the United States of America is a single-family house, it can be assumed that these low side ratios are not taken into account for the determination of the pressure coefficients.

The pressure coefficient of residence 4R-90° is plotted during the quasi-steady interval in Figure 4.11. The variation is in further figures displayed as an error bar of one standard deviation added and subtracted from the time-averaged value.

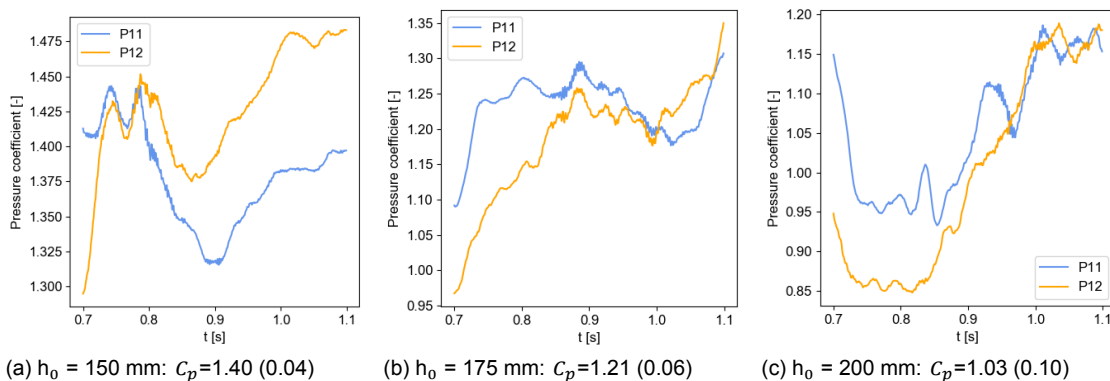


Figure 4.11: Pressure coefficients on the frontal face of 4R - 90° (standard deviation between brackets)

Furthermore, the effect of the length of the building is investigated. According to NEN-EN 1991-1-4 (see Appendix E) the pressure coefficients are equal for building 4R-0° and 8R, because the water depth-to-length of the buildings is equal. Figure 4.12a shows that the experimental data of the two buildings do not give equal coefficients and show a difference with the Eurocode: the coefficients at the frontal face are higher and those at the back face are smaller. This can be explained by the difference between two-dimensional and three-dimensional flow. In the case of the wind, the air will flow around and over the building (3D), whereas the water in the experiments flows only around the building (2D). An object piercing the surface of the water cause a blockage effect in both the width and height, where the vertical blockage of a submerged object such as the wind-action on a building is negligible compared to the horizontal blockage. The blocking effect of the emerged object influence the vortex shedding causing an increase of the drag-coefficient.

An increase in the side-ratio below the critical value of ± 0.6 , will cause an increase in drag coefficient according to Norberg (1993), the same applies for the B/h - and h/L -ratio. This effect can be seen in Figure 4.12b by the shift to the left when the side-ratio increases from 0.2 to 0.4. Above this critical value the opposite occurs, so an increase of the side-ratio causes a decrease of the pressure coefficient. By rotating the building with 90°, so aligning the longest side with the flow instead of the shortest side, the L/B -ratio increases from 0.4 to 2.5. A shift to the right is expected, which can not be seen for the experimental data when the side-ratio increases to 2.5. However, both the B/h -ratio, which should result in a smaller pressure coefficient according to P-55 (FEMA, 2011).

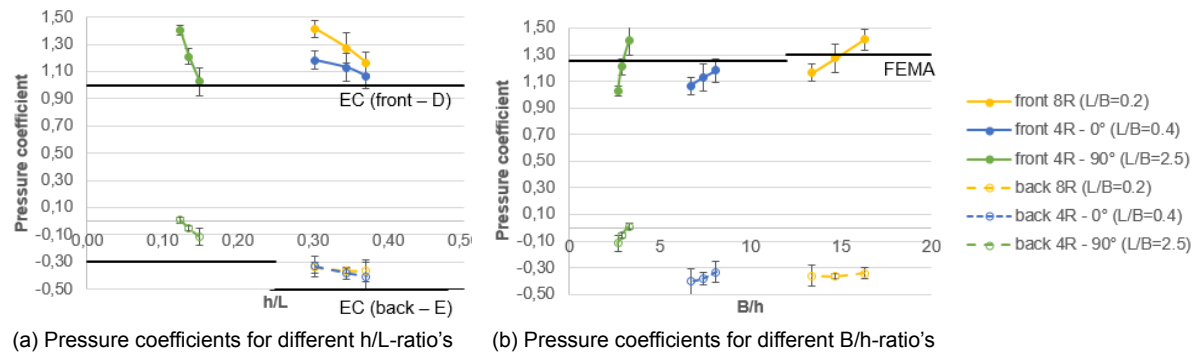


Figure 4.12: Influence of the side ratio and aspect ratio on pressure coefficient

The difference lies in the use of the drag coefficient which is derived from the pressure component aligned with the flow direction, F_D in Figure 4.13, and the friction along the faces. The effect of friction along the faces is not taken into consideration in this study, since this is relatively small compared to the component from perpendicular pressure. The pressure coefficient used in the previous figures is derived from the pressure perpendicular on the faces of the building, F_p . To make a better comparison with the figures from the literature study, the drag coefficients are calculated according to Equation 4.7.

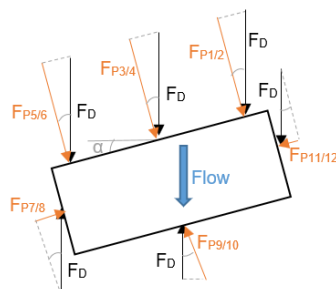


Figure 4.13: Drag force vs. pressure

$$C_D = \frac{1}{B'} \cdot \left(B \cos \alpha \cdot (C_{P1/2} + C_{P3/4} + C_{P5/6}) - L \sin \alpha \cdot C_{P7/8} - B \cos \alpha \cdot C_{P8/9} + L \sin \alpha \cdot C_{P11/12} \right) \quad (4.7)$$

When the drag coefficients are compared to the study of Norberg (1993), the decrease of the drag coefficient with a side-ratio of 2.5 can be seen now in Figure 4.14b. This is due to the decrease of pressure at the rear face of the building 4.12a when the h/L -ratio decreases, see also the values prescribed by the Eurocode in Appendix E. The current values are smaller than those found by others in wind-tunnel experiments shown in Figure 4.14b, which can be explained by the difference in aspect-ratio and type of flow. Where the wind-tunnel experiments have high h/L -ratios (>25) and are subjected to submerged (3D) flow, the current experiments have a small h/L -ratio (<0.5) and are subjected to emerged (2D) flow. The experimental values with a side ratio, L/B , of 0.4 are smaller than those of 0.2, due to the smaller aspect ratio, B/h , as described above and shown in Figure 4.12.

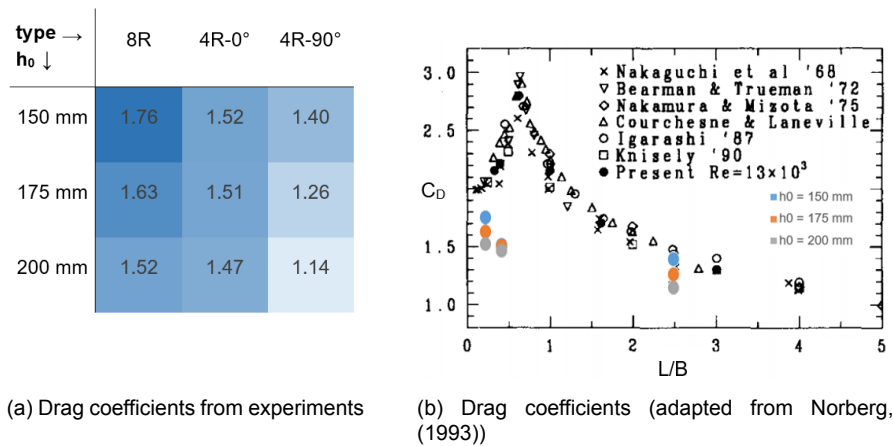


Figure 4.14: Influence of the side ratio on drag coefficients

The values above the x-axis in Figure 4.15 resembles the drag coefficient and below the x-axis mean pressure coefficients at the frontal area similar the Figure 4.10. The drag coefficients are derived from the combination between the positive pressure at the front face and negative pressure back face, so is in all situations higher than the pressure coefficient. The values from P-55 (FEMA, 2011) are closer to the pressure coefficients than the drag coefficients. Since this drag coefficient is used for different failure mechanisms, such as sliding, overturning and bending of the walls, an underestimation of the hydrodynamic action is made in case of total stability checks.

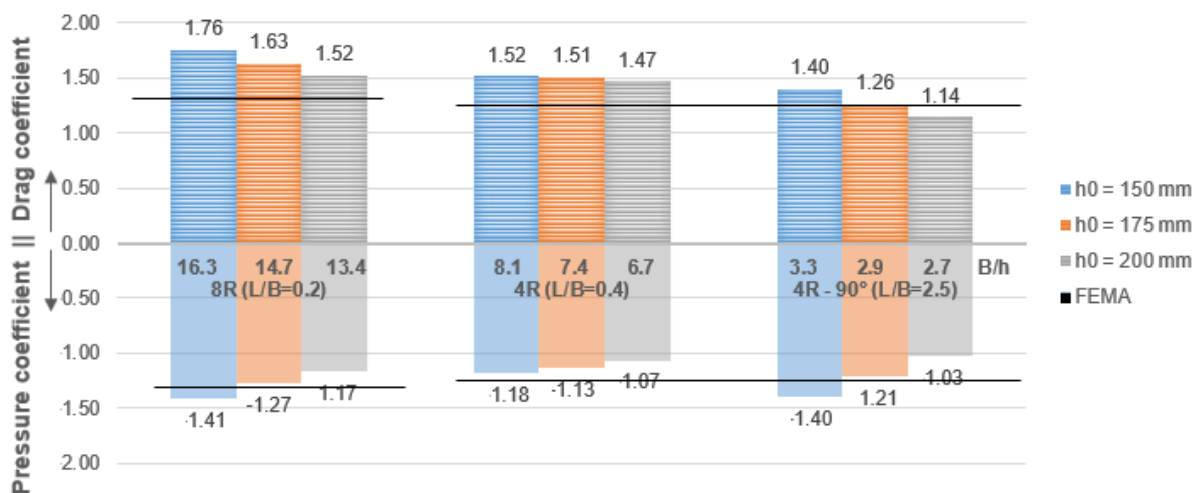


Figure 4.15: Drag coefficients (above x-axis) and mean pressure coefficients at the frontal area (below x-axis)

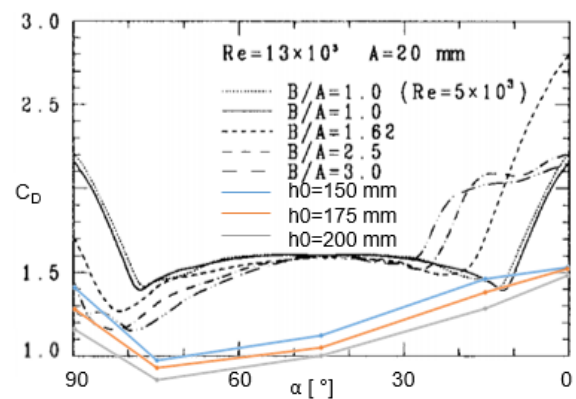
4.2.2. Orientation

To find the influence of the orientation of the building on the pressure coefficients, only experiments with building 4R are conducted. Since symmetry is used for the experiments on building 8R, it is impossible to experiment with other angles than 0° and 90° . The angle between the front side of the original orientation and the new orientation caused by rotating the building with an angle α shown in Figure 4.7. These rotations cause different angles of attack, ϕ , however, only the pressure perpendicular to the faces of the building can be measured with the pressure sensors.

First the data is compared to those of Norberg (1993) for a rectangular cylinder with $B/L=2.5$ similar to the building 4R in Figure 4.16b. A similar minimum is found with an angle of attack of 15° corresponding with a rotation of 75° . Also, the small difference between an angle of attack of 75° and 90° can be seen from the current result. Since the experiment is conducted for only five orientations, straight lines are drawn between the measurements, but it can be expected that these lines have a similar shape as those of $B/L=2.5$.

$\alpha \rightarrow$ $h_0 \downarrow$	0°	15°	45°	75°	90°
150 mm	1.52	1.45	1.11	0.96	1.40
175 mm	1.51	1.37	1.04	0.91	1.26
200 mm	1.47	1.27	0.99	0.84	1.14

(a) Drag coefficients for different orientations



(b) Drag coefficients (adapted from Norberg, (1993))

Figure 4.16: Influence of the orientation of the building on drag coefficients

To find the influence of the orientation on the pressure coefficient, the pressures on the centerline of the front face (P3 and P4) are compared, since these have a constant distance to the gate. Also, the pressures from the side face which is rotated towards the gate (P11/12) are shown in Figure 4.17. When the building is rotated, the angle of attack decreases for the front face, so the pressure from P3 and P4 decreases. The angle of attack for the side face increases, resulting in an increase of the pressure coefficient.

$\alpha \rightarrow$ $h_0 \downarrow$	0°	15°	45°	75°	90°
150 mm	1.17	1.17	0.89	0.45	0.26
175 mm	1.13	1.04	0.75	0.30	0.21
200 mm	1.07	0.92	0.65	0.27	0.19

(a) Pressure coefficients of P3/4

$\alpha \rightarrow$ $h_0 \downarrow$	0°	15°	45°	75°	90°
150 mm	-0.03	0.32	0.80	1.16	1.40
175 mm	-0.02	0.28	0.69	1.10	1.21
200 mm	0.01	0.27	0.62	1.03	1.03

(b) Pressure coefficients of P11/P12

Figure 4.17: Influence of the orientation of the building on pressure coefficients

The interaction between the decrease of the coefficient on one face and increase on the other face as presented in Figure 4.18a, causes partly the minimum of drag coefficient shown in Figure 4.16. The other part is due to the negative pressure at the rear side(s) of the building. If the pressure coefficient is plotted against the angle of attack, ϕ , in Figure 4.18b instead of the rotation of the building, a slightly steeper line can be observed for the smaller side (P11/12) compared to the larger side (P3/4). This can be explained by the increase of the distance of the centerline of the side face (P11/12) to gate, except for a rotation of 90° , see Figure 4.7, where there is a constant distance between the centerline of the front face (P3/4) and the gate.

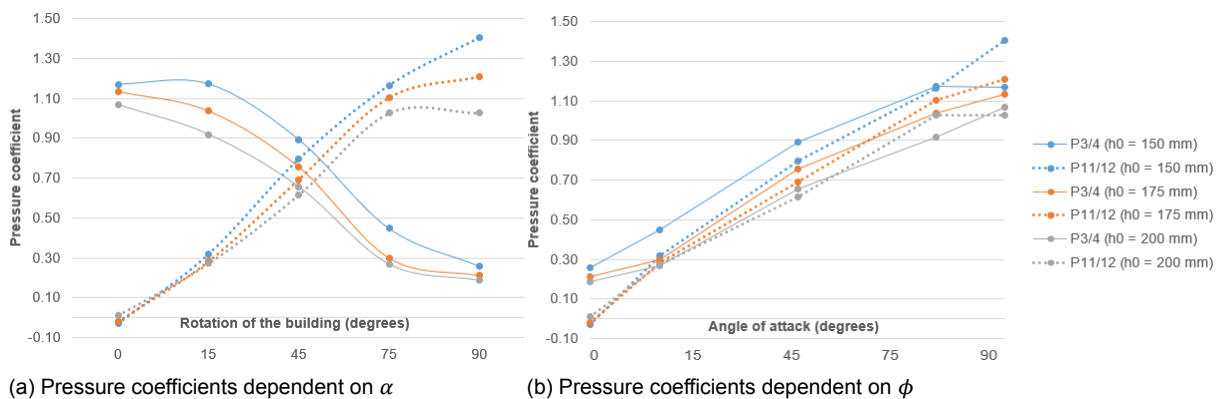


Figure 4.18: Pressure coefficient per rotation of the building or angle of attack

4.2.3. Conclusions on quasi-steady load

Only few geometries and orientation are considered, but based on the pressure coefficients determined from the physical experiments the following conclusions can be drawn:

- $B/h \uparrow C_p \uparrow$:
From this experimental data, it is clear that the pressure coefficient increases if the width-to-water depth increases. The similar to increase of the drag coefficient due to the increase of the B-h ratio in the design guidelines of P-55 (FEMA, 2011).
- if $L/B < 0.6$: $L/B \uparrow C_d \uparrow$ and if $L/B > 0.6$: $L/B \uparrow C_d \downarrow$:
The increase of the side ratio (side aligned with the flow over the side parallel to the flow) causes an increase in the drag coefficient for ratios below the critical value of ± 0.6 (Norberg, 1993). The opposite is valid for values higher than this critical side-ratio, see Figure 4.14b. This is mainly due to the decrease of pressure at the rear face of the building shown in Figure 4.12a when the h/L-ratio decreases similar to NEN-EN 1991-1-4 (see Appendix E).
- $\phi \uparrow C_p \uparrow$:
By rotating the building using different angles, α , around the centerline of its frontal face, the angle of attack, ϕ of the flow on the buildings faces change. An increase of the angle of attack, causes an increase in the pressure coefficient as well, see Figure 4.17. Where a similar minimum of the drag coefficient around a rotation of 75° is found as Norberg (1993), the pressure coefficients do not show this minimum.
- The drag coefficients prescribed in P-55 (FEMA,2011) are smaller than the drag coefficients derived from the current experimental data. If the prescribed drag coefficient is used to design flood-prone residences which are resistance to lateral sliding, the hydrodynamic load is underestimated according to the current data. These coefficients appear to be upper values for the current pressure coefficients of the frontal face, see Figure 4.15. However, the pressure at the front can exceed this 'upper' value for terraced houses with a smaller side ratio than common American single-family homes.

4.3. Overview of flood loads

The loads due to flooding act as accidental loads on the residence and depend mainly on the flood conditions, such as water depth and flow velocity. The other factors are the orientation and geometry of the residence. From the selection of flood action in Appendix D the residence will be subjected to hydrostatic, q_h , and hydrodynamic loads (quasi-steady, q_d , and wave, q_{Hd}). It is assumed that waves only occur during ponding, so the combination of the load due to wind-induced waves and the hydrodynamic load is not taken into consideration leading to the following load combinations displayed in Figure 4.19. The water depth, h , is with respect to the floor level, which is also the base of the wall.

1. Hydrostatic + quasi-steady hydrodynamic load
2. Hydrostatic + hydrodynamic wave load

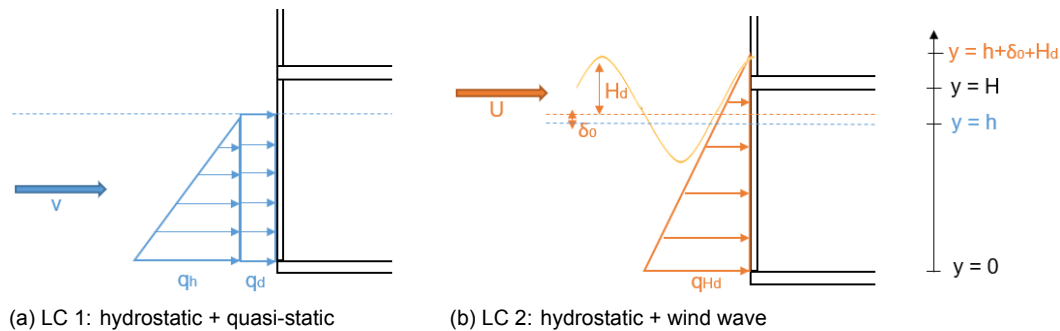


Figure 4.19: Load combinations subjected to the load-bearing leaf of the residence

Critical flood loads

Both the quasi-steady and wave load are the largest when the angle of attack is 90° . Failure of the load-bearing walls is one of the most important failure mechanisms of collapse, which are most vulnerable under lateral load. This situation occurs when the flow is perpendicular to the length of the building, so orientation 4R- 90° is used for the structural analysis.

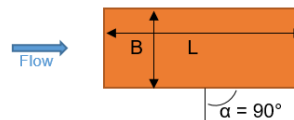


Figure 4.20: Critical orientation of the residence: 4R - 90°

- *Hydrostatic load*

The lateral hydrostatic pressure is taken into account as defined in Figure 2.4a. The flood infiltration rate is not included in this study, so is assumed that the residence will fill up as soon as the windows break and the residence will be empty before reaching the resistance of the glass pane. After failure of the window an equal water level in- and outside the residence is considered, so the hydrostatic load can be neglected from there since the part on the inside load cancels out the one on the outside.

$$q_H(h, y) = \rho g(h - y) \quad (4.8)$$

- *Quasi-steady hydrodynamic load*

The pressure coefficients found from the experiments appear to be influenced by several factors, so could be described as Equation 4.9 with a function of these factors. Due to limited data and the interest in the critical orientation only, a function based on the B/h -ratio only is derived instead of using all these factors. Since the width of the building is known, the coefficient can also be described as a function of the water depth only.

$$C_p = f\left(\frac{B'}{h}, \frac{L'}{B'}, \frac{b}{B'}, \alpha\right) \quad (4.9)$$

To define the quasi-steady load for the residence 4R in the critical orientation, the experimentally determined pressure coefficients of 1.40, 1.21 and 1.03 for water depths of respectively 2.6, 2.9 and 3.2 meters are used. The time-averaged pressure coefficients with the standard deviations are plotted in Figure 4.21, where a trendline through these data points is used as a function for the pressure coefficients. Higher water depths or smaller aspect ratios result in smaller pressure coefficients at the frontal face. Using the smallest value for higher water depths as well, the results will be on the conservative side. A minimum and maximum pressure coefficient of respectively 1.0 and 2.0 are used based on the values given by NEN-EN 1991-1-4 and FEMA (2011) in Appendix E.

$$q_D(h, v) = \frac{1}{2} C_p(h) \rho v^2 \quad \text{with } C_p(h) = \begin{cases} 2.0, & h < 1.7 \text{ m} \\ -0.6438h + 3.1083, & 1.7 \text{ m} < h < 3.3 \text{ m} \\ 1.0, & h > 3.3 \text{ m} \end{cases} \quad (4.10)$$

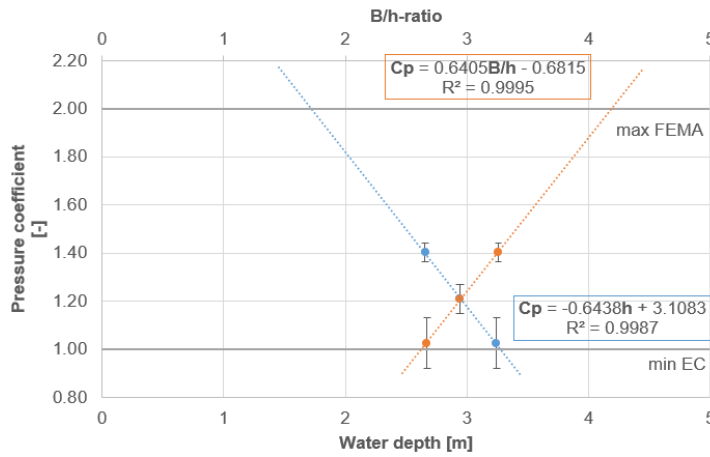


Figure 4.21: Pressure coefficient for residence 4R in its the critical orientation for collapse of the residence (90°)

- *Hydrodynamic wave load*

The lateral pressure due to wind-generated waves colliding into the building is shown in Figure 4.22a. To avoid a system of fifth-order differential equations in the structural analysis, the sum of the hydrostatic and wave load is approached by the hydrostatic load of the water surface being at the level of the maximum wave height, $h + \delta_0 + H_s$:

$$q_w(h, u, y) = \rho g(h + \delta_0 + H_d - y) \quad \text{with } H_d = H_s \quad (4.11)$$

The real load from the wave impact, F_w , and hydrostatic pressure, F_h , on a vertical wall is just smaller than the estimated load, F_{Hd} , as shown in Figure 4.22b. This results in a slightly conservative outcome for further calculations.

$$\begin{aligned} F_w &= p_0 h + \frac{1}{2}(p_1 - p_0)h + \frac{1}{2}p_1(\delta_0 + H_d) \\ F_h &= \frac{1}{2}\rho g h^2 \\ F_{Hd} &= \frac{1}{2}\rho g(h + \delta_0 + H_d)^2 \quad \approx F_h + F_{wave} \end{aligned}$$

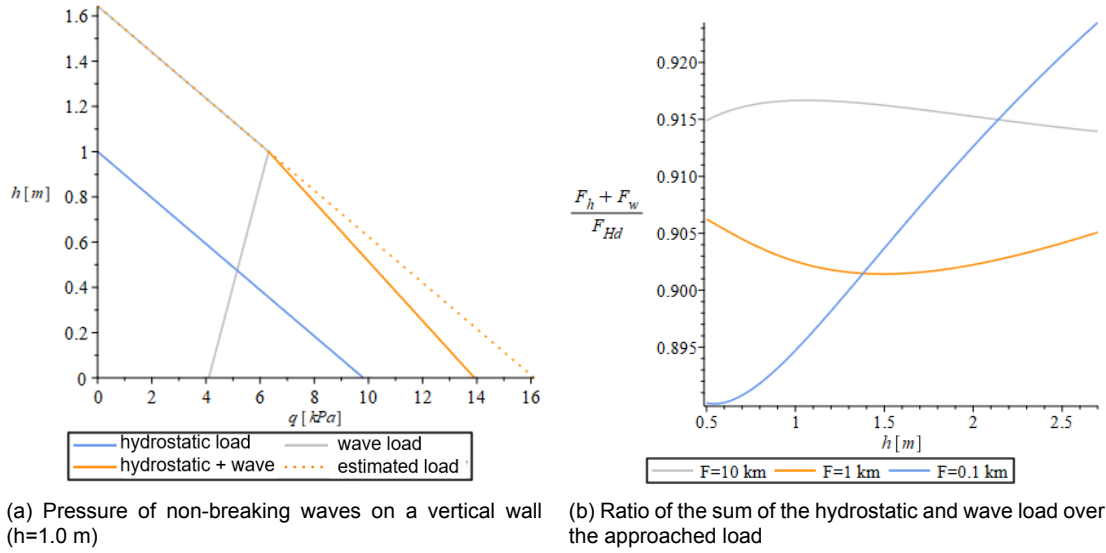


Figure 4.22: Wind induced wave load for different fetches with a wind velocity of 29.5 m/s

5

Structural damage of typical Dutch residences

This chapter deals with the resistance of the typical Dutch residence due to flood actions. Structural models of the residences are made by looking to the material properties of different structural elements and their interface conditions. Based on these models and the schematization of the load, the loads which cause collapse can be determined. By comparing the effects of the flood action with the resistance of the elements, the structural damage of a typical Dutch residence due to flood actions can be described.

5.1. Approach

Both the loads and the residences are schematized before the resistance to flood actions can be determined. The load-bearing wall is supported in the vertical direction by the stabilizing piers and in the horizontal direction by the floors and foundation. After determining the corresponding schematization of the supports, the different structural analyses are described.

5.1.1. Schematization

In general as described in Equation 5.1, an element collapses if the design value of the effect of the action, E_d , is larger than the design value of the resistance, R_d . Residential properties are classified as consequence class CC1 according to NEN-EN 1990. Since the resistance in case of flooding is of interest, the material factor for the accidental loading situation should be used, which is $\gamma_{Mm} = 1.3$ for masonry (NEN-EN 1996-1-1+A1/NB art. 2.4.3) and $\gamma_{Mc} = 1.2$ for concrete (NEN-EN 1992-1-1+C2/NB art. 2.4.2.4).

$$R_d \leq E_d \quad \text{with} \quad R_d = \frac{R_k}{\gamma_M} \quad (5.1)$$

- *Loads*

The self weight of the residence and the loads working on the residence are described. Furthermore, the load combinations due to flooding defined in Section 4.3 are assigned as accidental loads. The compression force on the lower load bearing (LB) wall is calculated in Equation 5.2, which is a summation of the self-weight of the roof construction, the wall of the first floor and the first and second floor construction. On top of that a minimum surface load on the floors is included to take into account the installations, furniture and inner partition wall. Since this force has a favourable effect on the resistance, a factor $\gamma = 0.9$ is used. An overview of the dead weights is given in Table I.1 per case-study residence.

$$N_{Ed} = \gamma(N_{roof} + N_{wall} + 2N_{floor}) \quad \left\{ \begin{array}{l} N_{roof} = 2.86 \text{ kN/m} \quad \text{see Equation 3.1} \\ N_{wall} = G_w H \\ N_{floor} = G_f \frac{B}{2} \quad (+G_{surface} \frac{B}{2}) \end{array} \right. \quad (5.2)$$

- *Edge support conditions*

Appendix I.1 describes the appropriate edge support conditions per case study residence. The vertical edge support conditions are provided by the facade perpendicularly on this panel. The junction between these load-bearing wall panel and the supporting piers or walls can be bonded, tied or untied as shown in Figure 5.1. It is assumed that movement joints are located at this locations as well, so no extra edges needs to be considered. Most of the residences have an open plan as in Figure 3.4, so no internal walls provide extra vertical supports.

The horizontal supports at the bottom and top of the wall panel are provided by the floors and type of foundation, which can be continuous or simple supported. The stiffness of the floor and the connection with the walls is important for the stability of the residence.

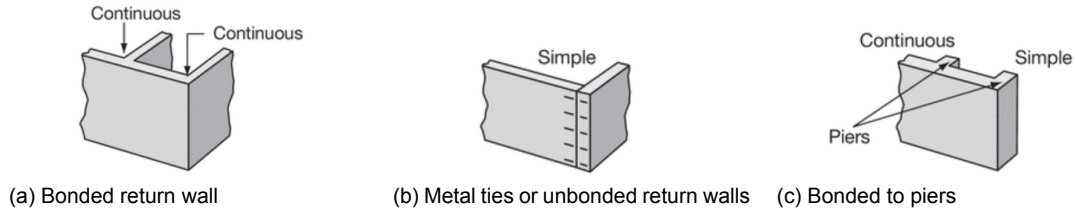
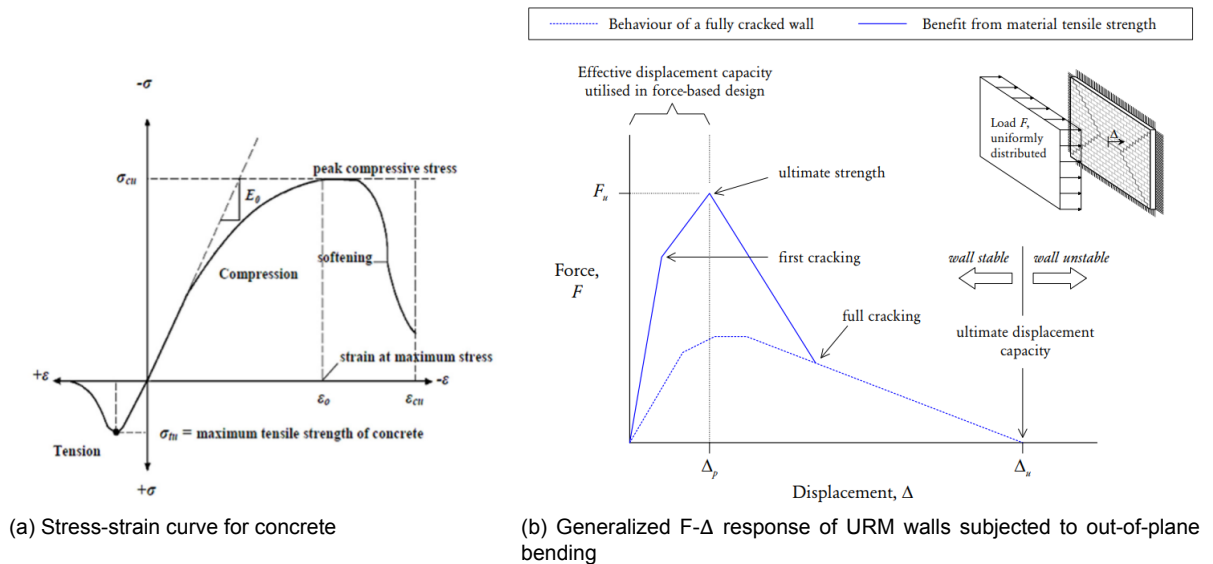


Figure 5.1: Vertical edge support conditions for masonry walls (Moore, 2008)

Structural analyses

Cracks in the part of the cross section in tension is allowed, since these cracks do not immediately lead to collapse of the wall. Both masonry and concrete are quasi-brittle materials with a compressive strength more than two times their tensile strength. Up to approximately 30% of the ultimate compressive strength, σ_{cu} in Figure 5.2a, the material behaves linearly-elastic. Then the first crack starts to develop and gradually the ultimate strength is developed in the part of the cross-section which is still intact. The stress distribution along this process can be found in Figure 5.11. At ultimate strength the process of softening of the material start until material is crushed at ultimate strain, ϵ_{cu} .



(a) Stress-strain curve for concrete

(b) Generalized $F-\Delta$ response of URM walls subjected to out-of-plane bending

Figure 5.2: Non-linear behaviour of quasi-brittle material (Vaculik,2012)

A linear analysis with redistribution of the forces or a plastic analysis would lead to a higher moment resistance as shown in Figure 5.2b: the ultimate strength of the wall is higher than the strength calculated with linear elastic analysis when assuming one-way bending.

In the traditional force-based design it is assumed that failure occurs at this point. Collapse however occurs when the ultimate displacement capacity, Δ_u , which is beyond in the scope of this study due to the complexity of the softening process. It is assumed that the ultimate strength is maintained until the other cracks are fully developed. An overview of the mechanic schemes for both linear and non-linear elastic analysis are presented in Figure 5.3 with corresponding section of further elaboration.

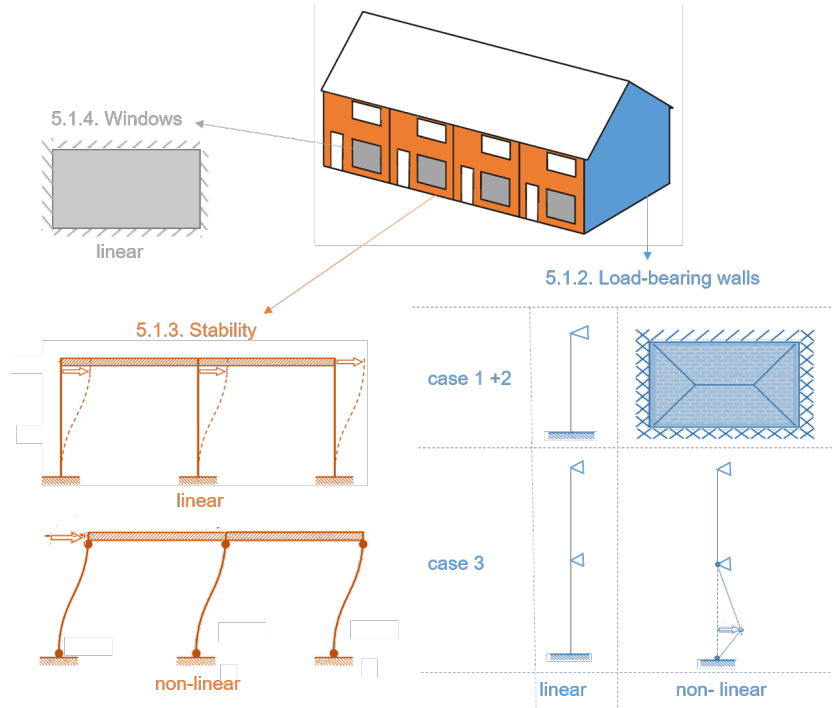


Figure 5.3: Overview of used mechanical schemes

5.1.2. Load bearing walls

Linear elastic analysis

The cavity wall consist of a load-bearing inner leaf, outer leaf and the ties connecting the two leaves. The inner leaves of the load-bearing walls are placed on top of the ground floor slab, which is assumed to be at ground level as displayed in Figure 5.4a. The water depths used in this section are all with respect to the base of this inner leaf.

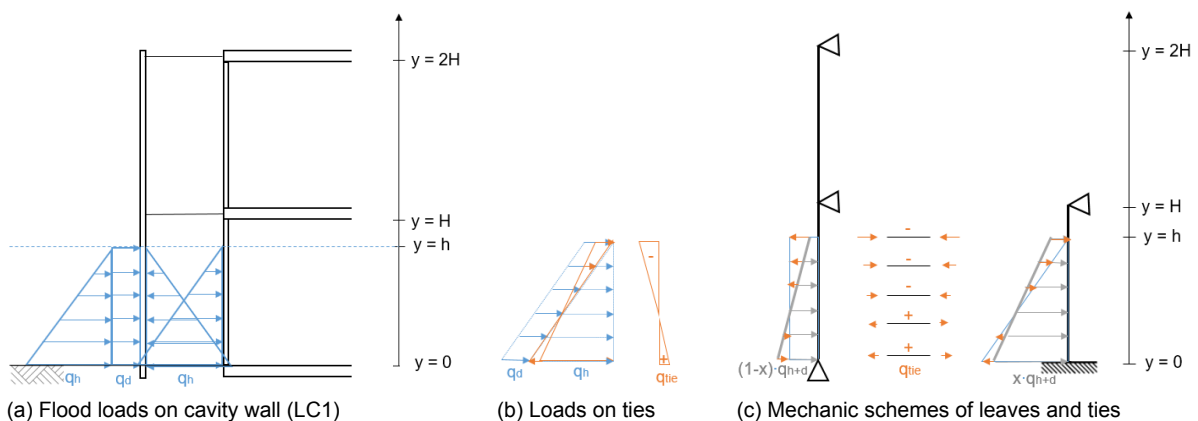


Figure 5.4: Schematization of loads acting on cavity wall

To equalize the air pressure in- and outside the cavity and allow water to drain out, air vents and weep joints are located at the base of the facade and interfaces with the non-structural elements. For a ventilated cavity wall, more than 1500 mm² perforations are required per meter wall (NEN 1068+C2 art. A.3.3), so it is assumed that the cavity will fill up through these weep joints. This causes an equal hydrostatic pressure on both sides of the outer leaf as pictured in Figure 5.4a, so this leaf is only subjected to the hydrodynamic load and the inner leaf to the hydrostatic load from the water inside the cavity (q_d and q_h in Figure 5.4c).

- *Ties*

If the ties are fully intact, it is assumed that both the combined load is distributed over the two leaves based on their relative stiffness according to Equation 5.3. The part of the load bearing upon the inner leaf, x , can be used to check if the ties are pushed out (- in Figure 5.4) or pulled out (+) due to this load transfer in Equation 5.4.

$$\begin{aligned} q_{LB,inner} &= x(q_h + q_d) \\ q_{LB,outer} &= (1 - x)(q_h + q_d) \end{aligned} \quad \text{with} \quad x = \frac{EI_{inner}}{EI_{inner} + EI_{outer}} \quad (5.3)$$

$$nF_{Rd,tie,-} \leq q_{tie} \leq nF_{Rd,tie,+} \quad \text{with} \quad q_{tie} = q_h - x(q_h + q_d) \quad (5.4)$$

- *Masonry*

The load-bearing walls have the minimum height-to-length ratio of $(2.7/8.64) \pm 0.30$ to consider the walls as two-way bending. According to NEN-EN 1996-1-1, they are allowed to design as vertically spanned walls by ignoring this two-way action due to the vertical supports. In I.2 the response of any one-way bending wall due to a lateral load is described with the help of differential equations, boundary- and matching conditions. These walls can be schematized with a simple support at the top ($y = H$) and partially fixed support at the base ($y = 0$) due to the gravity action of the self-weight and dead load from the roof, floor and wall above, see Figure 5.4.

- *Concrete*

The concrete frame with its walls and floors do not need other stabilizing elements, so the edges where the walls and slabs are connected to the façades can be modelled as free edges. This makes it possible to approach the slabs as one-way spanning and consider the residence as a non-bracing frame, since the transfer of loads will be similar. The load-bearing wall of the third case-study residence spans over two floors, so the load-bearing wall can be approached as a beam on three supports (ground, first and second floor), see Appendix I.2 for the corresponding boundary conditions.

Non-linear elastic analysis

In the upper right of Figure 5.2b, the collapse mechanism for a two-way wall supported on all four sides is displayed. The base is clamped due to the normal force in the wall, the top is simply supported by the floor and the vertical edges are clamped due to the bonded piers, see Figure 5.5b and Appendix I.2. This mechanism is defined as the crack pattern which occur due to displacement of a series of plates concentrated as rotations in these crack lines.

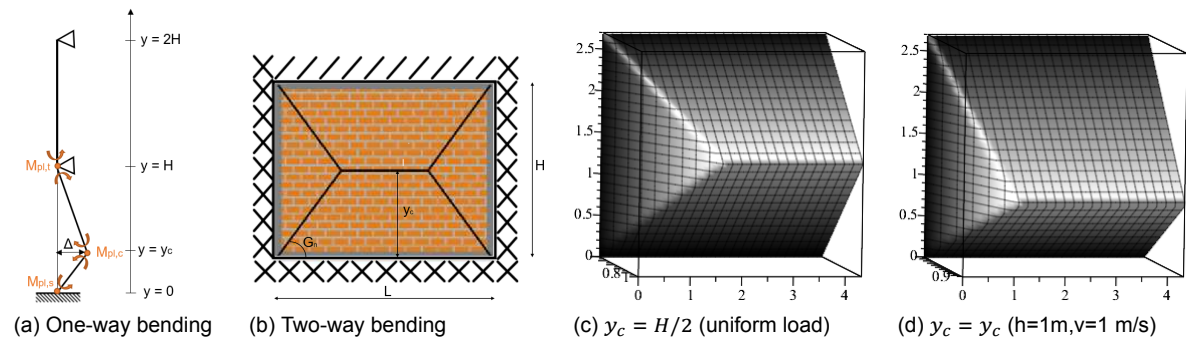


Figure 5.5: Crack patterns for half of the length of the wall due to a lateral load (based on Lawrence and Page (2013))

The assumption is made that the diagonal crack follows the natural slope of the masonry, G_n . In the Netherlands, most terraced houses are constructed in a half-overlap stretcher bond shown in Figure 5.9. Based on the nominal values found by Jafari et al. (2017) and the general thickness of the walls in Table I.1 the generally used sizes for bricks are derived: the clay bricks in LB1 have a 'Waalformaat' (100x210x50) and the calcium-silicate bricks in LB2 a 'Maas(120)-formaat' (120x214x82). Since the inner and outer leaf have the same thickness, it is assumed that both leaves consist of bricks in the same size.

Furthermore, the crack patterns from both the Eurocode as of the Australian code are based on uniform loaded walls, but the flood loads applied are not uniform. It is assumed that the location of the horizontal crack does not occur at mid-height as in the code but at the critical height, y_c , found from the one-way bending walls. The crack pattern belonging to the flood conditions in Figure 5.12 is assumed to be as shown in Figure 5.5d.

5.1.3. Stability

The floors function as horizontal supports for the load-bearing walls, so transfer the loads from these walls through the the stabilizing elements to the foundation. For the traditionally built case-study residences 1 and 2, the piers in the facade function as stabilizing walls. The piers on the edges of the facade, which are bonded to the party walls, are named engaged piers. The piers which are not bonded to a load-bearing walls are referred to as isolated piers. Case-study residence 3 gains the stability from the rigid connections between the walls and the floor.

Masonry

The width of the case-study residences is 5.4 meter, which have openings in the facade for the door (0.9 meters) and one or multiple windows (3 meters). This leaves three piers of 0.5 meters per residence acting as shear walls, see Figure 5.6a. When the horizontal force increases, the stress cannot be distributed linearly anymore. The most common failure modes of shear walls with a high aspect ratio like piers are rocking or toe crushing (Figure 5.6b) depending on the amount of vertical stress, where for lower aspect ratio diagonal tension cracks develop or sliding occurs. The pier is considered as a rigid body which rotates due to the in-plane inertial forces, but is restricted by the boundary conditions at the base and top. A crack occurs at the tension zone and opens up, so the effective area decreases leading to an increase of stress in the compression zone, L_c , until the maximum compression stress is reached and a full plastic hinge is developed.

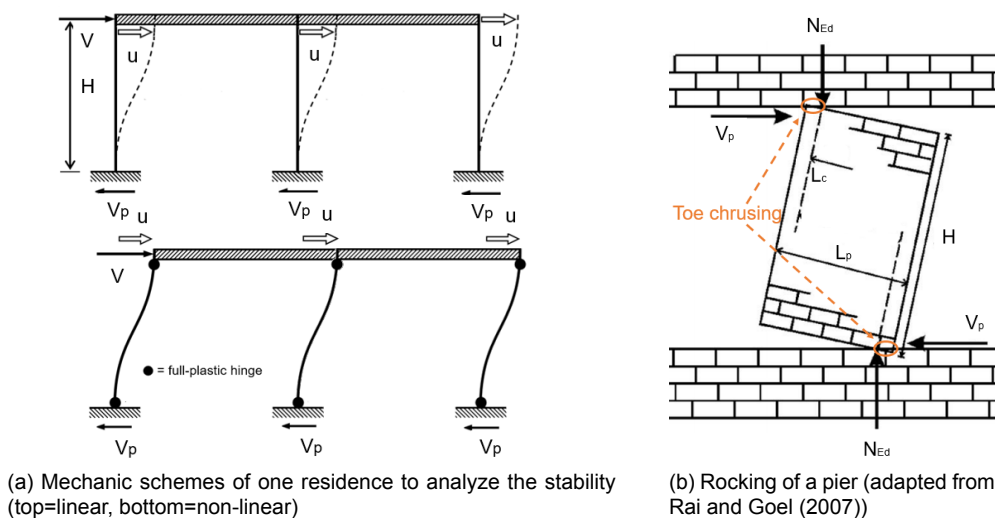


Figure 5.6: Schematization of piers for shear failure analysis

For of both case-study residences the distribution of the shear force is based on the relative rigidity of the piers despite the flexible diaphragm behaviour of the timber floor. The timber beams span in the same direction as the shear force (parallel to width of the residence), so can be considered rigid in this direction. This force distribution is similar to the one of the lateral load between the leafs of cavity wall in Equation 5.3, but since the piers consist of the same material, the distribution is solely based on the moment of inertia, see Appendix I.3. For both residences, the shear wall bonded to the party wall is subjected to the highest shear force.

Concrete

The party walls are assumed to provide the stability due to the larger thickness compared to the end-walls, respectively 250 mm and 120 mm, so the end walls can be schematized as 'pendelstaven'. The floor is continuous over multiple spans of 5.4 meters (width of a residence), so is assumed to have a thickness of 180 mm with $\pm 30 \text{ kg/m}^3$ reinforcement, corresponding with a net of $\text{Ø}8\text{-}150$ (VOBN). The flexural rigidity of these reinforced floors is approximately ten times bigger than those of the walls, so can be schematized as rigid similar to Figure 5.6a. The three party walls are equal, so the shear force can be equally divided over the three walls.

5.1.4. Windows

A window pane is approached as a simply supported thin plate as proposed by Kelman (2002). In case of double-glazed windows is assumed that the load will be shared between the two panes proportional to their stiffness similar as the cavity wall. The formulas of Westergaard and Slater (1921) approximate the moment for a uniform load on rectangular slabs by considering two strips in transverse direction through the center of the slab, see Figure 5.7.

The maximum deflection occurs in the center of the slabs and is equal in both strips. Since the shorter strip has a smaller radius of curvature, the stress is larger, so the moment in this direction will be governing. Due to the difference in distribution of the hydrostatic and hydrodynamic pressure will the maximum moment occur in different locations, so superposition of these moments is not feasible. An equivalent load, p_{eq} in Figure 5.8, is used to approach the maximum bending moment by spreading the linearly distributed hydrostatic load equally over the panel. Taking the Poisson's ratio into account, the bending moments at the center of the plate increase. Kelman (2002) gives an overview of the Poisson ratio for float glass and from that an upper value of 0.25 is used to approximate the governing moment in the plate with Equation 5.5.

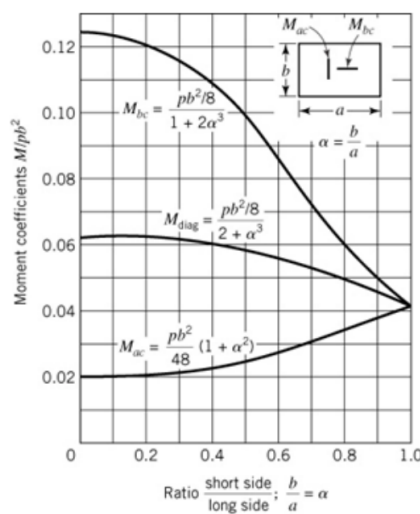


Figure 5.7: Bending moment coefficient, β (Westergaard and Slater, 1921)

$$M_{bcv} = M_{bc} + \nu M_{ac} = (\beta_b + \nu \beta_a) p b^2$$

$$M_{Ed} = \beta_v p_{eq} H_g^2 \quad (5.5)$$

with $\beta_v = \nu \frac{1+\alpha^2}{48} + \frac{1}{8+16\alpha^3}$

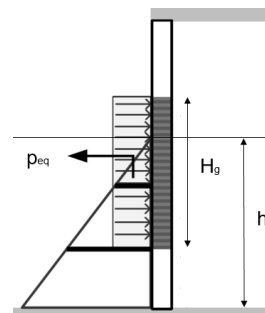


Figure 5.8: Equivalent load on window (adapted from Chen (2016))

5.2. Resistance

During flooding, the load-bearing walls need to resist the out-of-plane lateral load, so the bending moment and shear resistance is determined. If the non-structural elements such as the windows and the doors fails, different loads act on the wall, so the resistance of these elements are also of interest.

5.2.1. Load-bearing walls

The materials used for the structural walls, both load-bearing and stabilizing walls, have a high resistance in compression, but are vulnerable for tensile stresses. The walls are designed to withstand mainly gravity loads and wind loads, which do not lead to high tensile stresses, so reinforcement is in most walls not implemented. When higher lateral loading due to flooding occurs, these stresses can lead to brittle failure behaviour resulting in cracks in different directions shown in Figure 5.9.

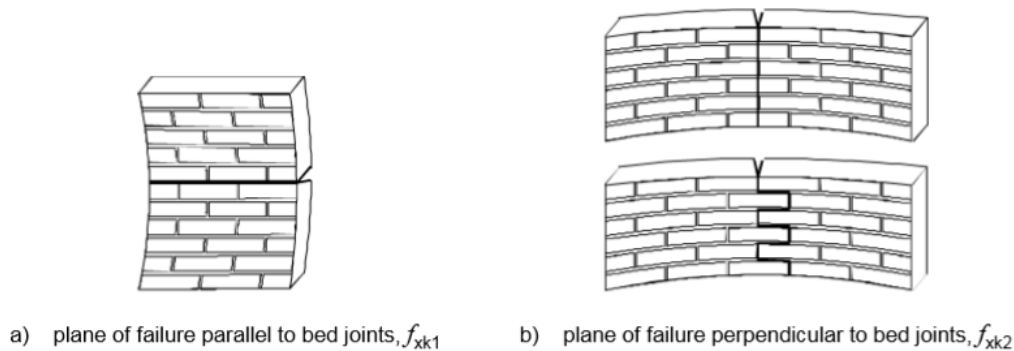


Figure 5.9: Planes of failure of masonry in bending (NEN-EN 1996-1-1+A1)

Linear elastic analysis

Distinction can be made between failure in the plane parallel to the bed joints due to a bending moment over the height of the wall (Figure 5.9a) and failure due to a bending moment over the length of the wall resulting in the failure plane perpendicular to the bed joints (Figure 5.9b). Concrete is an isotropic material, so the material properties are similar in both directions. For unreinforced concrete walls the direction of the cracks are similar as those in masonry. The used material properties of all materials can be found in Appendix G.2.

When looking to the the bending moment resistance over the height of the wall, M_{Rd1} , the vertical load due to self-weight and life load on the walls causes a compression stress, which has a favourable effect for the stresses in the cross section. In Figure 5.10 the linear-elastic stress distribution for this cross section is drawn, so before cracks occur. The minimum amount of vertical load is assumed to consider the worst case scenario, so when the wall is only carrying the dead weight of the walls and floors above. For the design moment resistance over the length of the wall, M_{Rd2} , no normal stresses are assumed ($\sigma_n = 0$). The moment resistance depends solely of the flexural strength of the material. A crack in the wall occurs if the acting moment calculated with the differential equations in I.2 is larger than the moment the wall can resist in Table 5.1.

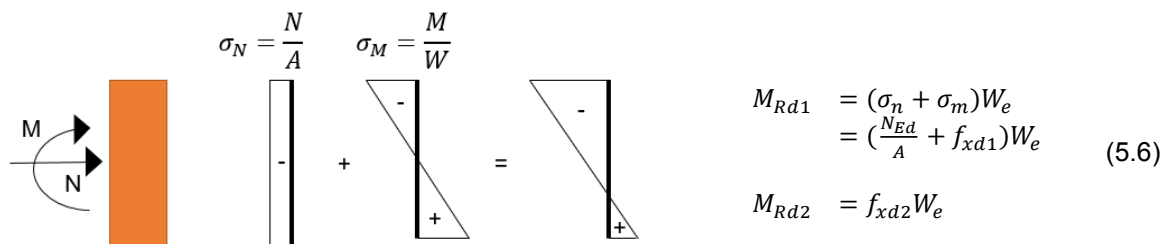


Figure 5.10: Stresses in cross section (linear-elastic beam theory)

Table 5.1: Moment resistance of lower walls (derivation of strengths in Appendix G.2)

Case	t [mm]	σ_n [MPa]	f_{xk1} [MPa]	f_{xk2} [MPa]	M_{Rd1} [kNm/m]	M_{Rd2} [kNm/m]
1:LB URM clay	100-50-100	0.13	0.29	0.81	0.59	1.04
2:LB URM CS	120-60-120	0.32	0.14	0.51	1.03	0.94
3:LB URC	120-60-120	0.30	1.55	1.55	3.95	3.10

Non-linear elastic analysis

The residual or post-cracking strength is obtained by the development of the moments along the crack lines. For every wall configuration there is a typical crack pattern found by various experimental studies, which are the base of plastic analysis, such as the 'virtual work-method' used in the Australian masonry code (AS 3700). It uses the principle of energy conservation by determining the internal work, E_{in} , which sum should be equal to the external work, E_{ex} , see Equation 5.7. The internal work is provided by the rotation of the wall, θ_i , along the cracks lines, l_i , multiplied by the moment resistance, $M_{Rd,i}$, along these cracks lines. The external work is caused by the applied load, q , multiplied by the displacement of the wall, u_i .

$$E_{ex} = E_{in} \quad \text{with} \quad \begin{cases} E_{ex} = \sum_{i=1}^n \int_{y_{Ai}}^{y_{Bi}} \int_{x_{Ai}}^{x_{Bi}} q(x,y) u_i(x,y) dx dy \\ E_{in} = \sum_{i=1}^n M_{Rd,i} l_i \theta_i = M_{Rd,v} l_v \theta_v + M_{Rd,h} l_h \theta_h + M_{Rd,d} l_d \theta_d \end{cases} \quad (5.7)$$

This method uses the assumption that the full moment capacities along the diagonal and vertical cracks are reached simultaneously. The moment contributions along horizontal crack lines are ignored in the code, since they form early in the damage process. The crack patterns of the loaded walls in the experiments of Vaculik (2012) however showed that the horizontal and diagonal cracks are fully developed when the ultimate strength is reached, while the vertical cracks are partially developed. The failure modes consists of a combination of different kind of cracks, which all three have their independent analytical expressions based on AS3700 adapted by (Vaculik, 2012):

- *Horizontal cracks (Figure 5.9a) due to vertical bending:*

The vertical moments due to gravity action during opening of the horizontal cracks will contribute to the ultimate strength of the wall (Vaculik,2012). Neglecting these contributions as prescribed by AS3700 will lead to a too conservative outcome, since the walls in the terraced houses have a high L/H-values, so long horizontal cracks are expected to form. The contribution of this residual moment is equal to the value calculated in the one-way bending analysis in Equation I.1. These moments will be present along both the crack at the base of the wall and at the critical height, y_c .

This residual bending moment capacity can be included to find a more realistic moment capacity of the wall after the linear bending stress is reached. The cracked section opens, so the normal stresses due to the vertical load should be transferred to the foundation through a smaller contact area, see Figure 5.11. The section is fully cracked, so no bond strength is present and it is assumed that the blocks above and below the crack behave as rigid blocks. This results in uniform stress along the contact zone, but a reduction factor should be applied to take into account the idealizing behaviour, which can be found between the brackets in Equation 5.9. The maximum moment can be reached when the masonry is crushing, which can be approximated in a similar way as reinforced concrete with the factor $\alpha_{cc} = 0.85$.

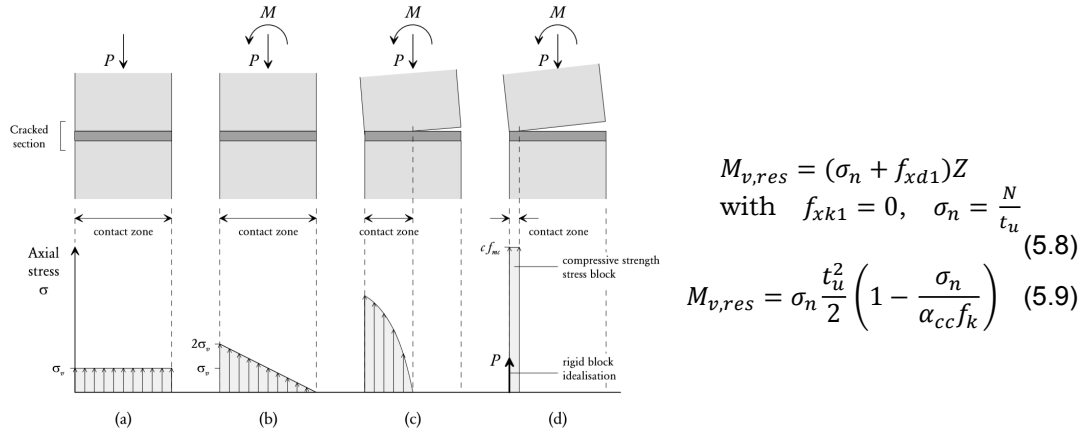


Figure 5.11: Normal stresses along a cracked section (Vaculik, 2012)

- *Vertical cracks (Figure 5.9b) due to horizontal bending:*

AS3700 assumes that the crack can develop in two different ways: in a straight line following the head joints (56% according to Equation 5.10) and cutting through the brick units (44%) or following the bed and head joint alternately resulting in stepped failure. In reality there are two parallel paths for a local crack to develop further depending on the material strength, so the mixed failure mode is lower than the individual modes. To take this variability of strength into account, the code prescribes a capacity reduction factor $\phi = 0.6$ for design of URM walls in flexure, which is sufficient to cover this effect according to Vaculik (2012).

$$M_{Rd,h} = \min \begin{cases} \Phi(0.44f_{ku}Z_u + 0.56f_{xk2}Z_p) & \text{for line failure} \\ 2.0\Phi k_p \sqrt{f_{xk2}} \left(1 + \frac{\sigma_n}{f_{xk2}}\right) Z_d & \text{for stepped failure} \end{cases} \quad (5.10)$$

The internal bending moments from diagonal cracks are gradually redistributed to the vertical cracks along the edges, which have some degree of rotational restraint due to the return walls. It is assumed that the ultimate strength is reached after the point where the moments along the diagonal cracks start reducing and before the vertical cracks are fully developed (Vaculik, 2012). Since the degree of development of these vertical crack are hard to predict, the moment resistance along the vertical cracks at the fixed connection with the shear walls are not included. This will lead to a slightly conservative value for the ultimate strength. After cracking, the wall separates from the vertical support, so is subjected to one-way bending and zero residual strength is obtained from this line failure.

- *Diagonal cracks due to diagonal bending:*

The ultimate moment resistance is obtained by a combination of flexure and torsion acting along the joints. Willis (2004) gives an analytical solution for this moment capacity based on the orthogonal ratio of the material and the assumption that only the bed joints contribute to the ultimate resistance:

$$M_{Rd,d} = M_{Rd,1} [\cos(\phi)^4 + \eta \sin(\phi)^4] \quad (5.11)$$

5.2.2. Stability

If the net horizontal load on the row of residences is larger than the shear resistance of both the engaged and isolated piers together, the total row has become unstable. NEN-EN 1996-1-1 art.6.2. only prescribes the resistance against sliding along a straight crack at horizontal bed joint as in-plane shear resistance, since cracking is considered as ultimate limit state. URM walls have some ductility as shown before in the non-linear analysis of bending of the load-bearing wall due to opening of the crack.

Linear elastic analysis

Compression in the cross section due to the normal force increases the shear resistance of the cross section similar to the bending moment resistance. A small part of the compression stress helps to resist the lateral load, see Equation 5.12. Only the part of the pier which is compressed, L_c , is able to transfer the shear force. No crack is allowed in this failure mechanism, so a linear elastic stress distribution is used to find this length. The total shear force can be determined for the different piers with the relative rigidity's, RR , from Table I.2 and Equation 5.14. The lowest value for the total shear force is found for the longest pier, since the portion this pier has to bear is the highest, leading to the value found in Table 5.2.

$$f_{vk} = f_{vk0} + \mu\sigma_n \leq 0.065f_b \quad \text{with} \quad f_{vk0} = f_{xk1} \quad (5.12)$$

$$V_{Rd,p} = f_{vd}tL_c \quad \text{with} \quad L_c = 3\left(\frac{L_p}{2} - \frac{V_{Rd}H}{N_{Ed}}\right) \quad (5.13)$$

$$V_{Rd} = \min \frac{V_{Rd,p}}{RR} \cdot 100\% \quad (5.14)$$

In the ultimate limit state, the tension strength of the unreinforced concrete is allowed to take into account to determine the shear resistance per meter width of the wall with Equation 5.15 (NEN-EN 1992-1-1+C2 art.12.6.3). The limited ductility should be accounted for in Equation G.3 by using $\alpha_{ct,pl} = 0.8$ in stead of $\alpha_{ct} = 1.0$ (NEN-EN 1992-1-1+C2/NB art.12.3.1). The shear force per meter length of the residence is approximately equal to the total shear force of the other residences, so this failure mechanism is further elaborated for case-study residence 1 and 2 only.

$$V_{Rd,i} = \frac{f_{cvd}L_c}{k} \quad \text{with} \quad \begin{cases} k = 1.5 \\ \sigma_{c,lim} = \frac{f_{cd,pl} - 2\sqrt{f_{ctd,pl}(f_{ctd,pl} + f_{cd,pl})}}{k} = 8.11\text{MPa} \geq \sigma_n \\ f_{cvd} = \sqrt{f_{ctd,pl}^2 + \sigma_n f_{ctd,pl}} = 1.12\text{MPa} \end{cases} \quad (5.15)$$

Table 5.2: Linear analysis of shear strength of a pier with a length of 0.5 meter

	f_{xk1} [MPa]	μ [-]	f_k [MPa]	σ_n [MPa]	f_{vd} [MPa]	L_c [mm]	$V_{Rd,p,l}$	$V_{Rd,l}$
1	0.29	0.89	6.64	0.04	0.52	12.8	0.39 kN	5.97 kN
2	0.14	0.43	5.05	0.04	0.17	36.6	0.36 kN	5.43 kN
3	1.55	-	20	0.17	1.12	2.6	1.93 kN/m	5.79 kN/m

Non-linear elastic analysis

Similar to the linear elastic calculation, the longest pier will reach its rocking strength, described in Equation 5.16 (FEMA 273 art.7.4.2), before the other piers do. The cracks opens up and grows horizontally from the corner under compression towards the other end of the pier. This pier cannot bear a higher load, but due to some ductility of the material it is assumed the pier can deform while maintaining this ultimate load. If additional lateral force is applied to the residence, the other piers take a higher percentage of the load. A different distribution of the load causes the other piers to crack as well until all the piers are cracked and the row of residence becomes unstable. The residual strength from redistribution of the load can be determined with Equation 5.17.

$$V_{Rd,p,nl} = 0.9\alpha N_{Ed} \frac{L_p}{H} \quad \text{with} \quad \alpha = \begin{cases} 1 & \text{fixed-fixed pier} \\ 0.5 & \text{fixed-free cantilever wall} \end{cases} \quad (5.16)$$

$$V_{Rd,res} = 2N \left(V_{Rd,p,nl} - \frac{V_{Rd,nl}}{100} RR_p \right) \quad (5.17)$$

Table 5.3: Non-linear analysis of shear strength of a pier with a length of 0.5 meter

	$V_{Rd,p,nl}$ [kN]	n [/facade]	RR [%]	$V_{Rd,nl}$ [kN]	$V_{Rd,res}$ [kN]	$V_{Rd,ult}$ [kN]
1:engaged	0.72	6	1.80	-	6.23	
engaged	1.43	3	13.08	10.94	-	17.16
2:isolated	0.34	4	0.89	-	1.42	
engaged	0.68	2	3.42	-	1.31	
engaged	1.36	3	13.20	10.28	-	13.01

Allowing cracks in the pier, almost doubles the shear strength of the pier. The total shear force the total row of 4 residences can resist increases from 5.97 to 10.94 kN for case-study residence 1 and from 5.43 to 10.28 kN for case-study residence 2. If the residual strength is also taken into account, this strength increases to respectively 17.16 and 13.01 kN.

5.2.3. Non-structural elements: windows

As stated in the description of most common failure mechanisms of the residences in Section 3.3, the failure of non-structural elements leads to openings in the facade. The acceptable failure probability as result of an accidental load is 10^{-5} per year (NEN-EN 1991-1-7+C1/NB art. 3.2), which for example corresponds to a failure probability of the material of 99% with an event with a return period of approximately 1000 years according to Equation 5.18. The probability of flooding in the Netherlands is much lower, so using strength of glass of 80 MPa which correspond with 99% failure probability is still on the conservative side. This gives a bending moment resistance of 0.21 kNm/m for single glass (4 mm) and 0.55 kNm/m for double glass (5-15-4 mm), where the resistance is equal to the summation of the panes according to Equation 5.19. If the bending moment due to the applied loads from the flooding is higher than the moment resistance, the glass will fail and water can enter the residence.

$$p_f = p_{f,m}^N = 0.99^{1000} = 4 \cdot 10^{-5} \quad (5.18)$$

$$M_{Rd} = \sigma_{Rd} W = 80 \cdot \frac{1}{6} (t_{g,inner}^2 + t_{g,outer}^2) \quad (5.19)$$

The Dutch code NEN 6702 provides tables with the bending moment coefficients for a number of slabs with various boundary conditions. These coefficients are obtained from a linear elastic calculation of a concrete slab under uniformly distributed load. Since the poisson's ratio of uncracked concrete and glass are close to each other, the coefficients belonging to panel I are used as comparison. Also the values of Chen (2016) are used to compare in Table 5.4, which are all just below the values found with Equation 5.5. This difference can be explained by the choice of a larger poisson's ratio in this study.

Table 5.4: Window pane

Height [m]	Width [m]	α	β_v	β_{NEN}	β_{Chen}	$\rho_{Rd,single}$ [kPa]	$\rho_{Rd,double}$ [kPa]
1.80	2.80	0.64	0.090	0.076	0.084	0.74	1.90
1.30	1.30	1.00	0.052	0.041	0.048	2.42	6.21
1.30	0.65	0.50	0.107	0.097	0.102	4.74	12.15

5.3. Structural damage

The moment resistance of the different elements is compared with the flood load acting on these elements for the two different load combinations as defined in Section 4.3:

1. Hydrostatic + quasi-steady hydrodynamic load
2. Hydrostatic + hydrodynamic wave load

5.3.1. Load-bearing walls

The first crack will form at the base of the wall ($y = 0$), because the hogging moment exceeds the flexural moment of resistance, M_{Rd} , before the sagging moment at the critical height ($y = y_c$) does (Appendix I.2: Figure I.2). If the acting moment at the base exceeds the flexural moment resistance, the stress distribution is not linear-elastic anymore, so a crack starts to develop at the base. Although the floor is not fixed to the wall, it prevents the wall from deforming due to the eccentricity of the normal force generating an additional moment. If more load is applied, the crack at base will open until this stability moment at the base is reached, $M_{stability}$.

An example is given for case study residence 1 subjected to a water depth of 0.75 meters and a flow velocity of 1 meter per second in Figure 5.12. With the help of a simple 'forget-me-not' the moment at the base is calculated, which is slightly higher than determined with the differential equations due to the use of point loads in stead of distributed loads. For small flow velocities, the hydrostatic pressure predominate (see Figure 5.12a), leading to a crack at the base of the wall at a water depth of 0.75 meters already:

$$\begin{aligned}
 F &= F_H + F_D = \frac{1}{2}\rho gh^2 + \frac{1}{2}C_p\rho v^2 h &&= 3.51 \text{ kN/m} \\
 y_F &= \frac{F_H \frac{h}{3} + F_D \frac{h}{3}}{F} &&= 0.28 \text{ m} \\
 M_{base} &= \frac{F(H - y_F)(H^2 - (H - y_F)^2)}{2H^2} = 0.82 \text{ kNm/m} < M_{stability} = 0.84 \text{ kNm/m}
 \end{aligned}$$

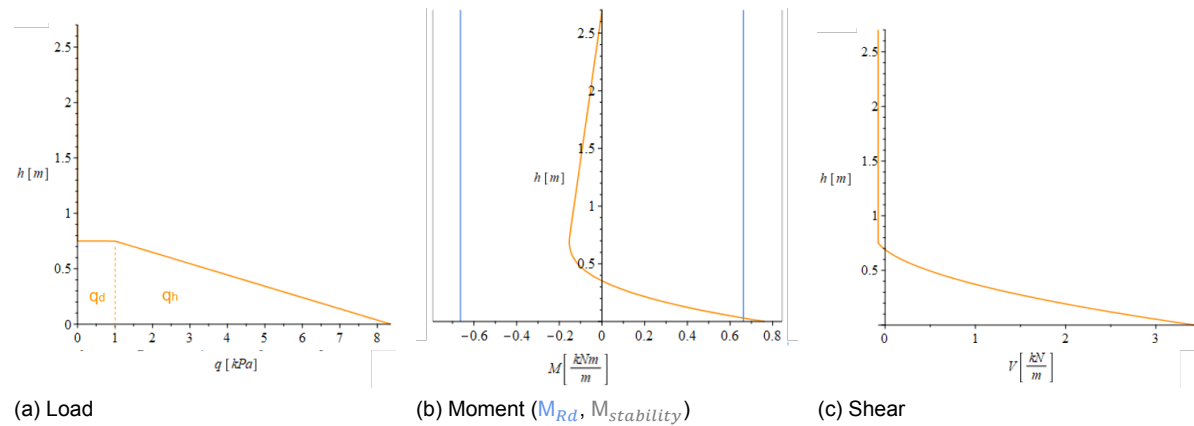


Figure 5.12: Load, acting moment and shear force in the wall ($h = 0.75$ m and $v = 1$ m/s)

In Figure 5.13 is shown for which flood conditions the wall is stable (green area) according to the linear elastic analysis, so when the flexural moment of resistance is larger than the acting moment. The yellow area resembles the combinations leading to opening of the the first crack until the stability moment is reached. Due to this rocking strength, the wall will not collapse due to the flood conditions from the example.

When the crack is totally opened, redistribution of the loads causes an increase of the sagging moment until the ultimate strength is also reached at this location. Due to the ductility of the masonry and concrete, it is assumed that the ultimate moment resistance at the base remains constant while the crack at the critical height develops to ultimate strength as well. The additional moment resistance due to redistribution of the forces is shown in Figure I.2. For case-residence 1 and 2, two-way bending of the wall allows additional moments to develop along the diagonal cracks. This is shown in Figure 5.13 as the orange area, where also the horizontal crack at the base, the critical height and top are fully developed. For case residence 3, also additional moments are assumed to develop at the critical height and at the top, but one-way bending is still applied as schematized in Figure 5.5a.

The failure graphs for the hv -combinations and the wind-generated wave load from a fetch of 100 meters are shown in Figure 5.13. The influence of the fetch is shown in Figure I.3, which shows a small difference especially for higher wind speeds. The differences between the rocking strength of the case-study residences imply that the influence of the dead weight carried by the wall in combination with the compression strength and thickness of the wall, is larger than the flexural strength of the wall. Furthermore, the residual moment resistance due to the two-way bending is quite large compared to the residual moment of case-study residence 3. All residences will fail under considerable lower water depths and flow velocities than the Clausen criteria of $h \cdot v \geq 7 \text{ m}^2/\text{s}$ displayed as the black line.

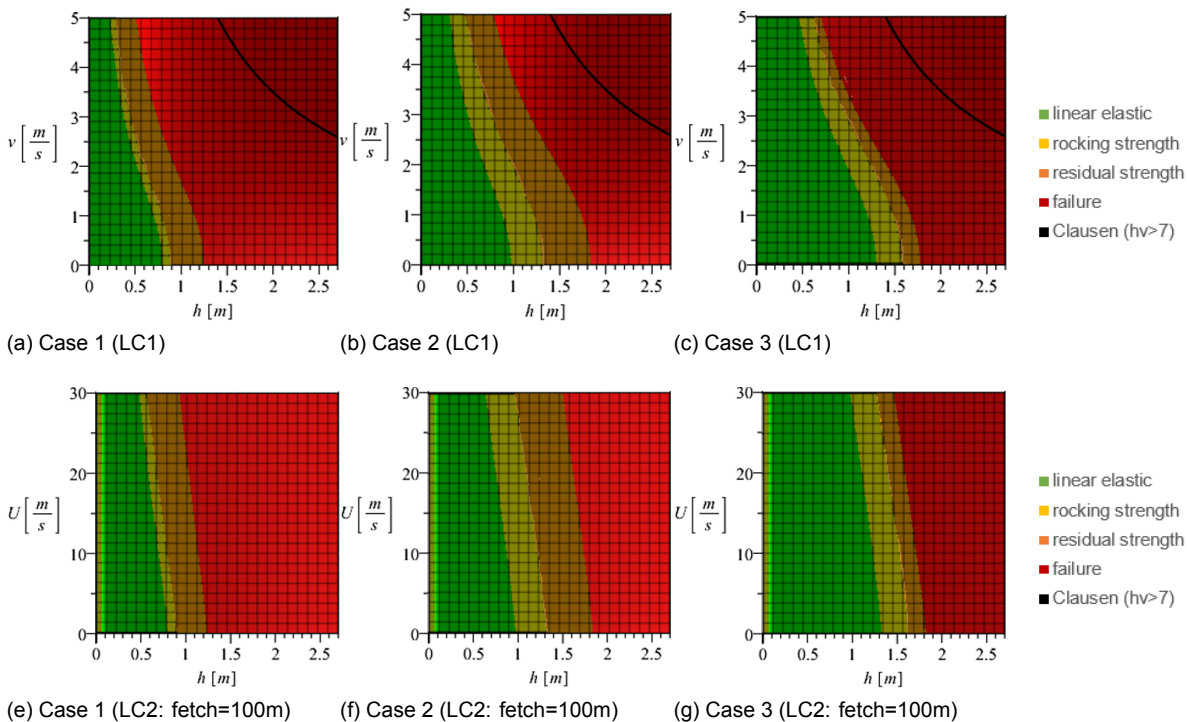


Figure 5.13: Failure graphs from nonlinear analysis for load combination 1 (a,b,c) and 2 (d,e,f) for all three case-study residences

The total resistance of the cavity wall depends on the capacity of the load-bearing inner leaf, outer leaf and the ties connecting the two leaves. The inner leaf should be able to resist the total force to prevent the residence from collapsing if the outer leaf fails under this load or the capacity of the ties is exceeded. The latter occurs when the maximum tension or compression force in the ties is reached due to the difference in hydrodynamic load on the outer leaf and hydrostatic load on the inner leaf according to Equation 5.4. Appendix J.1 shows for load combination 1 that more capacity is obtained when the load can be distributed between the leaves. However, the ability of the wall ties to transfer the force before being pulled or pushed out, depends strongly on the location.

5.3.2. Shear walls

Different than the local loads used to analyze failure of the windows and walls, the net force should be taken into account. The hydrostatic load is assumed to be equal on both sides, so only the hydrodynamic load causes a horizontal load on the row of residences. The positive pressure on the front wall and negative pressure on the rear should be combined, leading to the drag or wave load as only horizontal load. This net load will be divided over the support at the base of the wall and the top. Only the part of the load which is transferred to the first floor, so the shear force in the top of the wall is of importance. This load, V_{Ed} , can be determined to multiply the shear force at $y = H$ from the linear analysis of one-way bending of the load-bearing walls (Equations in I.2) with the length of the residence. The shear force per meter length of residence 3 is approximately equal to the total shear force of the other residences, so this failure mechanism is not expected to occur for case-study residence 3.

From Figures 5.14a and 5.14b, it can be seen that the difference between failure of the shear walls from the two different case-study residences is mainly due to their residual strength. Both the case-study residences fail before the Clausen criteria is reached, shown as the black line. For load combination 2, the influence of the fetch is also visible by comparing Figure 5.14d with 5.14e and Figure 5.14f with 5.14g. An increase of this length from 0.1 km to 10 km causes collapse of the residence for smaller water depth-wind velocity combinations.

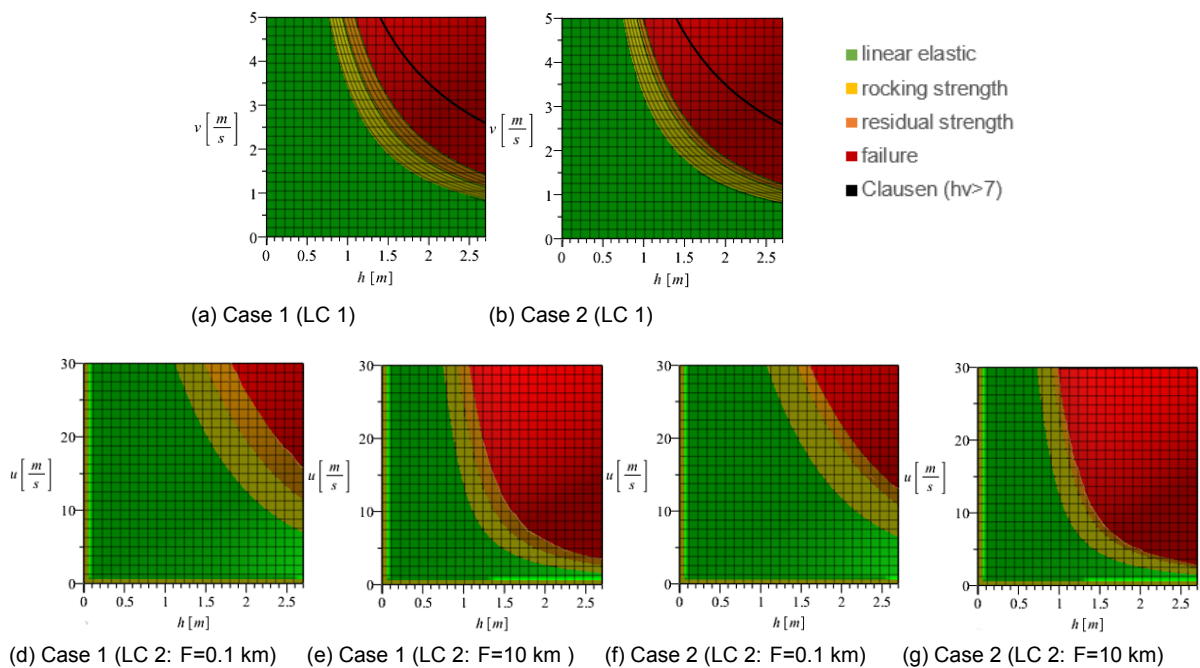


Figure 5.14: Failure graphs from nonlinear analysis for load combination 1 and 2

5.3.3. Conclusions on structural damage

The generated failure graphs in the previous sections show that out-of-plane bending of the load-bearing walls is critical compared to shear failure for both the load combinations. Furthermore, if the ties fail, there is no longer an interaction between the two leaves, so the load-bearing inner leaf should be able to resist all the load, $\alpha = 1$. Combining the failure-graphs of the inner leaf bearing all the load by itself (Figure 5.13a and 5.13b) with the failure-graphs of the inner leaf bearing part of the load due to the interaction with the outer leaf (Figure 5.15a and 5.15c) give Figure 5.15b and 5.15d.

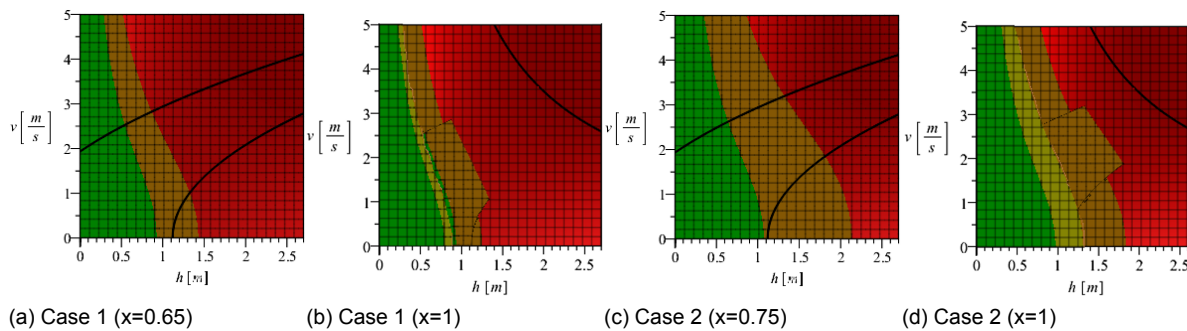


Figure 5.15: Failure graph for inner load-bearing leaf with tie failure included

The moment resistance shows an increase for only a small number of water depth-flow velocity combinations. Since these combinations depend highly on the location and conditions of the ties, it is advised to exclude the influence of the outer leaf on the resistance of the residence. Furthermore, it is assumed that the windows are placed in the façade, so along the width of the residence. In the critical orientation for collapse, the flow or wind direction is parallel to the façade where the windows are placed. The pressure coefficient, or wave impact due to the wind, becomes smaller than used in the failure graphs in Appendix J.2, leading to higher flow velocities before the windows fail. In the critical orientation, the load-bearing walls fail due to out-of-plane bending before the windows fail.

Only a few geometries and case-study residences are considered, but based on the pressure coefficients determined from the physical experiments and resistance of the case-study residences the following conclusions can be drawn:

- Adding residences to the row or considering wider residences results in a longer side aligned with the flow, L' , so a higher side ratio and a lower h/L -ratio for equal water depths. The L/B ratio causes an increase in drag coefficient and the decrease of the h/L -ratio does not make a significant difference. Overall, the pressure on the front face of the building (load-bearing wall of the corner residence) increases, so collapse will occur at smaller water depth-flow velocity combinations.
- Residences with a longer load-bearing wall result in a longer side parallel to the flow, B' , so a smaller side ratio and larger aspect ratio. Both changes in the ratio cause an increase in drag coefficient. In addition, the load-bearing walls will primarily span vertically, so influence of the moment resistance along the diagonal cracks becomes negligibly small. Failure is expected to happen due to smaller flood conditions than determined in Section 5.3. On the other hand, if partition walls are positioned perpendicular to the load-bearing walls, these can function as additional vertical supports. These supports prevent the load-bearing wall from bending at this location, so smaller moments are created due to the flood conditions, resulting in higher moment resistance.
- In case the window is located lower or the window has a larger area than assumed above, a smaller combination of the water depth and flow- or wind velocity can be resisted by the window before it breaks and the water level will equalize inside the residence. An equal hydrostatic water depth outside and inside the residence results in a smaller net load on the walls, so these walls can withstand higher combinations of the water depth and flow- or wind velocity than before failure of the windows.
- The inner leaves of the load-bearing walls are placed on top of the ground floor slab which is assumed to be at ground level (Figure 5.4a). The water depths in this study are all with respect to the base of the wall. If this reference level is elevated, the difference in elevation should be added to the water depth in this study to present the real situation.
- Calculations are conducted with the permanent load only, but also a variable load is allowed to take into account according to NEN-EN1990+A1+A1/C2 (load combination

6.11b). This gives an additional floor load of 0.53 ($\psi_2 q_k = 0.3 \cdot 1.75 = 0.53 \text{ kN/m}^2$), which provide an increase of the moment resistance of the walls. To approximate the real failure values more closely, the failure graphs from Figure 5.13 are recreated in Appendix K including this additional load. Also the characteristic strengths, f_{xk} , are used instead of the design strength, f_{xd} , and the safety factor, $\gamma=0.9$, for the dead load is excluded. For case-study residences 2 and 3, this gives an additional water height of $\pm 0.20 \text{ m}$ that can be resisted before the residence collapse. The difference for residence 1 and the combinations causing the first crack is smaller than 0.10 m .

Comparison with other studies

To place the outcome in perspective, the created failure graphs are compared with those from the studies of Korswagen Eguren (2016) and Kelman (2002). Korswagen Eguren (2016) shows that the boundary conditions are not relevant for the linear elastic analysis of a thin URM wall subjected to one-way bending due to a hydrostatic lateral load. The first crack occurs at comparable water depths for a wall clamped at the top and bottom, pinned on both ends and a combination of those. For a wall subjected to only self-weight (1 kN/m), the first crack occurs at a water depth of ± 0.70 meters and loss of stability is expected at almost the same water depth. For walls subjected to a higher axial load, for example due to the heavier system floors ($\pm 40 \text{ kN/m}$), a water depth of ± 1.00 meters causes the first crack, where a water depth of ± 1.25 meters causes a loss of stability.

The hv -combinations in the coloured area in Figure 5.16a resemble the first crack until the development of multiple cracks leading to mechanism according to linear elastic analysis. The values for the first crack, \bullet , and loss of stability, \times , of Korswagen Eguren (2016) show to be comparable with the values found from one-way bending of case-study 1 and 2 with zero flow velocity or wave height.

Kelman (2002) also used yield line analysis to find the ultimate lateral load a URM cavity wall can resist. Calculations are made for several hv -combinations for different kind of wall geometry and loads. The two storey-residence with a surface area of 55 m^2 is closest to case-study residence 1, so these results are shown in Figure 5.16b as 'light'. As concluded before, the load carried by the wall is of great importance, so also the results for adding an additional storey ('heavy') is displayed to take into account the higher load for case-study residence 1.

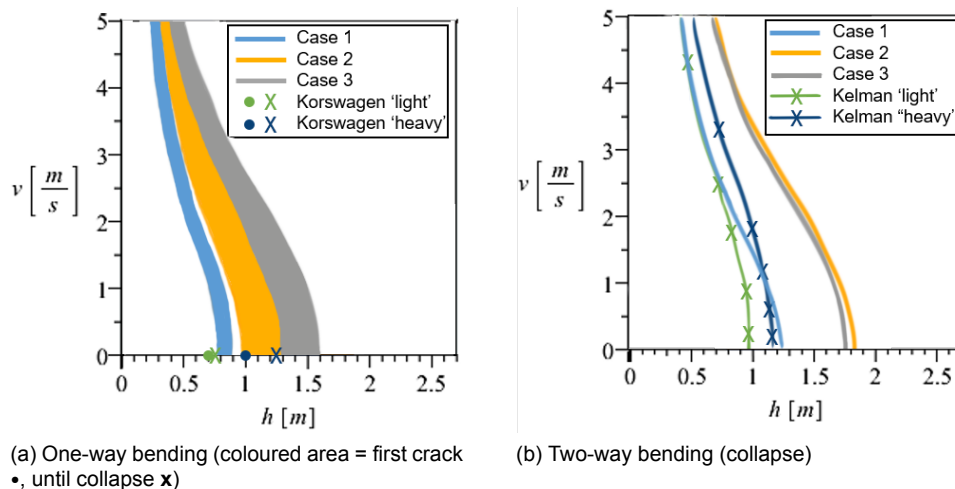


Figure 5.16: Comparison of current failure lines with those from Korswagen Eguren (2016) and Kelman (2002) with case 1: clay masonry walls with timber floors, case 2: calcium silicate masonry walls with system floors, case 3: casted concrete walls and floors

The differences between the case-study residences, also visible in Figure 5.16b, can be explained by looking to the sensitivity analysis of Kelman (2002) for the hydrostatic load to determine the influence of the parameters on the results:

- *Geometry:*

In this study, a height of 2.7 meters is used instead of 2.4 meters, which results in an additional water depth of 1 cm that can be resisted, so the difference in used height can be neglected. A wider wall is also used (8.64 m vs. 5 m), which approaches the one-way bending closer than the wall used by Kelman, but this difference seems to be negligible as well. A smaller width, however, shows a significantly higher water depth that can be resisted by the wall.

- *Load:*

In the current study, the dead load of the roof and floors are approximately double the magnitude of those used by Kelman, resulting in an additional water depth of 0.19 meters which the wall can resist according to the sensitivity analysis. The density of the masonry is also heavier in this study (1800 kg/m^3 vs. 1000 kg/m^3) resulting in an additional water depth of ± 0.11 meters. Furthermore, since fresh water is assumed to cause the flooding whereas Kelman uses seawater with a larger density (1000 kg/m^3 vs. 1026 kg/m^3), a small additional water depth is expected to be resisted by the wall.

- *Vulnerability matrices:* (Appendix B.1)

Also, vulnerability matrices are developed by Kelman (2002) for different residences with the flood depth along one axis and the flood velocity along the other axis. The cells present the expected damage scale based on failure of the URM cavity walls, glass failure and rise-rate of the flood water inside the residence. The rise-rate inside the residence depends mainly on the external residence perimeter, which is smaller for terraced houses since only two, or three for the corner residence, out of the four are exterior walls. Also, it is assumed the glass will fail at smaller h_v -values, since Kelman assumed both panes take half the load instead of changing the second moment of inertia as used in Appendix J.2. The differences in the rise-rate and windows failure could change the damage scales for the current case-study residences.

6

Discussion, Conclusions and Recommendations

This chapter presents the final remarks on the study. First, the application, interpretation, and implementation of the results due to the used methodology of the experiments and structural analysis are discussed. Subsequently, the research questions formulated at the start are presented followed by the conclusions. Finally, the study is concluded by recommendations on how to continue improving the determination of flood load on buildings and approaching realistic values of the flood conditions leading to collapse of the residence.

6.1. Discussion

The limitations, simplifications and assumptions due to the scope of the study are addressed followed by the insights that have been obtained to explore the significance of the study.

Methodology of the experiments

Creating a dam break wave can be done using several methods, all of which have their pros and cons. Using a finite reservoir results in a short interval where the flow is quasi-steady. As expected, due to the finite amount of water in the reservoir, the plateau-value (Ritter, 1892) for the water depth and corresponding flow velocity cannot be reached during this interval. Where a constant water depth is reached at a smaller value than the plateau-value, the flow velocity is larger than the value found by Ritter (1892). Furthermore, the time of rising and falling of the water level cannot be scaled to a real flood.

Another aspect of this method is the generation of a dam-break wave with a relatively short period leading to effects of unsteady flow. The Morison equation describes the load due to the movement of the water with the drag force and an inertia force due to the added mass. This last component is assumed to be small in comparison to the drag component due to the quasi-steady flow conditions. However, the unsteady force component could be high enough to make a significant difference between the different orientations and impoundment depths. The Keulegan-Carpenter number is often used to describe the relative importance of the drag component over the inertia component for bluff bodies in oscillatory flow. This parameter can be used to validate the assumption that the inertia component is negligible. On top of that, if dynamic loads appear to be more important than expected, the dynamic response of the residence could change the failure mechanisms.

$$F_{Morison} = \underbrace{\frac{1}{2} C_D \rho v^2 B}_{F_D(\text{drag})} + \underbrace{\rho C_M B L \frac{dv}{dt}}_{F_M(\text{inertia})} \quad (6.1)$$

The accuracy of the experimental data is not investigated. The temperature of the air and water during the calibration process could be different than those during the experiments. This can cause a minor difference in the offset of the velocity sensor and the pressure sensors. A difference is also observed if the velocity sensor stays submerged for a while or is subjected to a sudden wave. To minimize these effects on the results, all the runs for a certain set-up are conducted on the same day and the calibration functions are derived 6 weeks before the last experiments were conducted.

Interpretation of the results

Looking more closely at the interpretation of the results from the experiments, it is questionable which water depth and flow velocity should be used for the calculation of the loads on the building. The flow velocity used in the damage and mortality functions from the current flood models is not simulated correctly due to the spatial scale and used roughness (De Bruijn and van Kester, 2015). The development of the newer models with a higher resolution can make it possible to obtain local flood characteristics per neighbourhood or even per building. In the current study, both the water depth and velocity which are measured without the building being present, are used for the calculation of the pressure coefficient. However, the building being there influences the flow conditions, leading to different flood characteristics resulting in different loads.

In general, more data points lead to more reliable results. By isolating a certain variable and changing this while keeping the others constant, the influence of this variable can be found more accurately. A small number of experiments for the building at its critical orientation (long side aligned to the flow) are conducted for water depths where collapse initially was expected. Due to this small number, the relation between the pressure coefficients and the water depth is obtained from just a few data points, but collapse appears to already occur at smaller water depths. More experiments for different water depths improve the relationship between the geometry and pressure coefficient, C_p . Also, the determination of the interval where quasi-steady flow is observed is arbitrary; a different interval influence this relation.

Methodology of structural analysis

In the current study, the characteristic strengths of the material are used as prescribed in the codes. In other literature the mean strength obtained from experiments (Vaculik, 2012) or even an upgrade factor is used (Roos, 2003). This makes a significant difference for the linear elastic analysis, since the first cracks occur when the flexural strength is reached. Furthermore, approaching both two leaves and glass panes of the window as different elements instead of a combined thickness (Chen, 2016), a lower moment resistance is obtained as well.

The used failure mechanism for the non-linear analysis is based on wall panels subjected to a uniform lateral load. The location of the maximum moment from linear elastic analysis is considered to be the location of the crack which is usually at mid-height in case of uniform lateral load. The assumption that this is the appropriate failure mechanism has a substantial influence on both the internal and external work in the non-linear analysis.

New insights

The following new insights are obtained which indicate the significance of the current study and further research on the field of structural damage of residences due to flood actions:

- There is a difference between the residences during the Watersnoodramp in 1953 and the buildings in the current building stock. Due to the bad quality of the mortar, which had started dissolving in the seawater, the flexural strength was little to none. On top of that, the minimal dead load from the timber floors on the thin walls provided a negligible residual moment resistance. Similar to the residences then, terraced houses nowadays are also mainly vulnerable to out-of-plane bending of the load-bearing walls. Comparing the 'newer' residences with calcium-silicate masonry walls and system floors to the 'older' residences with slightly thinner clay masonry walls and timber floors, a substantial increase in bending resistance is observed.

- Similar relations are observed between the geometry of the residences and the drag coefficients (obtained from the hydrodynamic pressure in the experiments) and the geometry and the pressure coefficients (used for the lateral wind load). The pressure coefficients, however, show a larger dependence of the aspect-ratio, B/h , than the drag coefficient due to the emerged flow in stead of submerged flow.
- The wall ties connecting the inner and outer leaf of the cavity are of great importance, since they make it possible to distribute the lateral load. Due to the interaction between these leaves, the out-of-plane bending resistance of the wall is higher than that of a single leaf. The simplification of the distribution of the wall used in this study shows the dependence of the location of the ties.

6.2. Conclusions

Combining the findings of the two main objectives lead to the conclusion of this study and makes it possible to answer the main research question.

Which loads act on a building in a flood?

Flow velocity, v , causes an additional load, which depends on the geometry and orientation of the building with respect to the water height and flow direction. From the data obtained from the conducted experiments, the following conclusions concerning the drag coefficient, C_D , and pressure coefficient, C_p , can be drawn:

- An increase in the aspect-ratio (width of the residences, B , over the water depth, h) causes an increase of the pressure coefficient. The side-ratio (length, L , over width, B) shows a peak of the drag coefficient at a critical value of ± 0.6 . Below this value the drag coefficient increases when the side-ratio does, after this value it decreases. This is mainly due to the decrease of pressure at the rear face when the h/L -ratio decreases similar to the wind coefficients.
- The load-bearing wall of the residence orientated perpendicular to the flow direction (angle of attack, $\phi = 90^\circ$) results in the highest pressure coefficient, which decreases when the angle of attack decreases as well.
- The drag coefficients, prescribed in P-55 (FEMA,2011) are smaller than those derived from the current experiments. These coefficients appear to be upper boundaries for the pressure coefficients of the frontal face of the buildings used in the current experiments. However, the pressure at the front can exceed this 'upper' value for terraced houses with a smaller side ratio than common American single-family homes.

What is the strength of typical Dutch residences?

The terraced house is found as the typical Dutch residence from geometric information, defined as three case-study residences based on year of construction, building methods and materials from literature. Despite the higher flexural bending strength, the resistance of the older residences (1965-1975) with clay masonry walls and timber floors is smaller than those of the newer residences (1975-1994) with calcium-silicate masonry walls and system floors or casted concrete walls and floors. This is mainly due to the forming of early cracks in the wall resulting in zero tension strength after cracking and a higher normal force on the walls due to heavier system or concrete floors instead of timber floors. When the crack opens up, eccentricity of this normal force causes residual moment capacity, which is substantially higher in case of the newer residences.

Which flood conditions may lead to collapse of typical Dutch residences?

For all three case study residences, out-of-plane bending of the load-bearing wall is the critical failure mechanism, leading to the failure-graphs in Figure 5.13. Using design values for both the load and strength, the residence already collapses before the hv -product (water depth times flow velocity) of 7 m/s^2 is reached according to Clausen (1989). The residences located at the area of interest, all areas subjected to a flood depth of 2.0 meters or higher, are

used to find the typical Dutch residences. However, the resistance of out-of-plane bending of the load-bearing walls is already reached at lower water depths, especially in combination with high flow velocities, see Figure 5.13.

For the older residences (1965-1975) with clay masonry walls with timber floors, a water depth of ± 1.2 meters already causes the design moment resistance of the wall without taking the velocity or wave action into account. For the newer residences (1975-1994) with calcium-silicate masonry walls with system floors or concrete walls and floors, this ultimate resistance is reached due to a water depth of ± 1.8 meters. If the flood water has a flow velocity of 2 m/s or waves are generated by a wind speed of 29.5 m/s over a fetch of 100 m, the critical water depth reduces for both situation by ± 0.3 meters to respectively ± 0.9 and 1.5 meters.

6.3. Recommendations

This report started with the influence of collapse of residential buildings on the mortality. The damage- and loss functions used for mortality functions nowadays, obtained from statistical data from previous similar events are not representative anymore, since the building quality showed to have a large influence on the collapse. It is advised to use a physical approach, where the flood characteristics from the improving hydraulic models are used to determine the acting loads on the current buildings. To conclude this study, some recommendations can be given for further research into this physical approach from both the hydraulic and structural perspectives.

From the hydraulic perspective, important factors to include in the approach are the location of measuring the flood characteristics and the alternation of the flow due to the presence of the building. Furthermore, research is recommended in the following topics:

- The inclusion of more loads, such as the impact load and debris, provide more insight into the real structural damage. Experiments on partitions of walls with non-structural elements can provide realistic values for the flood infiltration rate. The inclusion of debris force is difficult due to the uncertainty of this debris actually colliding in the residence. A probabilistic approach of this load should be more appropriate than applying the debris force in different situations on the residence.
- Looking at the layout of a city, the residences are oriented differently, so the angle of attack and blockage also differ per street or block. Where one row of terraced houses will be subjected to load from a critical angle, others will experience lower loads. Physical experiments with multiple buildings having different orientations and blockage ratios can be used to find the influence of the layout on the pressures. Subsequently, the flood parameters generated by a hydraulic numerical model can give a damage estimation of a total city based on the loads from the experiments and the structural damage due to these loads.
- To derive the pressure coefficients for the hydrodynamic load from those used for the lateral wind load, more insight should be gained into the difference between submerged and emerged flow.

From the structural perspective the following topics are of interest, which are advised to be analyzed probabilistically to include multiple failure mechanisms:

- If dynamic loads appear to be more important than expected, the dynamic response of the residence should be taken into account in the structural analysis.
- Neglecting the contribution of the outer leaf leads to a conservative outcome, but assuming a certain strength of the ties without the knowledge of the condition leads to an overestimation. A balance should be found between these approaches to make a realistic calculation of the resistance of the total cavity wall. A combined system of the two different leaves with their flexural stiffnesses and boundary conditions connected by the wall ties, can be useful to approach this real behaviour of the cavity wall.

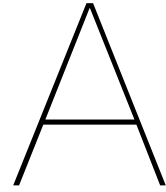
Bibliography

- NL Agentschap. Voorbeeldwoningen 2011: bestaande bouw. *Chapter*, 6:Rijwoning, 2011.
- Halldór Árnason. Interactions between an incident bore and a free-standing coastal structure. 2005.
- NEM Asselman. Consequences of floods—damage to buildings and casualties. *WL Delft Hydraulics report Q3668*, 3668, 2005.
- Riccardo Beretta, Giovanni Ravazzani, Carlo Maiorano, and Marco Mancini. Simulating the influence of buildings on flood inundation in urban areas. *Geosciences*, 8(2):77, 2018.
- Coastal Engineering Research Center. Shore protection manual. *Dept. of the Navy, Waterways Experiment Station, Vicksburg, MS*, 1984.
- Hubert Chanson. *Hydraulics of open channel flow*. Elsevier, 2004.
- X Chen. Impacts of overtopping waves on buildings on coastal dikes. 2016.
- LK Clausen. Potential dam failure: estimation of consequences, and implications for planning. *Unpublished M. Phil. thesis at the School of Geography and Planning at Middlesex Polytechnic collaborating with Binnie and Partners, Redhill*, 1989.
- Giovanni Cuomo, Gholamreza Shams, Sebastian Jonkman, and Pieter Van Gelder. Hydrodynamic loadings of buildings in floods. pages 3744–3756, 2008.
- Giovanni Cuomo, William Allsop, and Shigeo Takahashi. Scaling wave impact pressures on vertical walls. *Coastal Engineering*, 57(6):604–609, 2010.
- K De Bruijn and B van Kester. Possibilities to improve flood fatality functions for the netherlands. *Deltares*, 2015.
- Ministerie van Verkeer en Waterstaat, Directoraat-Generaal Rijkswaterstaat, and Dienst Weg-en Waterbouwkunde. *Hydraulische randvoorwaarden primaire waterkeringen: voor de derde toetsronde 2006-2011 (HR 2006)*. 2007.
- M Escarameia, A Karanxha, and A Tagg. Quantifying the flood resilience properties of walls in typical uk dwellings. *Building Services Engineering Research and Technology*, 28(3): 249–263, 2007.
- Rita Esposito, Francesco Messali, and Jan G Rots. Material characterization of replicated masonry and wall ties. final report 18 april 2016. 2016.
- FEBE. Schijfwerking, 2019. URL <http://www.febeefloor.be/febeefloor/nl/index.php?2007/05/22/19-schijfwerking>.
- FEMA. Coastal construction manual. *FEMA P55*, 2, 2011.
- FEMA. Guidelines for design of structures for vertical evacuation from tsunamis. *FEMA P646*, 2012.
- ASJ Foster, T Rossetto, and W Allsop. An experimentally validated approach for evaluating tsunami inundation forces on rectangular buildings. *Coastal Engineering*, 128:44–57, 2017.
- VP Gupta and SC Goyal. Hydrodynamic forces on bridge piers. *J. of Institution of Engineers. India*, 56, 1975.

- Samira Jafari, Jan G Rots, Rita Esposito, and Francesco Messali. Characterizing the material properties of dutch unreinforced masonry. *Procedia engineering*, 193:250–257, 2017.
- S.N. Jonkman. Loss of life estimation in flood risk assessment; theory and applications. 2007.
- Ilan Kelman. *Physical flood vulnerability of residential properties in coastal, eastern England*. PhD thesis, University of Cambridge, 2002.
- Bas Kolen, Robert Slomp, Wim Van Balen, Teun Terpstra, Marcel Bottema, and S Nieuwenhuis. Learning from french experiences with storm xynthia; damages after a flood. *ISBN 978-90-77051-77-1*, 2010.
- Paul A. Korswagen Eguren. Structural damage to masonry housing due to earthquake-flood multi-hazards. 2016.
- PB Laurengo, Jan G Rots, and Johan Blaauwendraad. Two approaches for the analysis of masonry structures: micro and macro-modeling. *HERON*, 40 (4), 1995, 1995.
- SJ Lawrence and AW Page. Manual 4: Design of clay masonry for wind and earthquake. In *ThinkBrick Technical Manuals*. Artarmon, NSW 1570 Australia, 2013.
- Robert Lijbers, Christophorus Carolus Franciscus Thijssen, and Henk Westra. Woningvoorraad 45-75. 1984.
- Tristan Oliver Lloyd. *An experimental investigation of tsunami forces on coastal structures*. PhD thesis, UCL (University College London), 2016.
- D Lumbroso and F Vinet. A comparison of the causes, effects and aftermaths of the coastal flooding of england in 1953 and france in 2010. *Natural Hazards and Earth System Sciences*, 11:2321–2333, 2011.
- B Maaskant, B Kolen, R Jongejan, SN Jonkman, and M Kok. Evacuatieschattingen nederland. *Rapport PR1718*, 10, 2009.
- Joshua Macabuag, Tiziana Rossetto, Ioanna Ioannou, Anawat Suppasri, Daisuke Sugawara, Bruno Adriano, Fumihiko Imamura, Ian Eames, and Shunichi Koshimura. A proposed methodology for deriving tsunami fragility functions for buildings using optimum intensity measures. *Natural Hazards*, 84(2):1257–1285, 2016.
- Massey. *Mechanics of fluids*. Van Nostrand Reinhold Company Ltd., 1970.
- Frank Messner and Volker Meyer. Flood damage, vulnerability and risk perception—challenges for flood damage research. pages 149–167, 2006.
- JFA Moore. *Manual for the design of plain masonry in building structures to Eurocode 6*. Institution of Structural Engineers, 2008.
- C Norberg. Flow around rectangular cylinders: pressure forces and wake frequencies. *Journal of wind engineering and industrial aerodynamics*, 49(1-3):187–196, 1993.
- K Nore, Bert Blocken, and JV Thue. On cfd simulation of wind-induced airflow in narrow ventilated facade cavities: coupled and decoupled simulations and modelling limitations. *Building and Environment*, 45(8):1834–1846, 2010.
- Younes Nouri, Ioan Nistor, Dan Palermo, and Andrew Cornett. Experimental investigation of tsunami impact on free standing structures. *Coastal Engineering Journal*, 52(01):43–70, 2010.
- Shinichi Oka and Takeshi Ishihara. Numerical study of aerodynamic characteristics of a square prism in a uniform flow. *Journal of Wind Engineering and Industrial Aerodynamics*, 97(11-12):548–559, 2009.

- J Peakall and J Warburton. Surface tension in small hydraulic river models-the significance of the weber number. *Journal of Hydrology (New Zealand)*, pages 199–212, 1996.
- Aimilia K Pistrika and Sebastiaan N Jonkman. Damage to residential buildings due to flooding of new orleans after hurricane katrina. *Natural Hazards*, 54(2):413–434, 2010.
- ZX Qi, I Eames, and ER Johnson. Force acting on a square cylinder fixed in a free-surface channel flow. *Journal of Fluid Mechanics*, 756:716–727, 2014.
- Durgesh C Rai and Subhash C Goel. Seismic strengthening of rocking-critical masonry piers. *Journal of structural engineering*, 133(10):1445–1452, 2007.
- Anton Rietmeijer. Rear-slope revetment stability approached by the wave overtopping simulator: Experiments regarding the stability of single-layer cube revetment on breakwater crests and rear slopes. 2017.
- Rijkswaterstaat. Over overstroomik?, 2019. URL <https://overstroomik.nl/over-overstroomik.html>.
- August Ritter. Die fortpflanzung der wasserwellen. *Zeitschrift des Vereines Deutscher Ingenieure*, 36(33):947–954, 1892.
- Ian N Robertson, H Ronald Riggs, Solomon C Yim, and Yin Lu Young. Lessons from hurricane katrina storm surge on bridges and buildings. *Journal of Waterway, Port, Coastal, and Ocean Engineering*, 133(6):463–483, 2007.
- W Roos. Damage to buildings. *DC1-233-9*, 2003.
- Navaratnarajah Sathiparan, WAV Anjalee, and KKS Kandage. The scale effect on small-scale modelling of cement block masonry. *Materials and Structures*, 49(7):2935–2946, 2016.
- J Schwarz and H Maiwald. Empirical vulnerability assessment and damage description for natural hazards following the principles of modern macroseismic scales. 2012.
- AG Sebastian, KT Lendering, BLM Kothuis, AD Brand, SN Jonkman, PHAJM van Gelder, B Kolen, M Comes, SLM Lhermitte, KJMG Meesters, et al. Hurricane harvey report: A fact-finding effort in the direct aftermath of hurricane harvey in the greater houston region. 2017.
- K Slager and D Wagenaar. Standaardmethode 2017 schade en slachtoffers als gevolg van overstromingen. *Deltares*, 2017.
- Kees Slager. *De ramp: een reconstructie: 200 ooggetuigen over de watersnood van 1953 verhalen om nooit te vergeten...* De Koperen Tuin, 1992.
- KBM Tennakoon. Parameterisation of 2d hydrodynamic models and flood hazard mapping for naga city, philippines. 2004.
- Christophorus Carolus Franciscus Thijssen. Bouwconstructieve analyse van naoorlogse eengezinshuizen in de non-profit huursector 1946-1980. 1999.
- Jaroslav Vaculik. *Unreinforced masonry walls subjected to out-of-plane seismic actions*. PhD thesis, 2012.
- P Van Boom, WH Maessen, DJ Noy, and JGM Raadschelder. Jellema 8-woningbouw. *ThiemeMeulenhoff, Utrecht/Zutphen*, 2005.
- A.G.M Van Paasen, G. IJsseldijk, and M.E.M.E. Van Kuik. Woningbouw - prefab beton. URL <http://betonplaza.nl/Documenten/PBTO-hoofdstuk-09.pdf>.
- Steffie Van Wijlick. Nut en noodzaak: Wel of geen geventileerde spouwmuur?, 2018. URL <http://www.vekemans.nl/nut-en-noodzaak-wel-of-geen-geventileerde-spouwmuur/>.

- VOBN. Construeren van gietbouwcasco's. URL http://www.joostdevree.nl/bouwkunde2/jpgc/casco_4_construeren_gietbouwcasco_www_gietbouwcentrum_nl.pdf.
- Zhangping Wei, Robert A Dalrymple, Alexis Héroult, Giuseppe Bilotta, Eugenio Rustico, and Harry Yeh. Sph modeling of dynamic impact of tsunami bore on bridge piers. *Coastal Engineering*, 104:26–42, 2015.
- Harold Malcolm Westergaard and Willis Appleford Slater. Moments and stresses in slabs. In *Journal Proceedings*, volume 17, pages 415–538, 1921.
- Craig Robert Willis. *Design of unreinforced masonry walls for out-of-plane loading*. PhD thesis, 2004.
- Davide Wüthrich, Michael Pfister, Ioan Nistor, and Anton J Schleiss. Experimental study of tsunami-like waves generated with a vertical release technique on dry and wet beds. *Journal of Waterway, Port, Coastal, and Ocean Engineering*, 144(4):04018006, 2018.
- Historische Vereniging Zwijndrecht. De watersnoodramp 1953, 2018. URL <https://www.swaen.org/geschiedenis/bijzonder/watersnoodramp-1953>.



Durability of masonry

Factors affecting durability of masonry are taken into account in Annex A of NEN-EN 1996-2+C1 by classifying masonry based on micro conditions of exposure including macro conditions. Based on the environment or situation, the class can be selected and the right brick and mortar can be used:

- **MX1 - In a dry environment**

Examples of masonry in this class are interior walls of a residential or office building and rendered masonry in exterior walls not exposed to water or damp. Also no heavy loads can be subjected to this type of masonry during construction.

- **MX2 - Exposed to moisture or wetting**

Distinction is made between masonry that exposed to moisture, MX2.1, and exposed to severe wetting, MX2.2. Moisturized walls can be interior walls in a laundry, exterior walls not exposed to severe rain or frost and masonry in well drained non-aggressive soil. These last class includes exterior walls with cappings or flush eaves, parapets, freestanding walls, in the ground or under water.

- **MX3 - Exposed to moisture or wetting plus freeze/thaw cycling**

The same distinction is made as in MX2 between masonry exposed to moisture or wetting classified as MX3.1 and severe wetting of masonry, MX3.2. The difference with MX2 is the exposure to frost, which is included in this class.

- **MX4 - Exposed to saturated salt air, seawater or de-icing salts**

This class includes masonry in coastal areas or adjacent to roads that are salted during the winter.

- **MX5 - In an aggressive chemical environment**

When masonry has contact with ground or groundwater containing a significant level of sulfates or acid, it is classified as MX5. It also includes masonry near to industrial areas where aggressive chemicals are airborne or with contaminated ground or groundwater.

In the regular building sector, a cavity wall is ventilated, but it is not water- and/or air tight. These walls can be classified as MX3.2 or in exceptional situations as MX2.2. Buildings in coastal areas or close to a road, where during winters salt for de-icing is used, even the regulations which belong to class MX4 should be used. For mortar a similar classification is defined as followed:

- **P - Masonry subjected to passive exposure**

This type of mortar can only be used for masonry in class MX1 if during construction no moisture or frost is involved.

- **M - Masonry subjected to moderate exposure**

For masonry in class M2.1 and M3.1 it can be used without conditions, for M2.2 this type is only applicable if no bricks with soluble salts in category S1 are used. Otherwise the mortar should be resistant to sulfates.

- **S - Masonry subjected to severe exposure**

This can be used for masonry in class 1 to 3, if no soluble salts.

- **Specific composition**

For masonry classified as MX4 or MX5, a specific mortar should be used based on the amount of moisture, salts and other chemicals present in the environment.

B

Damage grade

To make it possible to take the collapse of houses into account in the mortality functions, the definition of *collapse* needs to be specified first. Schwarz and Maiwald (2012) developed a damage classification method for flood risk analysis, based on the earthquake damage assessment EMS-98 for masonry buildings. Damage grades D_i link the flood impact and loss of the houses, where it can be seen from Figure B.1 that collapse of the building is comparable with damage grade 5. In this research partial collapse of a key structural element as described in Section 3.3 will be assigned to total collapse of the building as well.









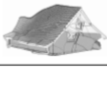

D_i	Damage		Description	Drawing	Example
	Structural	Non-structural			
D_1	no	slight	penetration and pollution only		
D_2	no to slight	moderate	slight cracks in load-bearing members broken doors and windows contamination replacement of extension elements		
D_3	moderate	heavy	major cracks and/or deformations in load-bearing walls and slabs settlement replacement of non-load bearing elements		
D_4	heavy	very heavy	structural collapse of load-bearing walls, slabs replacement of load-bearing elements		
D_5	very heavy	very heavy	collapse of the building or of major parts of the building demolition of building required		

Figure B.1: Definition of flood damage grade D_i and assignment to damage cases from the flood 2002 in Saxony (Schwarz and Maiwald, 2012)

B.1. Vulnerability matrices

Kelman (2002) developed vulnerability matrices for different residences, which can be used as a tool for determining the mitigation options and risk- and damage assessment. Along the axes the difference in flood depth in- and outside and the flood velocity can be found. The cells present the expected damage scale based on failure of the URM cavity walls, glass failure and rate of rise of the flood water inside the residence. The two storey-residence with a surface area of 55 m² closest to case-study residence 1, so this vulnerability matrix is displayed in Figure B.2a. Due to the importance of the load carried by the wall, so also the results for adding an additional storey ('heavy') is displayed in Figure B.2c.

Maximum Flood Velocity	Maximum Flood Depth Differential				
	0.0 m	0.5 m	1.0 m	1.5 m	2.0 m +
0.0 m/s	DS0	DS2 Even if glass doors, DS3 unlikely	DS4	DS4	DS5
0.5 m/s	DS0	DS2 Even if glass doors, DS3 unlikely	DS4	DS5	DS5
1.0 m/s	DS0	DS2 Even if glass doors, DS3 unlikely	DS4	DS5	DS5
1.5 m/s	DS0	DS2 Even if glass doors, DS3 unlikely	DS4	DS5	DS5
2.0 m/s	DS0	DS2 Even if glass doors, DS3 unlikely	DS4	DS5	DS5
2.5 m/s	DS0	DS2 Even if glass doors, DS3 unlikely DS4 if weak wall panels	DS4	DS5	DS5
3.0 m/s	DS0	DS2 Even if glass doors, DS3 unlikely DS4 if weak wall panels	DS4	DS5	DS5
3.5 m/s	DS0	DS4	DS4	DS5	DS5
4.0 m/s	DS0	DS4	DS5	DS5	DS5
4.5 m/s	DS0	DS4	DS5	DS5	DS5
5.0 m/s	DS0	DS4	DS5	DS5	DS5



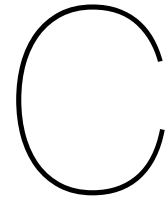
(a) Vulnerability profile for 2-storey residence comparable with case-study residence 1 (b) Residences with 2 storeys

Maximum Flood Velocity	Maximum Flood Depth Differential				
	0.0 m	0.5 m	1.0 m	1.5 m	2.0 m +
0.0 m/s	DS0	DS2 Even if glass doors, DS3 unlikely	DS2 Even if glass doors, DS3 unlikely DS4 if weak wall panels	DS4	DS5
0.5 m/s	DS0	DS2 Even if glass doors, DS3 unlikely	DS4	DS4	DS5
1.0 m/s	DS0	DS2 Even if glass doors, DS3 unlikely	DS4	DS4	DS5
1.5 m/s	DS0	DS2 Even if glass doors, DS3 unlikely	DS4	DS4	DS5
2.0 m/s	DS0	DS2 Even if glass doors, DS3 unlikely	DS4	DS4	DS5
2.5 m/s	DS0	DS2 Even if glass doors, DS3 unlikely	DS4	DS5	DS5
3.0 m/s	DS0	DS2 Even if glass doors, DS3 unlikely	DS4	DS5	DS5
3.5 m/s	DS0	DS2 Even if glass doors, DS3 unlikely DS4 if weak wall panels	DS4	DS5	DS5
4.0 m/s	DS0	DS2 Even if glass doors, DS3 unlikely DS4 if weak wall panels	DS4	DS5	DS5
4.5 m/s	DS0	DS4	DS4	DS5	DS5
5.0 m/s	DS0	DS4	DS5	DS5	DS5



(c) Vulnerability profile for 3-storey residences comparable with case-study residence 1 (d) Residences with 3 storeys

Figure B.2: Vulnerability matrices for residences (Kelman, 2002)



Impact modelling

There are internationally multiple models and functions to assess the impacts of the floods. A distinction is made between micro-, meso- and macro-scale approaches to assess damage and flood fatalities in Table C.1. The smaller the scale, the more accurate the estimate, but the more input parameters are needed. When looking especially at the damage, in a macro-approach the spatial distribution of damage potential is equal over the whole municipality. In the meso-approach a more realistic localization is used, such as a difference in the urban and rural areas by making use of data in Geometric Information Systems (GIS). For the micro-approach local hazard parameters are used to calculate damage to individual buildings.

Table C.1: Different approaches of flood modelling based on (Jonkman, 2007) and (Messner and Meyer, 2006).

Scale	Area	Type of information	Damage level
Micro	Local	Individual causes/circumstances	Object
Meso	Regional	Flood events	Land-use types
Macro	National	Global statistics	Municipalities

The impact of large scale floods from the main Dutch water courses is assessed with the 'Standard Flood Damage and Fatality Assessment Model' (Slager and Wagenaar, 2017) or in Dutch 'Standard Schade en Slachtoffer Model' (SSM2017). This model cannot be classified as one of the approaches above, as it combines elements from all three types: The considered area is usually a dike ring, where flood parameters are based on models which include land-use category, such as rural or urban areas (meso-scale). Small-scale socio-economic data is used to assign for example house type, number of employees and inhabitants to a geographic unit (micro-scale). The direct and indirect amount of damage can be estimated with damage- and mortality-functions, which are determined based on data from historic events in comparable areas (macro-scale).

C.1. Dutch mortality functions

- Breach zone

$$F_{D,B} = 1 \quad \text{if } hv \geq 7m^2/s \quad \text{and} \quad v \geq 2m/s \quad (\text{C.1})$$

- Zone with rapidly rising water levels

$$F_{D,S}(h) = \phi_N \left(\frac{\ln(h) - \mu_N}{\sigma_N} \right) \quad (\text{C.2})$$

$$\mu_N = 1.46 \quad \text{and} \quad \sigma_N = 0.28$$

$$\text{if } (h \leq 2.1m \quad \text{and} \quad \frac{dh}{dt} \leq 4m/hr) \quad \text{and} \quad (hv < 7m^2/s \quad \text{or} \quad v < 2m/s)$$

- Transition zone

$$F_{D,T}(h) = F_{D,O} + (w + 0.5) \frac{F_{D,S} - F_{D,O}}{3.5} \quad (\text{C.3})$$

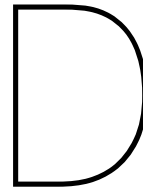
$$\text{if } (h \leq 2.1m \quad \text{and} \quad 0.5 \leq \frac{dh}{dt} < 4m/s) \quad \text{and} \quad (hv < 7m^2/s \quad \text{or} \quad v < 2m/s)$$

- Zone with slow rising water levels

$$F_{D,O}(h) = \phi_N \left(\frac{\ln(h) - \mu_N}{\sigma_N} \right)$$

$$\mu_N = 7.60 \quad \text{and} \quad \sigma_N = 2.75$$

$$\text{if } ((\frac{dh}{dt} < 0.5m/hr) \quad \text{or} \quad (\frac{dh}{dt} \leq 0.5m/hr \quad \text{and} \quad h < 2.1m)) \quad \text{and} \quad (hv < 7m^2/s \quad \text{or} \quad v < 2m/s) \quad (\text{C.4})$$



Flood actions

Selection of flood actions

Hydrostatic:

For the lateral hydrostatic pressure only the most extreme situation is *included*. This is the case without any infiltration of the flood water in the residence ($h_i = 0$), which causes the largest lateral load since there is no equalization. The flood infiltration rate is taken into account by various researches, see section D.1, but the differences in values per residence are too large to consider other situations as well.

Both buoyancy and capillary rise are *excluded* in further analysis, since timber frame residences are rare in the Netherlands and the effect of capillary rise is negligible to the hydrostatic loads.

Hydrodynamic:

Since the value of the drag coefficient, C_d , varies in different studies and practise documents, more research is done on this factor, so the quasi-static loads are *included* in both Section 2.2.2 and the experiments. The wind waves will not be generated in the physical model, because these loads can be *included* in the structural analysis by making use of known methods in Section 2.2.3. It is assumed that in the Netherlands mainly inundation floods occur due to the failure of a levee, so without the development of a bore when the flood travels further inland over the relatively flat surface. Only near the breach the impulsive loads could develop, so these forces are *excluded* from further analysis.

Geotechnical:

Scour of the subsoil can only start when the top layer is washed away. This layer in the Netherlands consist mainly of grass or pavement, which has a critical flow velocity of 5 m/s (Roos, 2003). Since this velocity is quite high, it is assumed that collapse of the walls has occurred before scour will have an effect. Also the effect of deposition is assumed to be negligible compared to the lateral hydrostatic force, so geotechnical actions are *excluded*.

Debris:

Modelling of the loads due to debris on a building is quite complex due to scaling effects and uncertainties, so these actions will not be quantified with the physical model. Due to the high uncertainty of the occurrence and magnitude, these are *excluded* in the structural analysis.

Non-physical:

Although these actions are assumed to have played a major part of the collapse of residences in 1953, but are nowadays assumed to be only relevant for damage and not for collapse, so these actions are *excluded* in the further analysis.

D.1. Flood infiltration rate

As soon as the water depth exceeds the lower part of the lowest window equalization is starting according to Roos (2003). Kelman (2002) suggest to use the flood rate inside a residence (FRR in m/s), since water starts infiltrating into the building immediately through pores and cracks. This value depends on the flood infiltration rate (FIR in m^3/s) and the footprint of the building (A in m^2), with a typical upper bound value of:

$$FRR_{typical} = FIR/A \approx 0.005m/s = 18m/hr \quad (D.1)$$

Infiltration through the walls, interfaces of wall and window/door, pipes, postal flaps and through the floor are considered. The smaller the water depth and flow velocity, the smaller the infiltration rate.

In 2007 laboratory experiments for DCLG (Escameia et al., 2007) found an average leakage rate of $0.15 m^3/hr$ per meter of typical cavity wall made out of bricks with a difference in water level of one metre. Multiplying with the typical perimeter and diving by the typical area used by Kelman (2002) in Equation D.1, give a value of $0.16 m/hr$.

D.2. Impulsive load

The impulsive (or impact) load is caused by the leading edge of a bore or surge passing the building in case of a tsunami or dam-break. Árnason (2005) observed the initial impact for the rectangular cross section, which assumed to be 50% larger than the resistance force during passing of a small bore. FEMA P646 (2012) used these laboratory data to derive an amplification factor of 1.5 for the impulsive force in Equation 2.5. Nouri et al. (2010) also observed a force reduction of approximately 55 to 60% after the initial impact force for an impoundment waterdepth to width/length ratio of 3.75, 4.25 and 5. For a ratio of 2.5 this drop was only 30% followed by a gradual increasing force due to run-up of the bore on the column.

However, there is another approach of simulating tsunamis which create longer waves with a volume-driven wave-maker by releasing a column of water of a specified volume at a controlled rate. The inundation flow is gradually varying in these experiments and can be considered as steady. So, impulsive loads are rarely observed and are preliminary proposed to be neglected for long wave periods from 20 to 240 s in the updated design guidance for tsunamis by Foster et al. (2017).

The magnitude of the impulsive loads are strongly influenced by the air entertainment due to friction with the "virtually" dry bottom, since perfectly dry is difficult to achieve. This results in Euler and Cauchy number which are too large. To compensate for these overestimation due to air effects a correction according to Cuomo et al. (2010) can be applied, based on the Bagnold number, $Bgn = \frac{\rho_w k_w v^2}{\rho_0 D}$, of both the model and in reality, see Figure D.1.

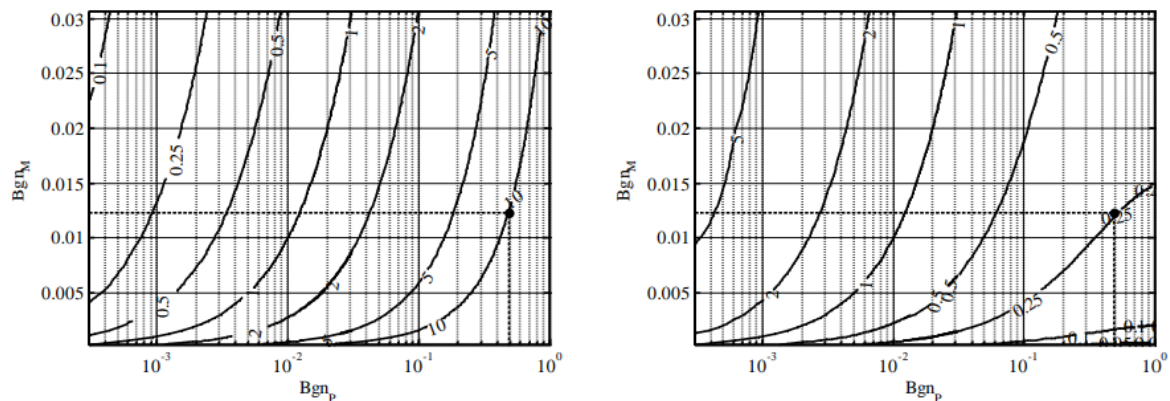


Figure D.1: Scale factors (left) and correction factors to Froud (right) as function of the Bagnold number (Cuomo et al., 2010)

D.3. Blockage effect

The ratio of the width of the building to the width of the flume is known as the blockage ratio, B/b , and can be used to take into account the presence of adjacent buildings. Empirically determined drag coefficients are strongly influenced by the blockage, which cause an increase of the average flow outside the wake. In some cases there is also a water level difference between the upstream and downstream side of the building, which cause a contribution of a hydrostatic pressure to the stream wise load. Recent research to the impact of this effect on the hydrodynamic force is summarized.

Árnason (2005) conducted experiments to study the interaction of a hydraulic bore with free-standing structures on a dry bed. In this research the *coefficient of resistance*, C_R , instead of C_D in Equation 2.4 are determined for a cylindrical, rectangular and rhomboidal cross sections, which appear to be constant for either orientations of the square column. This approach is similar to the research on steady flows around bridge piers by Gupta and Goyal (1975): $C_R = \frac{F_x}{\frac{1}{2}\rho Av^2}$.

Qi et al. (2014) proposed a framework where the relation between the blockage factor and the magnitude of the hydrodynamic force can be quantified for turbulent flow, which is shown by Foster et al. (2017) to be representative for the force of a tsunami inundation on buildings (Lloyd (2016) and Foster et al. (2017)). For damage to buildings these quasi-steady force estimation provides the best fit to damage data for three different tsunami areas by Macabuag et al. (2016). The blockage ratio influence the Froude number, which determines the flow regime to be subcritical or choked leading to the corresponding quasi-static or mean drag force as followed:

$$F_D = \begin{cases} \frac{1}{2}C_D\rho v_1^2 B h_1 & \text{Subcritical, } Fr_1 < Fr_{1c} \\ \lambda B g^{\frac{1}{3}} v_1^{\frac{4}{3}} h_1^{\frac{4}{3}} & \text{Choked, } Fr_1 \approx Fr_{1c} \end{cases} \quad (D.2)$$

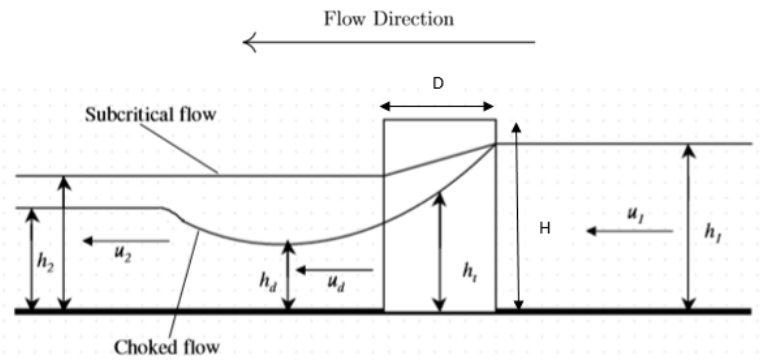


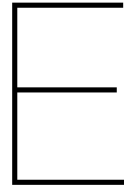
Figure D.2: Schematic diagram indicating the quantities described by the framework of Qi et al. (2014) adapted from Lloyd (2016)

The two different formulas are introduced to take into account the difference in waterdepth on both sides of the object in case of the choked regime shown in Figure D.2. This hydraulic jump downstream of the object cause a hydrostatic force component due to hydrodynamic actions. In the experiments of Qi et al. (2014) this component varies in a choked regime from 25 to 60% when the blockage ratio increase from 0.1 to 0.4. Wei et al. (2015) also observed a 10 to 20% larger hydrodynamic peak force than solely from the drag effect for blockage ratios between 0.2 and 0.28, depending on the shape of the object. This effect is included in the empirical factor λ in Equation D.2 defined as:

$$\lambda = \frac{1}{2}C_D Fr_1^{\frac{2}{3}} + \frac{1}{2}C_H \left(\frac{1}{Fr_1^{\frac{4}{3}}} - \frac{1}{Fr_d^{\frac{4}{3}}} \right) \quad \text{with} \quad \begin{cases} C_D = C_{D0} \left(1 + C_{D0} \frac{B}{2b} \right)^2 \\ C_H = 0.58 \end{cases} \quad (D.3)$$

After this peak, the flow is less transient and a linear relationship between the blockage fraction and the magnitude of the force is observed by Wei et al. (2015). Qi et al. (2014) describes this as the subcritical regime, where a modification of the unbounded drag coefficient, C_{D0} , is used, which is the drag coefficient of the submerged object in an unblocked turbulent flow.

The blockage ratio also influence the magnitude of the impulsive force according to the experiments of Nouri et al. (2010) on square structures. By changing this ratio from 0.125 to 0.250 and 0.375, the impulsive force increase up to respectively 125, 140 and 125% of the initial force in an unblocked flow. The general form of the measured forces in time however remains the same. Furthermore, the orientation of the object is important: both Árnason (2005) and Wei et al. (2015) observed a less violent initial impact on when there is a clear separation point in the leading edge of the object, which is the case for a diamond shaped object.



Drag and pressure coefficients

Width to Height Ratio (b/H)	Drag Coefficient (C_d)
1-12	1.25
13-20	1.3
21-32	1.4
33-40	1.5
41-80	1.75
81-120	1.8
>120	2.0

Figure E.1: Drag coefficients from P-55, Coastal Construction Manual (FEMA, 2011)

E.1. Windload according to NEN-EN 1991-1-4

For the design of the walls against wind loads, the worst combination of external and internal forces needs to be considered. The internal pressures coefficients depends on openings in the façade of the residence, which are none if the windows are not shattered yet. The building can be considered as 'closed' and internal pressure coefficients of ± 0.3 can be used.

$$F_w = \sum \begin{cases} F_{w,e} = c_s c_d \sum_{Surfaces} w_e A_{ref} & w_e = q_p(z_e) c_{pe} \\ F_{w,i} = \sum_{Surfaces} w_i A_{ref} & w_i = q_p(z_i) c_{pi} \\ F_{fr} = c_{fr} q_p(z_e) A_{fr} \end{cases} \quad (E.1)$$

Zone	A		B		C		D		E	
	$c_{pe,10}$	$c_{pe,1}$	$c_{pe,10}$	$c_{pe,1}$	$c_{pe,10}$	$c_{pe,1}$	$c_{pe,10}$	$c_{pe,1}$	$c_{pe,10}$	$c_{pe,1}$
5	-1,2	-1,4	-0,8	-1,1	-0,5		+0,8	+1,0	-0,7	
1	-1,2	-1,4	-0,8	-1,1	-0,5		+0,8	+1,0	-0,5	
$\leq 0,25$	-1,2	-1,4	-0,8	-1,1	-0,5		+0,7	+1,0	-0,3	

Figure E.2: Pressure coefficients

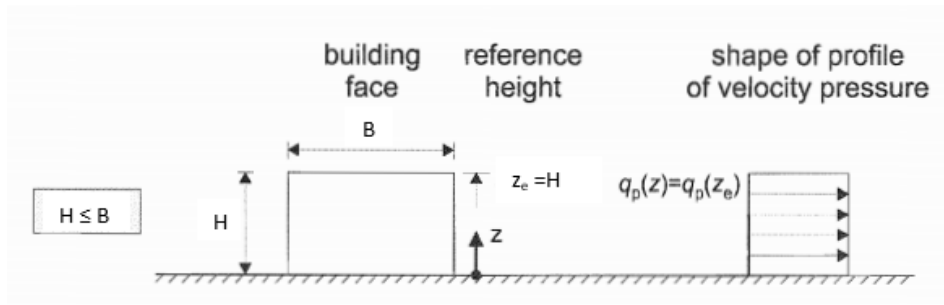
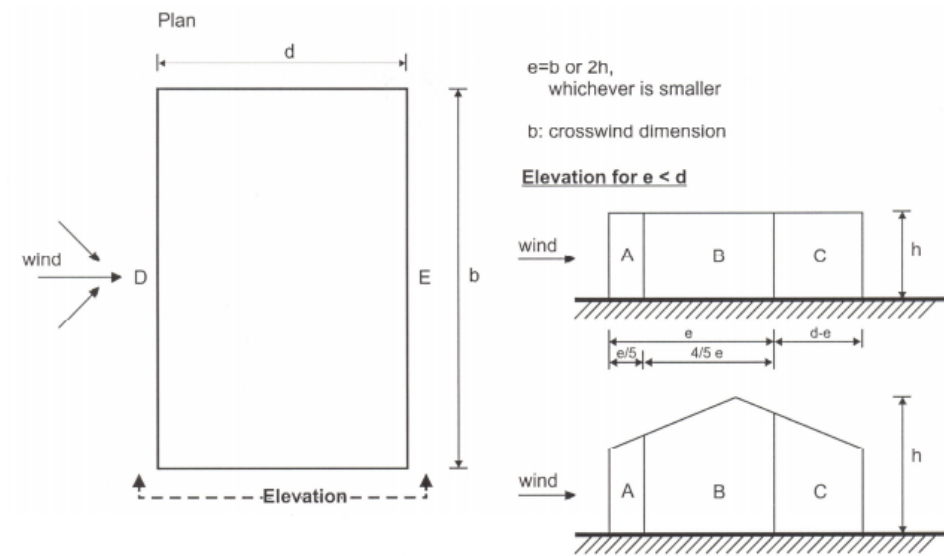
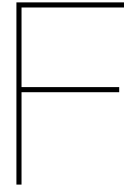
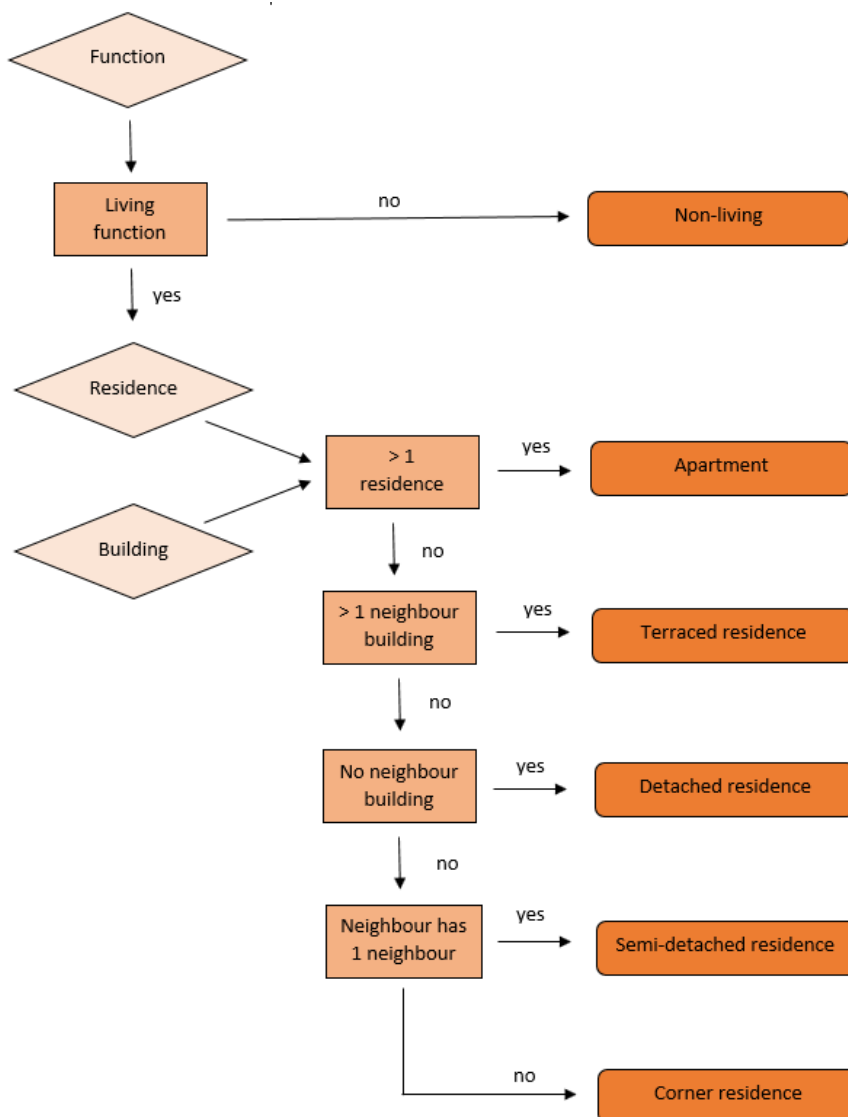
Figure E.3: Velocity pressure profile for a building where $H < B$ 

Figure E.4: Windload on vertical walls of a building with a rectangular footprint



Selection of case-study residences

F.1. Type of residence BAG



F.2. Building quality over the years

There are a five general periods where a lot of single-family residences were built with their own specific points of attention. Between 1947 and 1956 there was a lot of variation in the construction of terraced residences, which is changed with a variation factor of 3.1 to 1.7 due to the massproduction of residences between 1957 and 1973 (Thijssen, 1999). The information about the construction of the buildings are gained from Kennisbank Bestaande Woningbouw, Lijbers et al. (1984) and Thijssen (1999).

Blocks of terraced houses consist of 4 to 8 residences next to each other, up to 12 before 1965. The dimensions vary in time: for the most common width from 6 meter (60's), 5.7 (70's), 5.4 (80's) to 4.8 (90's) and depth from 7.5 (60's), 8.5 till 9.2 (70-80's) to 9.8 (90's) (Thijssen, 1999). The height of the residence is decreased from 2.8 in the sixties to 2.4 in the eighties, where in the building codes over the years a smaller height is required for the sleeping areas compared to the living area.

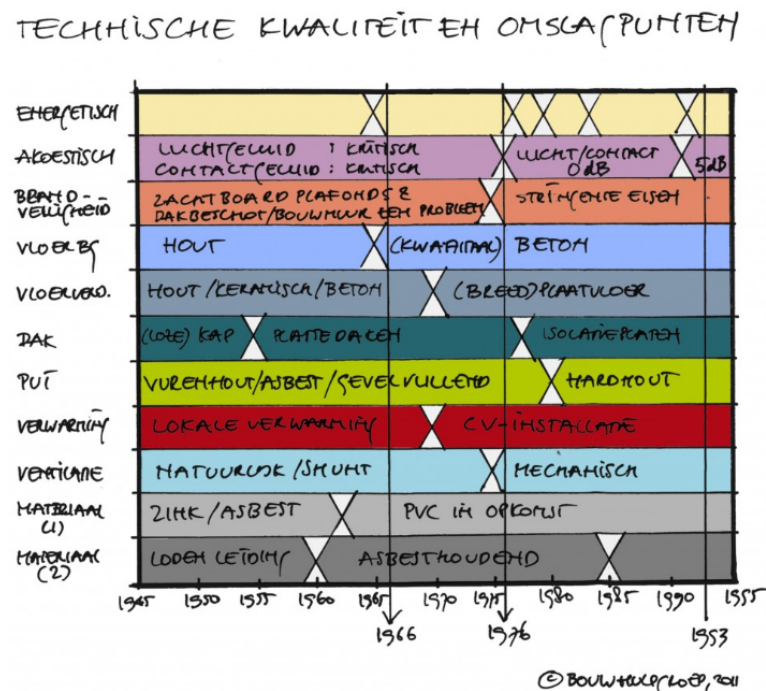


Figure F.1: Development of building quality of the years (Kennisbank Bestaande Woning Bouw)

Pre-war residences (< 1945)

Residences built after the first world war were obligated to fulfill the requirements of the first Woningwet of 1901. These are built with the traditional building method with high quality, durable materials. First a masonry or concrete foundation is built on timber piles if a shallow foundation is not able to withstand the forces. On top of that, walls consisting of single stone (wall thickness of ± 20 cm) or half stone brick wall (wall thickness of ± 10 cm) are placed, whereafter timber frame floors and roof.

Early-postwar residences (1945 - 1964)

Reconstruction after the Second World-war started slowly due to shortage of material and construction workers. Most buildings are built traditionally with hollow brick cavity walls with timber floors and roofs. From 1960, attics were able to enter through a timber floor. The use of non-traditional building elements, or the "system building method" increase from 1953, for example the use of concrete reinforced or stone-like material (hollow masonry) floors on concrete foundation on timber or concrete piles. Walls can consist of large hollow block of porous concrete, prefab concrete elements or in-situ concrete.

The focus in this period and the next one was to built affordable single-family residences for the socially disadvantaged resulting in sober and cheap plans, fixed in standard selection plans also known as "normaalwoningen" or the follow-up "keuzeplanwoning". Most frequently built is the "doorzonwoning" in the top figure of Figure 3.3b, characterized by the stretch of the living room from front to back facade resulting in a lot of light in the room and the load-bearing wall in the middle of the building. In this period almost 1.4 million of these kind of residences are built in both the traditional as the system building method. Approximately 450,000 residences are built from 1950 to 1979 as a "system residence".

Housing shortage residences (1965 - 1974)

In the sixties and seventies a lot of houses are built to overcome to housing shortage for especially lower income families. Social housing corporations used an industrial approach to construct fast, so prefabrication of large elements and in-situ concrete (in Dutch: gietbouw) become popular. Due to this production of large quantities of residences and quick development in building techniques, the risk of poor quality is higher than before. Due to the use of precast concrete panels as floor (in Dutch: breedplaatvloer) in 1970, floors could span one residence with a width of 5.4 meter, which leads to a new selection plan without a load-bearing wall in the building as shown in the bottom figure of Figure 3.3b.

Energy crisis residences (1975 - 1994)

In this period insulation requirements to floors, roofs and facades were introduced as result of the oil crisis in 1973. The load-bearing walls are made of masonry or concrete and are built on top of a concrete foundation with concrete piles. The cavity wall facades consist of an inner leaf from calcium silicate or concrete elements, insulation material with a thickness of ± 6 cm and a wood-based or masonry panel as outer leaf.

Bouwbesluit residences (1995-2005)

In this period the government assigned areas in and around cities which needed to be used for development of residences, called VINEX-location (Vierde Nota Ruimtelijke Ordening Extra). These neighbourhood should combine living, working and services at the edges of existing cities resulting in a decrease of pressure on the large cities. At 418,000 locations are more than 680,000 residences built, resulting in a living space for almost 790,000 people (CBS).

Renovation (> 2005)

In this period the focus is on the current building stock in stead of the development of new buildings, where a choice needs to be made between demolishing or renovation based on the ease of replacing components. System residences are renovated by replacing the facade-elements with new isolated elements or in case of traditional built residences isolation material is placed in between the hollow cavity walls.

F.3. Case-study residences

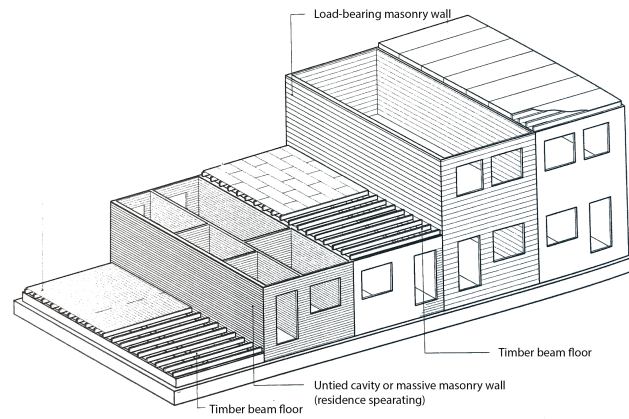


Figure F.2: Traditionally built residences with masonry cavity walls and timber floors

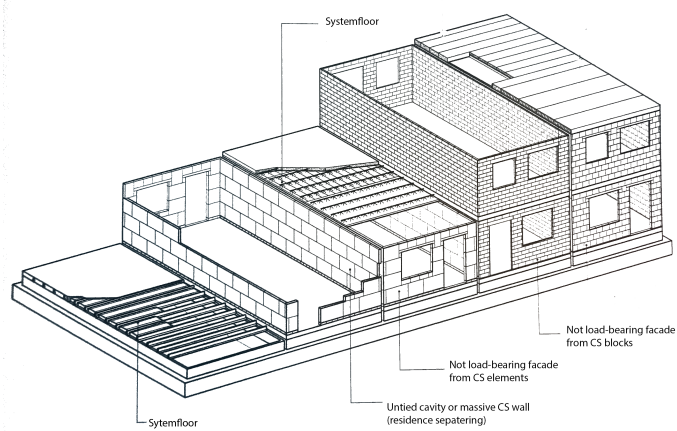


Figure F.3: Traditionally built residences with masonry cavity walls and system floors

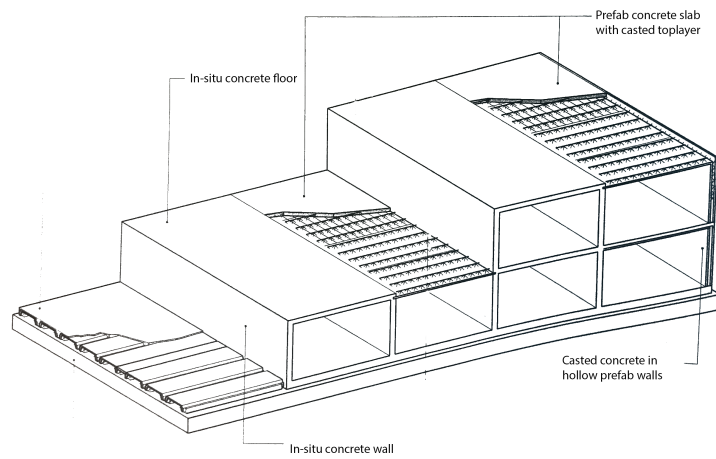


Figure F.4: In-situ concrete walls and floors

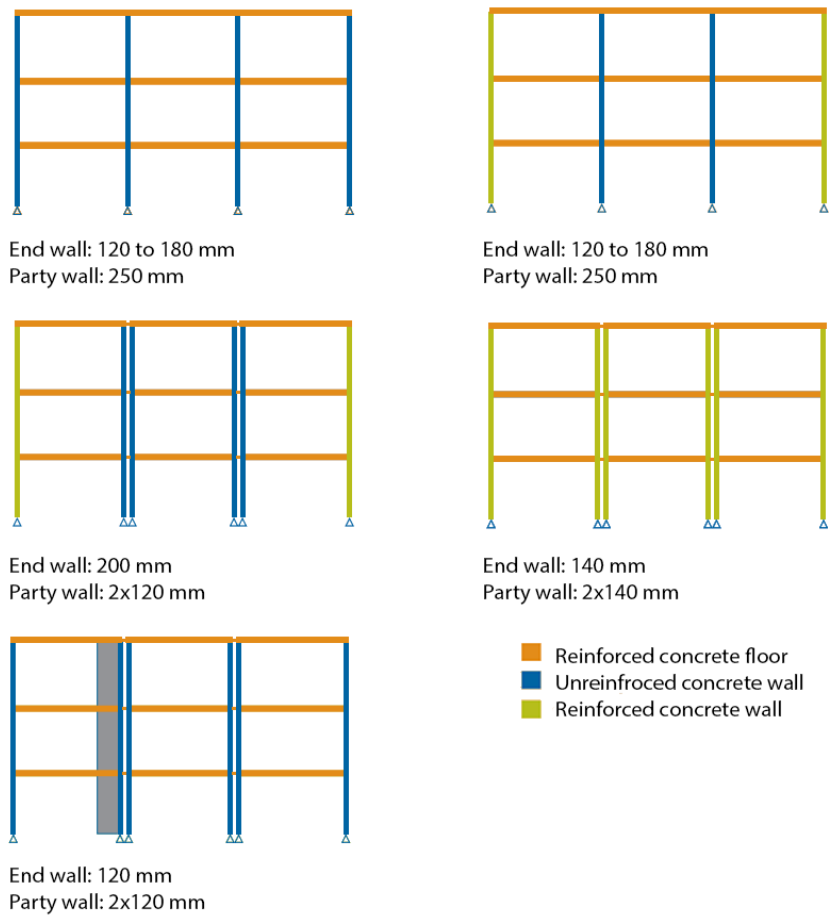


Figure F.5: Stability systems in-situ concrete residences adapted from VOBN

G

Material models and properties for structural analyses

G.1. Model approaches

To model this composite material, three common approaches are described in Figure G.1. Figure G.1 (b) and (c) shows a discrete model, where the joints and units are modelled as separate materials. A difference can be made between a detailed micro-model (b), where the mortar is modelled as a continuum element and the interface by discontinuous elements and the simplified micro-model (c), where the behavior of the mortar joints and unit-mortar interface are combined in discontinuous elements.

Another approach is to model the units and mortar as a homogeneous, an-isotropic material, which is called macro-modeling pictured in Figure G.1 (d). This is a phenomenological approach, so material parameters must be obtained from experiments on masonry. For global structural behaviour such as collapse, the use of a continuum model is preferred since this approach is less time-consuming and exact knowledge of the unit-mortar interaction is generally not required (Laurenco et al., 1995). Since global structural behaviour is of interest and laboratory test have already been conducted on similar masonry as the studied residences, this last approach is used.

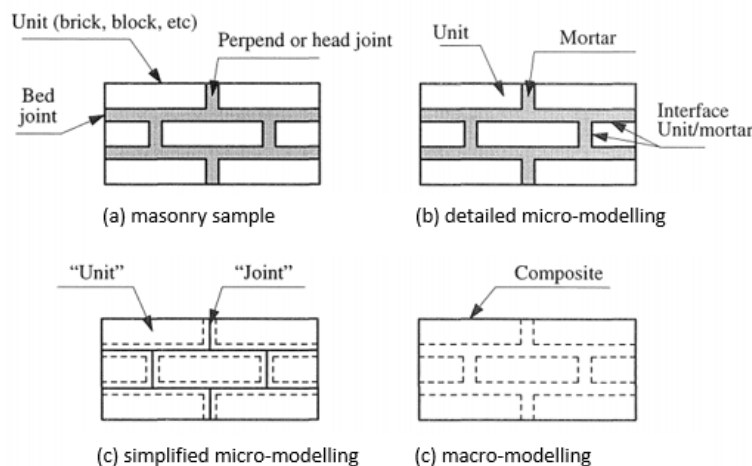


Figure G.1: Modeling strategies for masonry structures (Laurenco et al., 1995)

G.2. Material properties

The properties defined in the studies from experiments on samples from existing building (Jafari et al., 2017) and replicated masonry (Esposito et al., 2016) are summarized in Table G.1.

Table G.1: Material properties for masonry (coefficient of variation between brackets)

Test specimen	f_m [MPa]	f_{x1} [MPa]	f_{x2} [MPa]	f_{v0} [MPa]	μ [-]
sample solid clay > 1945	17.7 (0.38)	0.43 ^[1] (0.38)	1.22 (0.09)	0.45	0.89
sample perforated clay > 1945	20.7 (0.13)	0.15 ^[1] (0.20)	0.87 (0.09)	0.82	0.66
replicated perforated clay	14.73 (0.07)	0.40 (0.26)	1.12 (0.25)	0.15	0.87
sample CS < 1985	12.4 (0.20)	0.18 ^[1] (0.33)	0.72 ^[2] (-)	0.24	0.81
replicated CS	5.93 (0.09)	0.21 (0.25)	0.76 (0.47)	0.14	0.43

^[1] $f_{xk1} = f_{wk}$ (NEN-EN 1996-1-1+A1/NB)

^[2] $f_{xk2} = f_{xk1} * 4$ (NEN-EN 1996-1-1+A1/NB)

For structural analysis, the characteristic values of the material properties are needed. These values have a probability of non-exceedance of 5% and can be determined from the tests by assuming a normal distribution of the strength properties over the samples. For the compressive strength of the masonry, f_m , the covariance, V , is needed. For the flexural strength, the value should be divided by 1.5 and the 80%-value should be taken for the characteristic initial shear strength.

$$\begin{aligned} f_k &= f_m - 1.645\sigma \quad \text{with} \quad \sigma = f_m V \\ f_{xki} &= f_{xi}/1.5 \\ f_{vk0} &= 0.8 * f_{vk} \end{aligned} \quad (G.1)$$

The characteristic tension stress which can develop in the concrete without forming cracks, $f_{ctk0,05}$, is given in Equation G.2 (NEN-EN 1992-1-1+C2 art. 3.1.3) for the lowest quality URC used for residences C20/25 (Van Boom et al., 2005). Using Equation G.3 under accidental loading, gives a design tThe characteristic shear tension the wall can resist can be calculated with Equation G.4 (NEN-EN 1992-1-1+C2/NB art. 6.2.2.). Both values are larger than those of masonry in Table G.1.

$$f_{ctk0,05} = 0.7 * f_{ctm} = 0.7 * (0.3 * f_{ck}^{2/3}) = 1.55 \text{ MPa} \quad (G.2)$$

$$f_{ctd} = \frac{\alpha_{ct} f_{ctk0,05}}{\gamma_{Mc}} = \frac{1.0 \cdot 1.55}{1.2} = 1.29 \text{ MPa} \quad (G.3)$$

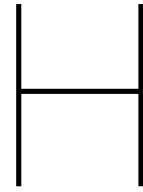
$$v_{min} = 0.035k^{3/2} f_{ck}^{1/2} = 0.44 \text{ MPa} \quad \text{with} \quad k = 1 + \sqrt{\frac{200}{t}} \leq 2.0 \quad (G.4)$$

The number of ties per square meter should be more than 2 according to the Eurocode, which lead to 4 ties in practice by the use of a standard number of ties per isolation plate. For residences built in the period with galvanized steel ties (residence 1), the number of ties is reduced to 2 to take into account the uncertainty of the state of the ties. The force the tie can bear before buckling (in case of compression) or before pulled out of the mortar (in case of tension), can be found in Table G.2 (Esposito et al., 2016). It is assumed the ties are able to transfer an uniform load, q_{Rd} , from one leaf to the other:

$$q_{Rd,tie} = \pm F_{k,tie} N \quad \text{with} \quad F_{k,tie} = F_{tie} - 1.645(F_{tie} V) \quad (G.5)$$

Table G.2: Characteristic material properties for ties (coefficient of variation between brackets)

Case	$F_{tie,-}$ [kN]	$F_{tie,+}$ [kN]	N [$/m^2$]	$q_{Rd,tie,-}$ [MPa]	$q_{Rd,tie,+}$ [MPa]
1+3: perforated clay	-1.83 (0.08)	+2.76 (0.16)	2	-2.61	+3.84
2: CS	-1.09 (0.37)	+1.4 (0.08)	4	-1.48	+3.40



Experimental set-up

H.1. Instrumentation

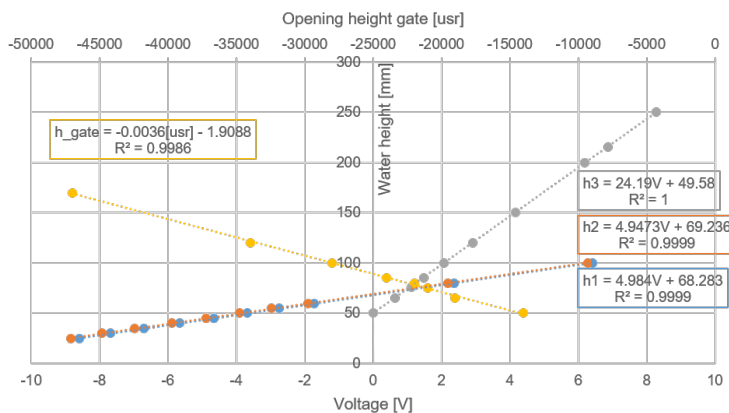
Gate

The Wave Overtopping Simulator can be controlled with the software SoMove 2.5. The software uses the unity, *usr*, to describe both the opening height under the gate, velocity and acceleration of the gate. The relationship between the height in *usr*-p and mm is created simultaneously as calibration of the wave gauges. When the bottom of the gate touches the water level, the water depth (in mm) and opening height (in *usr*-p) are saved to describe this relationship. The maximum opening height is 0.23 m, so avoiding the influence of the gate opening on the formation of the wave is only possible for impoundment depths lower than 0.23 m.

The time of opening of the gate is determined with a video record of 60 frames per second. An acceleration of 10,000 *usr*-a and velocity of 6,000 *usr*-v gives an opening time of 0.13 and 0.20 seconds for opening heights respectively -30,000 and -60,000 *usr*-p. Using the calibration for the height, these periods are in between the values of Equation 4.1. These velocity and acceleration are used in all the following experiments.

Wave gauges

Wave gauges generate electric signals (in volt), which correspond to a certain water depth. This relationship (Equation H.1) can be described by the process of calibration: The flume is filled to a certain water level, which can be verified with tapeline on the see-through side of the flume. To create an equal water level in the flume and reservoir, the gate is open during this process. The voltage from the wave gauges which correspond to this water depth are saved and a trendline can be drawn through these points as shown in Figure H.1.



$$h[\text{mm}] = \text{gain} \cdot V + \text{offset} \quad (\text{H.1})$$

Figure H.1: Calibration of Wave Overtopping Simulator and wave gauges

EMS

The velocity in the direction aligned with the flow is measured with an electromagnetic velocity sensor (EMS). The probe modifies an electric signal which is proportional to the flow velocity parallel to the plane of the electrodes. Velocities are expected to exceed the small range of 0 to +/- 1.0 m/s, so the larger range is chosen. A voltage of 1 V is comparable to a flow velocity of 0.10 m/s. To capture the occurring flow velocities, the EMS is set on 7.3 at stagnant water, leading to the following calibration equation:

$$v \text{ [m/s]} = \frac{7.3 + V}{10} \quad (\text{H.2})$$

Also the elevation of the EMS is of importance, because the results are only reliable when the probe is under water. Furthermore, the velocity profile should be taken into account, although it is assumed this is uniform over the height for the drag force. When looking to experiments of bores propagating over a wet bed, it can be seen that this uniformity starts from $\pm 0.1h_0$ (Wüthrich et al., 2018).

Pressure sensors

The buildings contain 12 sensors shown in Figure 4.3. These sensors measure the difference in pressure inside the building (atmospheric pressure) and the external pressure due to the flood wave perpendicular on the faces of the building. Calibration of the sensors is done in the same way as the wave gauges, so the output in voltage can be converted to a height as presented in Figure H.2. This height resembles the hydrostatic pressure due to a water column with this height.

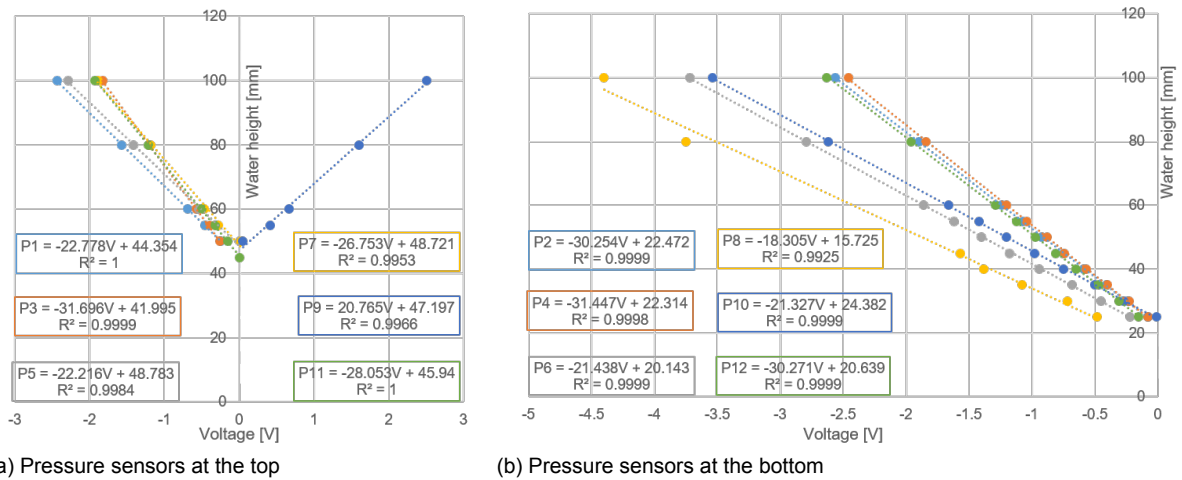


Figure H.2: Calibration of pressure sensors

H.2. Scaling

The following three criteria needs to be met to provide similitude:

1. Geometric similarity: The shape should be the same and is defined as the ratio of geometric dimensions, λ_L , so the real length, L_r to the length used in the model, L_m .
2. Kinematic similarity: Geometric similarity + similarity in motion
3. Dynamic similarity: Forces should act in the same ratio on the corresponding mass through the entire flow field = Geometrical + kinematic similarly and identical force ratios:

$$\text{Froude number} \quad (\text{inertia} - \text{gravity}) \quad Fr = \frac{v}{\sqrt{gh}} \quad (\text{H.3})$$

$$\text{Reynolds number} \quad (\text{inertia} - \text{viscosity}) \quad Re = \frac{vL}{\nu} \quad (\text{H.4})$$

$$\text{Weber number} \quad (\text{inertia} - \text{capillary force}) \quad We = \frac{\rho v^2 L}{\sigma} \quad (\text{H.5})$$

$$\text{Cauchy number} \quad (\text{force} - \text{elastic force}) \quad Ca = \frac{\rho v^2}{E} \quad (\text{H.6})$$

$$\text{Euler number} \quad (\text{pressure force} - \text{inertia}) \quad Eu = \frac{p}{\rho v^2} \quad (\text{H.7})$$

Scaling

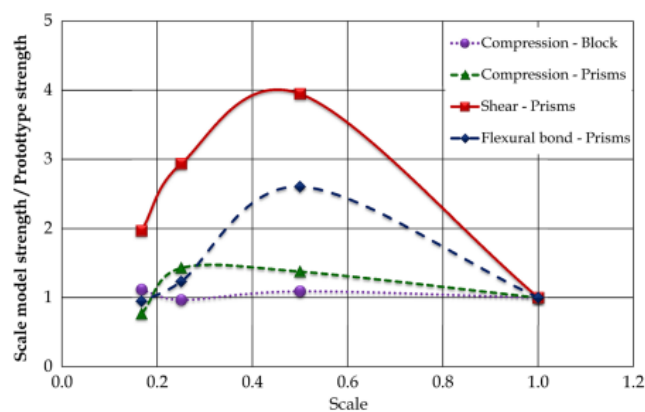
The scale of the model or scale ratio, λ is usually defined as the ratio of geometric dimensions, λ_L . To scale the other parameters in the same way, scale rules needs to be applied according to the most relevant force ratio. For the impact of water on structures the most important one are gravity and inertia, so these should be the same in the model and reality. In experiments this can be accomplished by scaling according to Froudes law, where the dimensionless Froude number, $Fr \frac{v}{\sqrt{gh}}$, should be equal in the model and in reality as well. A scale of 1:30 or 1:60 is typically used for models which imply a Froude similitude.

The scaling of different parameters can be found in Figure H.3a. An example is given for velocity: Since the gravity is the same in the model as in reality, $\lambda_g = 1$ and the length is scaled according to the scale of the model, $\lambda_L = \lambda$, the flow velocity should be scaled with $\lambda_v = \sqrt{\lambda}$, to provide $\lambda_{FR} = 1$.

Scaling of the building material, in this case masonry, is hard due to the difficulty in scaling down of the modulus of elastic, stiffness, density and interaction between the blocks. For this reason experiments are mainly done with the same material, which leads to more scale effects depending on the failure mode of the masonry element shown in Figure H.3b. If there is no effect due to scaling, the ratio of the strength of the scale model and the prototype (full scale/real) strength along the y-axis should be 1. The variation of compressive strength and stiffness is negligible, but there is an increase of shear stiffness and strength of the scale model compared to the prototype with a reducing scale. Also the flexural bond strength at the block-mortar interface is influenced by the scale factor, which is partially due to the variation in water absorption and porosity (Sathiparan et al., 2016).

Parameter	Dimension	Froude
Geometric similarity		
Length	[L]	λ
Area	[L ²]	λ^2
Volume	[L ³]	λ^3
Rotation	[-]	1
Kinematic similarity		
Time	[T]	$\lambda^{1/2}$
Velocity	[LT ⁻¹]	$\lambda^{1/2}$
Acceleration	[LT ⁻²]	1
Discharge	[L ³ T ⁻¹]	$\lambda^{5/2}$
Dynamic similarity		
Mass	[M]	λ^3
Force	[MLT ⁻²]	λ^3
Pressure and stress	[ML ⁻¹ T ⁻²]	λ
Energy and work	[ML ² L ⁻²]	λ^4
Power	[ML ² T ⁻³]	$\lambda^{7/2}$

(a) Scale ratios for Froude scale



(b) Ratio of scale model strength to real masonry strength for different scales (Sathiparan et al., 2016)

Figure H.3: Scaling of hydraulics and masonry

Scale effects

Since the model is made based on Froude scaling and the model fluid is identical to the real-world fluid (water), only one force ratio can be met and dynamic similarity is not possible. The remaining force ratios result in scale effects, which increase with the scale ratio.

The material properties of water, like viscosity, density and surface tension, cannot be scaled when this same fluid is used in the experiments. This makes it impossible to make sure the Reynolds and Weber number are the same in the model and reality. The ratio of inertia to respectively viscosity in Equation H.4 is independent of the Reynolds number when the flow is turbulent with $Re > 2000$. To maintain similar breaking characteristics, so take into account the ratio between inertia and capillary force (i.e. surface stress) at the interface air-water in Equation H.5, the Weber number cannot become below 120 according to Peakall and Warburton (1996).

There is also a difficulty in scaling of the atmospheric pressure and elasticity of the object, so the Euler and Cauchy number are too large. The Cauchy number results in a structure interaction which behaves too stiff and strong and the impact of the water and air are too large as well. Both result in an over prediction of the impact pressures, so the model is conservative compared to reality. For impulsive loads this should be compensated for, see Appendix D.2, but for quasi-static loads this is well accepted.

The dimensionless numbers are checked for the baseline measurements to see if scale effects should be taken in account. In Figure H.4 it can be seen that these numbers are well above the critical values of 120 for the Weber number and 2000 for the Reynolds number, so scale effects can be neglected.

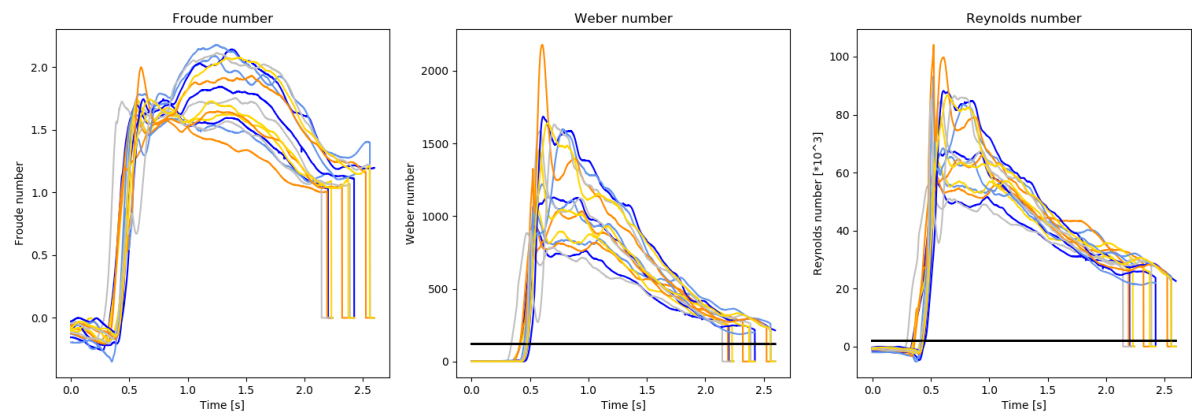


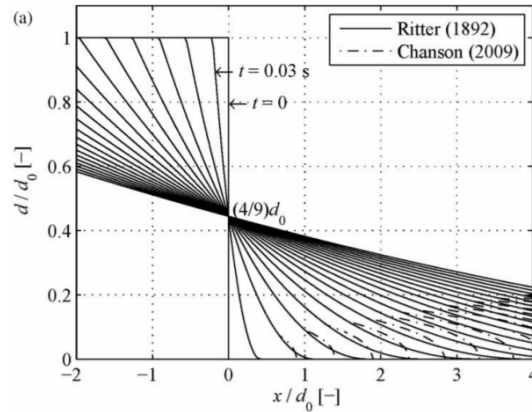
Figure H.4: Dimensionless numbers at the building from measurements of 5 runs with impundment depth $h_0 \approx 200$ mm

H.3. Analytical solution for a dam-break wave

Ritter (1892) determined an analytical solution for a one-dimensional dam-break wave on frictionless bed based on mass and energy conservation in Equation H.8 and H.9. The propagation speed of the front of the positive wave is not accurate enough, so Chanson used the Saint-Venant equations for a prismatic or rectangular channel with frictionless horizontal bed to predict the wave tip profile. The difference of the free surface profile is visible in Figure H.3.

$$h = \frac{1}{9g} \left(2\sqrt{gh_0} - x/t \right)^2 \quad (H.8)$$

$$v = \frac{2}{3} \left(\sqrt{gh_0} + x/t \right) \quad (H.9)$$



FEMA 55 (2011) give an lower and upper bound for the design flood velocity in Equation H.10 , where the initial velocity deduced from Equation H.9 is in between these boundaries with $v = \frac{2}{3}\sqrt{gh_0}$.

$$h_1/t \leq v \leq \sqrt{gh_1} \quad \text{with} \quad t = 1sec \quad (H.10)$$

In case of a steady flow the energy at any point of the streamline is constant according to the Bernoulli equation of conservation of energy head. With zero kinetic energy upstream and zero water depth downstream, the velocity can be calculated as followed:

$$\frac{1}{2}\rho v_0^2 + \rho gh_0 = \frac{1}{2}\rho v_1^2 + \rho gh_1 \quad \rightarrow \quad v_1 = \sqrt{2gh_0} \quad (H.11)$$

Linear elastic approach

The non-load bearing (NB) wall is the pier in the facade are needed to provide stability to the residence, the party walls provide the stability of case-study residence 3. The normal force in this wall is caused only by the self-weight of the facade. An overview of the dead weights is given in Table I.1 per case-study residence.

Table I.1: Normal forces on the lower walls

Case	Material	t [mm]	ρ [kg/m ³]	G [kN/m ²]	$N_{element}$ [kN/m]	N_{Ed} [kN/m]
1: floor	timber	-	-	0.30 (+1) ^[3]	0.81 (+2.7)	
LB wall	URM clay	100-50-100	1800	1.77	4.77	13.19
NB wall	URM clay	100-50-100	1800	1.77	4.77	4.77
2: floor	system	-	-	5.40 (+1) ^[3]	14.57 (+2.7)	
LB wall	URM CS	120-60-120	-	2.01 ^[1]	5.43	38.55
NB wall	URM CS	100-50-100	-	1.68 ^[2]	4.52	4.52
3: floor	RC	180	2500	4.41 (+1) ^[3]	11.92 (+2.7)	
LB wall	URC	120-60-120	2400	2.83	7.63	35.76
party wall	URC	250	2400	5.89	15.89	43.19

^[1] $G = g\rho = 9.81 \cdot 205/1000 = 2.01 \text{ kN/m}^2$ (Van Paasen et al.)

^[2] $G = 2.01/120 \cdot 100 = 1.68 \text{ kN/m}^2$

^[3] surface load due to installations, furniture ect. kN/m^2

I.1. Edge conditions

The façades on both sides are non-load bearing and consist of masonry wall panels with openings for the windows and doors. It can be assumed that the arrangement of the units provide a bonded connection between the load-bearing wall and façade. Depending on the ability of the masonry pier to rotate in torsion, the edge condition can be defined as continuous (Figure 5.1 a) or simple (Figure 5.1 c).

A small opening can be dealt with by subtracting the area of the opening from the total area to calculate the strength if a suitable frame is built in this opening. It is also possible that the parapets are constructed of wood-based panels in stead of masonry, which are glued to the floor and tied to the piers. To find the resistance of the façade, it can be divided into sub-panels by defining the material and edge conditions. For the out-of-plane behaviour, the parapet itself has only an clamped boundary condition at the base and the at the intersection of the masonry piers and the parapet, free edges can be assumed since no shear can be transferred.

Over the years three types of floors are commonly used resulting in the following boundary conditions:

- *Timber floors* can be assumed to function as a simple edge condition based on the capacity of the anchors. Since the beams span in one direction, the floor behaves stiff in the direction of the beams and flexible in the transverse direction. Due to this behaviour and the non-load bearing function of the façade itself, a flexible façade-floor connection is created and schematized as a free edge, so torsion of the piers is not restrained.
- "*System floors*" are placed on top of the load-bearing walls and fixed with mortar resulting in a stiff diaphragm behaviour of the floor. Although the floor spans in the same direction as the timber floor, this behaviour make it possible to provide a lateral support in both the direction of the load-bearing wall and the non load-bearing façade wall.
- When the *concrete floor* is a fixed to the load-bearing walls by pouring concrete at the edges and continuous or overlapping reinforcement through the elements, stability can be found without adding piers. Both moments and shear can be transferred between the walls and floors, so this is a continuous edge condition.

Beside the floors, also the type of foundation can be seen as an edge conditions for the wall. The foundation consist of a shallow foundation or in combination with pile underneath, resulting both in a fixed support at the base of the wall. Also the presence of a damp proof course (dpc) needs to be considered based on the shear resistance of the material, which can cause a discontinuity in the lateral load distribution. This layer, introduced around 1975, is usually placed at ground level in between the units to prevent capillary rise of ground water in the wall. Initially it is assumed the shear force can be transferred through this foil, so schematized as a simple supported edge.

I.2. Linear elastic response

The differential equations describe the linear elastic response of any wall due to a lateral load. If the stability moment of resistance (moment of the base in Equation I.1) exceeds the maximum moment without the partially fixed base, it should be schematized as a propped cantilever.

$$M_{Rd,s} = N_{Ed} * z \quad \text{with} \quad z = \frac{t}{2} - \frac{t_c}{2} = \frac{t}{2} - \frac{N_{Ed}}{(2f_d)} \quad (I.1)$$

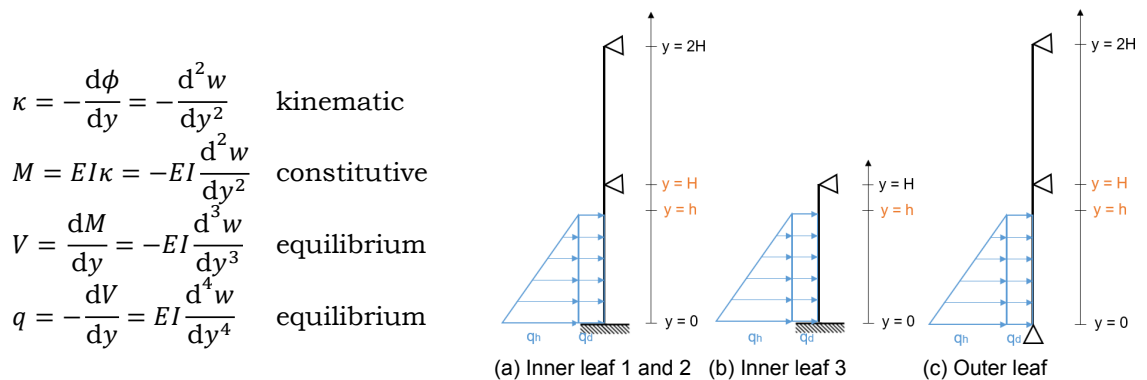


Figure I.1: Mechanic scheme of inner walls

Boundary conditions	propped	$w = 0$	$\phi = 0$	—	—
	simple support	$w = 0$	—	—	$M = 0$
Matching conditions	end load	$w_l = w_r$	$\phi_l = \phi_r$	$V_l = V_r$	$M_l = M_r$
	simple support	$w_l = 0$ $w_r = 0$	$\phi_l = \phi_r$	—	$M_l = M_r$

Failure however occurs when the stability moment at the base is exceeded, so the opening of the crack until reaching this stability moment, is colored yellow. For the second case-study residence this rocking strength provides additional moment capacity, where this is negligible for the first case-study residence. When the crack is totally opened, redistribution of the loads cause an increase of the sagging moment until the ultimate strength is also reached at this location (orange area in Figure I.2c and I.2g).

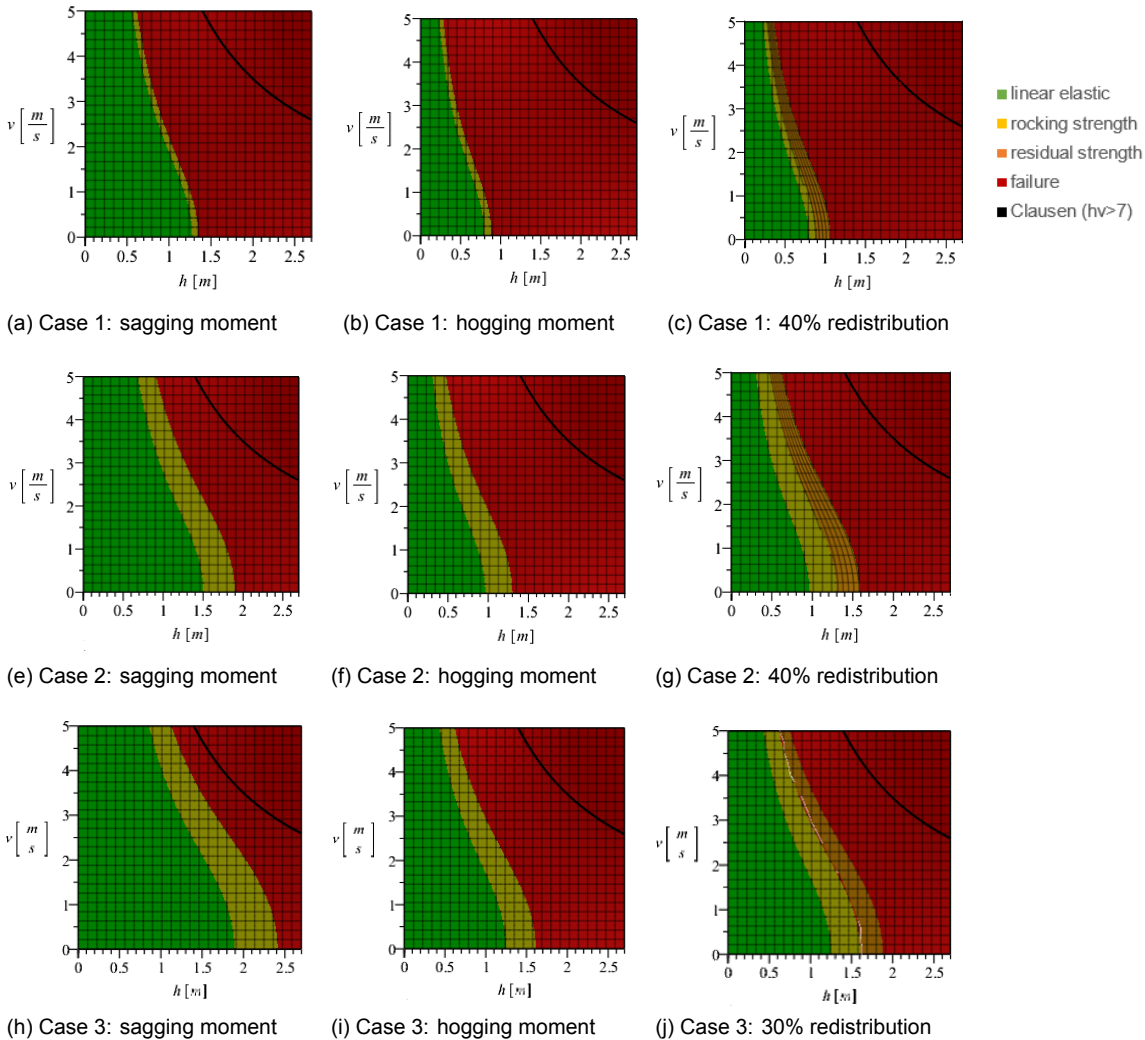


Figure I.2: Failure graph for one-way bending of the load-bearing inner leaves

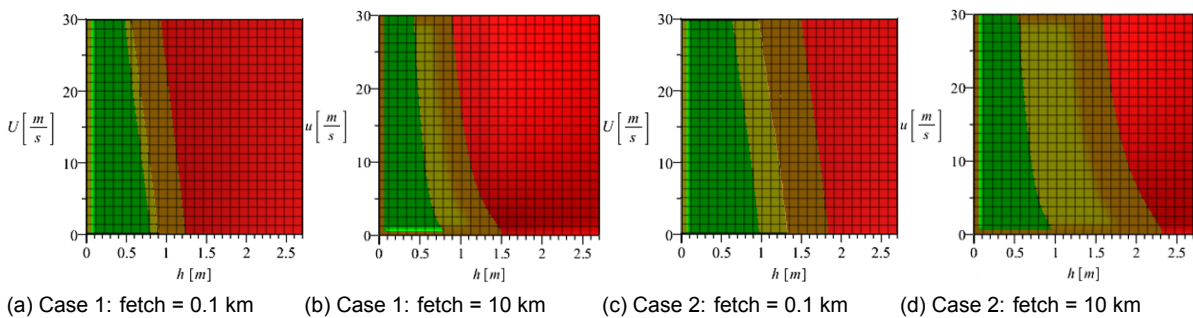


Figure I.3: Failure graph for out-of-plane bending of inner leaves for load combination 2

I.3. Load distribution over shear walls

The shear force subjected to a pier consist of a direct component and a torsional component due to the distance of the net force to the center of rigidity, see Equation I.2. In case the front and back facade have openings at the same locations, the latter component is zero due to symmetry.

$$\left. \begin{aligned} V_{v,p} &= V \frac{EI_p}{\sum_{i=1}^n EI_{p,i}} \\ V_{t,p} &= Ve \frac{EI_p d_p}{\sum_{i=1}^n EI_{p,i} d_p^2} = 0 \\ I_p &= \frac{tL_p^3}{12} \end{aligned} \right\} V_p = V_{v,p} + V_{t,p} = V \frac{I_p}{\sum_{i=1}^n I_{p,i}} \quad (I.2)$$

All the piers in case-study residence 1 are engaged due to the additional load-bearing wall in the residence, where the pier in between the door and window(s) is isolated for case-study residence 2. The moment of inertia for the engaged piers are much larger due to the bonded load-bearing wall, which partially act as flange of the shear wall according to NEN-EN 1996-1-1 art.5.5.3. The moments of inertia for the different piers and the number of piers present in a row of 4 residences are given in Table I.2. In the last column the percentage of the total load which the pier should resist according to Equation I.2 can be found.

Table I.2: Moment of inertia, amount and relative rigidity of piers in a row of 4 residences

Case	L_p [m]	t [mm]	L_{LB} [m]	t_p [mm]	N [/facade]	I [$\cdot 10^9$ mm ⁴]	RR [%]
1:engaged	0.5	100	0.54 ^[1]	100	6	2.13	1.80
	engaged	1.0	100	0.54	3	15.48	13.08
						$\Sigma I = 59.19$	
2:isolated	0.5	100	0.54	120	4	1.04	0.89
	engaged	0.5	100	0.54	2	4.02	3.42
	engaged	1.0	100	0.54	3	15.52	13.20
						$\Sigma I = 58.77$	

^[1] minimum of $H/5$, $\frac{L-t_{LB}}{2}$, $\frac{H-h_{floor}}{2}$, $6t_{LB}$ (NEN-EN 1996-1-1 art.5.5.3)

J

Tie and window failure

J.1. Tie failure

The load-bearing walls are cavity walls, so both leaves should not have to bear the total load. The maximum load can be applied to the wall if the load will be distributed between the leaves in the ratio 0.65:0.35 for case-study residence 1 and 0.75:0.25 for case-study residence 2 displayed in Figure J.1. Where the Clausen criteria is closely approached by the failure graph of case-study residence 2, the difference between the Clausen criteria and the failure graph of case-study residence 1 remains big.

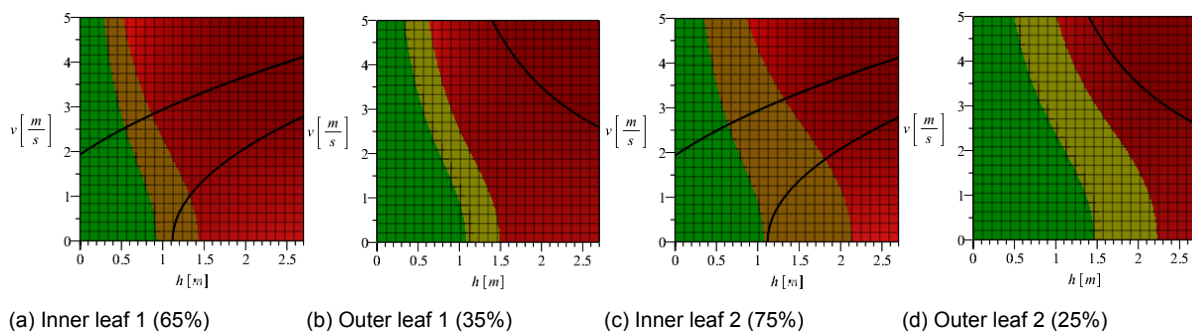


Figure J.1: Failure graphs for inner and outer leaf of case-study residences

It should be checked if the ties can bear this load transfer from one leaf to the other during this the optimal load distribution. The location of check makes a big difference as can be seen in Figure J.2a and J.2b, where the lower lines are the maximum tension force at a certain location before pulling out of the ties and the upper line is the maximum compression force before the ties will buckle. The boundaries at halfway of the water depth are shown in the Figure 5.15a and 5.15d as well to compare this failure with bending failure of the load-bearing inner leaf.

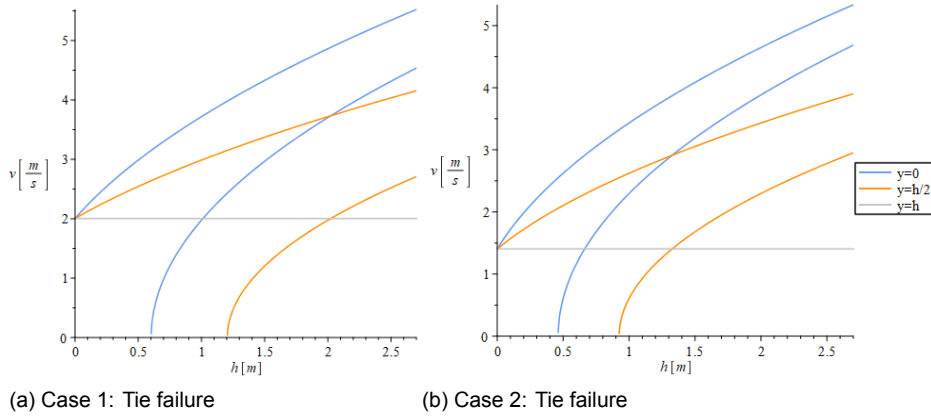


Figure J.2: Failure graph for ties of case-study residences

J.2. Windows

The red area in Figure J.3 represents the flood situation combination, which cannot be resisted by the window pane. For load combination 1 is this the combination of water depth and flow velocity, where for load combinations 2 a combination of water depth and the wind-generated waves is given. The orange part represent the failure in case of a single-glazed window, which fails at a slightly lower pressure. If this situation occurs, the window is assumed to be broken and the water depth will equalize inside the residence. In the graphs only the critical orientation for failure of the windows is taken into account, so the *glass panes perpendicular to the flow or wind direction*.

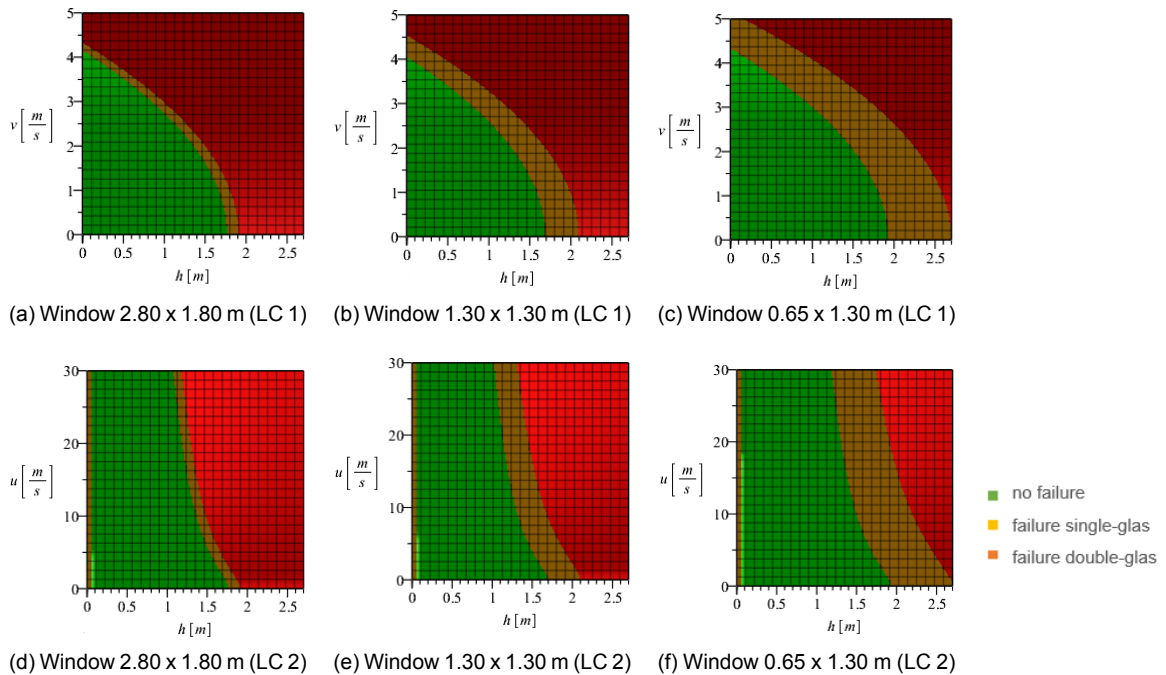
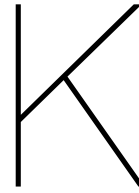


Figure J.3: Failure graph for windows of different dimensions for load combination 1 (a,b,c) or 2 (c,d,e)



Failure graphs without the safety factors

To approximate the real failure values more closely the additional floor load, $G_{surface}$, of 0.53 ($\psi_2 q_k = 0.3 \cdot 1.75 = 0.53 \text{ kN/m}^2$) is included and the safety factor, $\gamma=0.9$, for the dead load is excluded. Also the characteristic strengths, f_{xk} , are used instead of the design strength, f_{xd} , leading to the values in Table K.1. The failure graphs from Figure 5.13 are recreated in Figure K.1. For case-study residences 2 and 3, this gives an additional water height of $\pm 0.20 \text{ m}$ that can be resisted before the residence collapse. The difference for residence 1 and the combinations causing the first crack is smaller than 0.10 m.

Table K.1: Moment resistance of lower walls (design values between brackets)

Case	t [mm]	σ_n [MPa]	f_{xk1} [MPa]	f_{xk2} [MPa]	M_{Rk1} [kNm/m]	M_{Rk2} [kNm/m]
1:LB URM clay	100-50-100	0.22 (0.13)	0.29 (0.22)	0.81 (0.62)	0.85 (0.59)	1.35 (1.04)
2:LB URM CS	120-60-120	0.43 (0.32)	0.14 (0.11)	0.51 (0.39)	1.36 (1.03)	1.22 (0.94)
3:LB URC	120-60-120	0.42 (0.30)	1.55 (1.29)	1.55 (1.29)	4.73 (3.95)	3.72 (3.10)

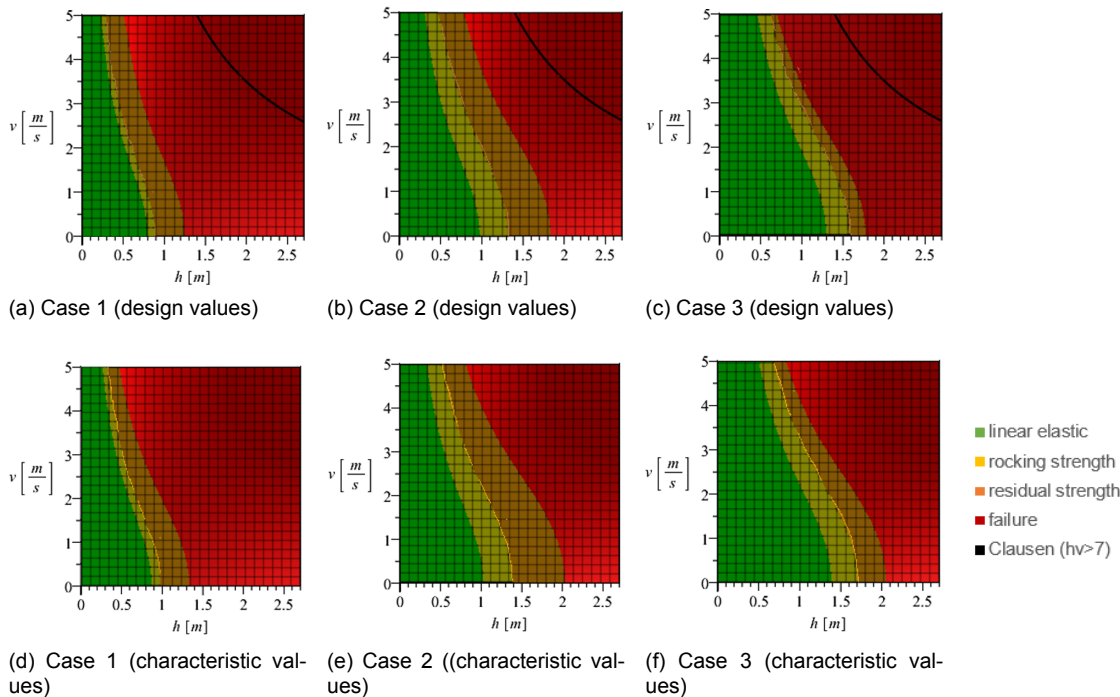


Figure K.1: Failure graphs from nonlinear analysis for load combination 1 for all three case-study residences